2015

Functional Dissection of Brainstem Circuitry

Alexander Ryan Nectow

FUNCTIONAL DISSECTION OF BRAINSTEM CIRCUITRY

A Thesis Presented to the Faculty of

The Rockefeller University

in Partial Fulfillment of the Requirements for

the degree of Doctor of Philosophy

by

Alexander Ryan Nectow

June 2015

FUNCTIONAL DISSECTION OF BRAINSTEM CIRCUITRY

Alexander Ryan Nectow, Ph.D.

The Rockefeller University 2015

Eat. Sleep. Breathe. Move. These functions, critical to an individual's survival, are controlled by highly conserved neurotransmitter and neuromodulatory systems, which are principally located in the brainstem. These different brainstem neural populations, while performing apparently simple life-sustaining functions, are remarkably complex. For proper function, survival circuits need to receive information from brain regions responsible for sensing survival needs, and rapidly exert broad control over the brain to generate adaptive behavior like foraging during energy deficit and escape from predation. How can survival circuits generate such autocratic control?

Survival circuits principally affect global brain function in two ways: diffuse projection patterns and transmitter co-release. Through these two mechanisms, cell types small in number can have an enormous impact on neural processing and behavioral output through combinatorial complexity. However, the properties that allow these systems to address critical survival needs also make them exceptionally difficult to study; and current technology is no match to the complexity of the circuit. To understand the role that these neural circuits play in the functioning animal, it is necessary to develop technologies that can identify molecular markers,

which will provide an access point for the study and manipulation of different cell types.

The current work presents studies that I've performed over the past three and a half years, where I have sought to functionally dissect neural circuits of the brainstem. Through the development and application of a number of novel molecular technologies, we have gained critical insight into the molecular and neural basis of behavior. The first part of this work describes the functional dissection of dorsal raphe cell types to elucidate their role in modulating survival functions. The second part outlines the development of a novel technology, Retro-TRAP, which we developed to address a critical, unmet need in neuroscience: molecular profiling of neurons based on their connectivity. In these studies, a particular emphasis was placed on the dopaminergic and serotonergic nuclei of the midbrain (the ventral tegmental area/substantia nigra pars compacta and dorsal raphe, respectively), as they are essential for key survival behaviors, such as feeding and locomotion. These populations of neurons are therefore ideal for studying the generation of purposive behaviors in the context of survival circuitry.

ACKNOWLEDGMENTS

I am incredibly grateful for all of the assistance, support, and instruction that I've received over the course of my graduate work. The following work would not have been possible without the help from so many different people.

First, I'd like to thank Jeff Friedman for his mentorship and patience with my work. In the Friedman lab, I have been able to run free with any crazy idea that has popped into my head, and I have been given incredible resources and opportunities (not to mention a number of excellent sushi dinners).

I would also like to thank the members of my Faculty Advisory Committee (FAC), Mary Beth Hatten and Winrich Freiwald, who have both been incredible resources, full of excellent advice. Winrich has also spent countless hours helping me with applications for independent positions, job talks, and just chatting good science. This has been critical for my success over the past few years. I would also like to thank Brad Lowell from Harvard University, for serving as the external examiner on my committee.

This work also critically relied on two people: Mats Ekstrand, my collaborator for the development and application of Retro-TRAP (and some other crazy molecular technologies), and Bianca Field, a technician who worked with me on the functional dissection of the dorsal raphe nucleus. Mats initially trained me in all things molecular biology, and grew into a great collaborator and friend. I would also like to thank the Friedman lab for their input at group meetings and informal conversations, in particular: Olof Dallner, Lisa Pomeranz, Kaamashri Latcha, Wei Shen, and Susan Korres. Additionally, Yupu Liang was invaluable in helping with bioinformatics and Hongxing Zhang and Ming-Hu Han for electrophysiology.

A number of other people have been an excellent source for advice, mentorship, and great conversation. The list is too long to write down, but just to name a few: Eric Nestler, Nick Stavropoulos, Stephan Lammel, Dragana Rogulja, Mike Crickmore, Eric Schmidt, and Marcelo Dietrich.

I would like to offer special thanks to a number of my friends (Brian, Jeremy, Eli, Dibble, Marc, Branden, Ping, Doug, and Horwitz) for their visits and overall shenanigans. In particular, Jon Miller has been a source of humor and great conversation, especially during times when my work wasn't going well. I also have to thank my extended family and friends for their kindness, patience, and encouragement throughout the duration of this work.

Lastly, and most importantly, I have to thank my mom, dad, Gramps and my late Grammy, for their endless love, support, and encouragement over the years. Without them, this work would not have been possible. I dedicate this work to my Grammy.

TABLE OF CONTENTS

LIST OF FIGURES

CHAPTER 1

CHAPTER 3

CHAPTER 4

CHAPTER 5

LIST OF TABLES

CHAPTER 5

CHAPTER 1: INTRODUCTION

A basic goal of biology is to understand the mechanism underlying how an organism's structure informs and determines its function. For the brain, this goal has proven to be somewhat elusive. The role of the brain is to interpret an animal's environment and convert it into an actionable sequence of events, behavior, which are critical for keeping the animal alive and reproducing. However, this simple goal belies the brain's remarkable complexity.

Unlike most other organs, the brain simultaneously operates at length and time scales spanning many orders of magnitude. Single synapses operate at nanometer lengths with millisecond-precision signaling, while neural circuits can span many centimeters and (in the case of something like memory) retain information over the course of years. With this daunting level of complexity, the study of neural circuitry requires a number of different approaches. The functional unit of the nervous system is the neuron, and it comes in many different flavors (cell types): different shapes and sizes (morphology), activity (excitability), anatomy (connectivity), composition (molecules), and function (effect on behavior). Recent work has demonstrated that cell types even in the same anatomic locus can bidirectionally influence behavior, whether it is feeding (Aponte et al., 2011), drinking (Oka et al., 2015), locomotion (Kozorovitskiy et al., 2012; Kravitz et al., 2010), valence (Jennings et al., 2013; Lammel et al., 2013), or stress/anxiety (Chaudhury et al., 2013; Kim et al., 2013). It is thus becoming increasingly clear that the identification

and functional dissection of specific cell types is critical for understanding how the brain gives rise to sophisticated behaviors.

Cell types are embedded within defined neural circuits, which ultimately determine their functionality. It is therefore essential to not only identify cell types, but to also define their unique input/output architecture. A cell type's inputs provide context for how an individual neural population interprets its internal and external environment, whereas its outputs determine how it converts this representation into actionable consequences. This is particularly important when studying brainstem neural circuitry, which is a critical locus for mediating key survival-related behaviors. The brainstem sends and receives information throughout the brain, and thus can exert autocratic control over the organism. How it does this is poorly understood.

The current work describes an approach to tackling the neural circuitry of the brainstem using novel, state-of-the-art molecular technologies in tandem with circuit mapping and functional optogenetic tools. Here, I describe the application of these tools to understand the molecular and anatomic organization of brainstem neural circuits, and then apply these findings to functionally interrogate these circuits in the freely moving animal. The insights gained from these studies have informed how the animal may adapt to its local environment to promote survival.

1.1 Functional dissection of the dorsal raphe

Innate behaviors such as feeding and locomotion address basic needs that are critical to survival. However, the neural circuits underlying these actions exhibit a remarkable degree of complexity, which is required to assemble the critical behavioral state. The dorsal raphe nucleus (DRN), which is thought to play a key role in modulating reward- and survival-related functions, is a prototypical example of survival circuitry: it is comprised of a mosaic of partially overlapping cell types (Figure 1.1) and has a diffuse, highly collateralized neural circuit architecture (Gagnon and Parent, 2014). The cell types underlying dorsal raphe-controlled behaviors have not been conclusively identified (Warden et al., 2012). The DRN also house's the single largest population of serotonergic neurons in the mammalian brain (Lowry et al., 2008). It is thus thought to play a critical role in modulating serotonin-dependent behaviors. These behaviors include feeding (Heisler et al., 2006), arousal/locomotion (Jacobs and Fornal, 1993; Waterhouse et al., 2004), and possibly reward (Liu et al., 2014; Rompre and Miliaressis, 1985). However, given the DRN's molecular heterogeneity, parsing out its role in controlling behavior is no easy task. The contribution of each of these cell types to behaviors associated with activity of the dorsal raphe nucleus is as yet unknown.

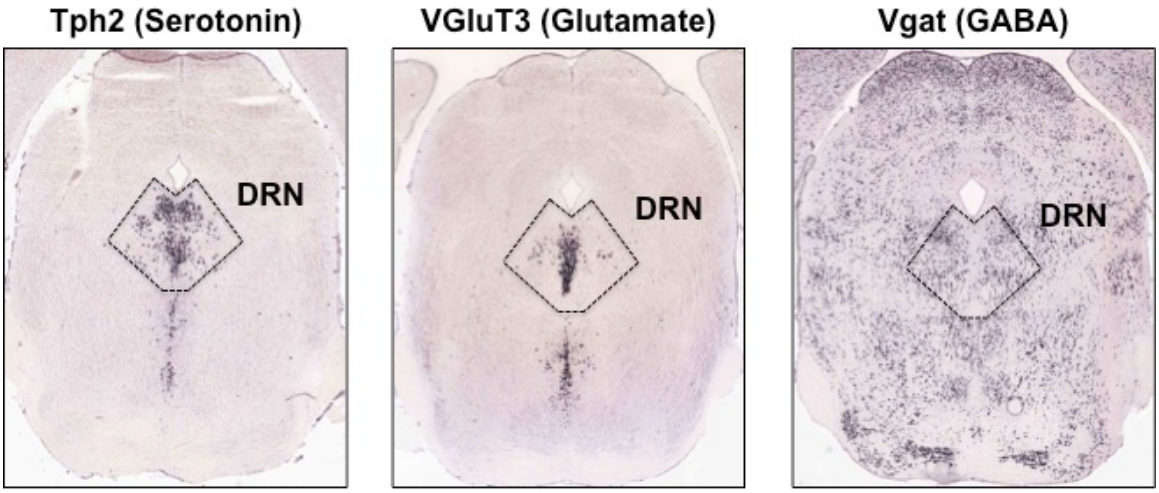

Figure 1.1. The Dorsal Raphe Nucleus is Comprised of a Mosaic of Cell Types. The three predominant cell types within the raphe are serotonergic (marked by Tph2, **left**), glutamatergic (marked by VGluT3, **middle**), and GABAergic (marked by Vgat, **right**). A rough outline of the dorsal raphe nucleus (DRN) is delineated by dashed lines.

We set out to test the contribution of each of these cell types to survival-related behaviors (feeding, locomotion, and reward) through cell-type-specific optogenetic activation utilizing freely available Cre-driver lines. In the current work, we surprisingly find that acute manipulation of DRN serotonin neurons does not affect survival-related function; rather, we find that the DRN modulates acute behavioral output principally through the activity of GABAergic (*Vgat*-expressing) and non-canonical glutamatergic (*VGluT3*-expressing) neurons, the latter of which overlap substantially with serotonergic neurons. These GABAergic and glutamatergic cell types contribute to different aspects of reward- and survival-related behaviors and together are able to bidirectionally control food intake, reminiscent of the AgRP/POMC neuron opponency exhibited by the arcuate nucleus of the hypothalamus (Aponte et al., 2011). Taken together, this work elucidates a novel cell-type-specific neural circuit mechanism through which the brain addresses critical survival needs.

1.2 Molecular profiling with viral translating ribosome affinity purification (vTRAP)

Translational profiling methodologies enable the systematic characterization of cell types in complex tissues. These methods have proven particularly useful for molecular studies of the mammalian central nervous system, where neuronal isolation is exceptionally difficult. Here, we report the development of a viral strategy for rapidly profiling CNS cell types. We engineered an adeno-associated virus to Cre-conditionally express an EGFP/large ribosomal subunit fusion protein

(AAV-FLEX-EGFPL10a), which we have used in combination with numerous Cre-driver lines to validate its utility as a tool to access translating mRNAs from genetically and anatomically defined neural populations. We then applied AAV-FLEX-EGFPL10a to melanin-concentrating hormone neurons of the lateral hypothalamus, identifying a number of novel marker genes for this cell type using high-throughput RNA sequencing. We have also produced and tested this AAV in a number of serotypes, making this new viral TRAP (vTRAP) technology broadly applicable for profiling the CNS and other cell types for which a Cre-driver line is available.

Molecular characterization of cell types within the brain is essential for understanding central nervous system (CNS) function. The complexity and heterogeneous nature of the CNS and the relatively few cell-type-specific marker genes have made such studies historically challenging. Over the last decade, a variety of innovative approaches have yielded significant advances in our ability to profile gene expression from defined cell populations. These include laser capture microdissection (LCM) (Lammel et al., 2008; Li et al., 2013) of anatomically identified cells, fluorescence activated cell sorting (FACS) of labeled cells (Lobo et al., 2006; Arlotta et al., 2005; Molyneaux et al., 2014), immunopanning (Dugas et al., 2008), and manual cell sorting (Sugino et al., 2006). While powerful, these methods are labor intensive, rely on postmortem identification of cell types, and are not amenable to rapid, high-throughput *in vivo* analyses.

The translating ribosome affinity purification (TRAP) technique is a direct, rapid affinity purification method for isolating polysomal RNA from genetically defined cell populations *in vivo* (Heiman et al, 2008). TRAP is part of a growing class of techniques, referred to as translational profiling, that directly access the translating mRNAs of defined cell types based on the expression of specific marker genes (Heiman et al., 2008; Doyle et al., 2008; Sanz et al., 2009), connectivity (Ekstrand et al., 2014), or even activity (Knight et al., 2012). These techniques are particularly effective due to the limited perturbations required to access genetic material from the cell types of interest. In contrast to lengthier cellular isolation methods, TRAP avoids possible adaptations and RNA degradation by substantially reducing the amount of elapsed time between animal sacrifice and mRNA purification by the affinity purification of tagged polysomes from whole tissue homogenates (Heiman et al., 2008, Heiman et al., 2014). TRAP has become widely used and has been employed to profile translation in dozens of cell types in the mouse CNS (Doyle et al., 2008**;** Schmidt et al., 2012**;** Gorlich et al., 2013; Mellen et al., 2014; Nakajima et al., 2014), visceral organs (Grgic et al., 2014; Liu et al., 2014; Zhou et al., 2013), and has even been adapted for use in other species including zebrafish (Tryon et al., 2013), frogs (Watson et al., 2012), flies (Thomas et al., 2012), and even plants (Wang and Jiao, 2014).

While simple and effective, to date the application of TRAP to study the mammalian CNS has been dependent on obtaining the proper transgenic mice. This has been achieved through the generation of completely new BAC transgenic mouse lines

(Doyle et al., 2008) or crossing Cre-driver lines to floxed tag alleles (Sanz et al., 2009; Stanley et al., 2013; Liu et al., 2014; Zhou et al., 2013). We thus set out to expand the use and accessibility of TRAP by generating novel Cre-conditional adeno-associated viruses (AAVs) that make it possible to profile molecularly defined, anatomically-restricted neural populations for which Cre-driver lines already exist. This approach allows for rapid access to translating mRNAs in discrete neural populations through viral tagging of ribosomes in anatomically and molecularly defined subsets of neurons. From the time of injection, enrichments for marker genes are observed as early as three weeks post-infection, demonstrating that this approach is an effective way to rapidly and accurately profile targeted cell types.

As a proof of concept, we validated this novel viral TRAP (vTRAP) methodology using a number of readily available Cre-driver lines, representing cell types throughout the brain (specifically, within the brainstem, hypothalamus, and cortex). In particular, we focused on a population of lateral hypothalamic neurons expressing melanin-concentrating hormone (MCH), which are implicated in feeding and arousal-related behaviors (Jego et al., 2013; Shimada et al., 1998). High-throughput RNA sequencing (RNA-seq) of the MCH neurons led to the identification a number of known cell type markers, and revealed a number of marker genes with relevance to feeding behavior and metabolic state. Taken together, the current work provides a highly efficient means for targeting neuronal ribosomes in a cell-type-specific, anatomically restricted fashion using viral-mediated gene transfer.

1.3 Molecular profiling of neurons based on connectivity using Retro-TRAP

An important goal in neuroscience is to understand how neural circuits control behavior. Toward this end, intensive efforts are being made to delineate the complete wiring diagram, or connectome, of the mammalian brain. High-throughput electron microscopy has been used to define micro-scale connectivity (Helmstaedter et al., 2013), while tracing strategies utilizing virally-encoded fluorophores have allowed for milli-scale circuit mapping (Wickersham et al., 2007), with postsynaptic cell-type-specificity in some cases (Wall et al., 2010; Wall et al., 2013). While these studies have elegantly dissected a number of complex circuits, they are not designed to provide molecular information about the presynaptic neural populations. The identification of marker genes for neurons comprising circuits enables testing of their functional role, which is key to understanding how the brain controls complex neural processes.

Methods for identifying markers expressed in molecularly defined neurons in the mammalian nervous system have been developed by translationally profiling cells through the expression of a ribosomal tag (Heiman et al., 2008; Sanz et al., 2009). Translating ribosome affinity purification (TRAP) can yield molecular profiles of defined neural populations using cell-type-specific expression of a GFP-L10 fusion protein through BAC transgenesis or conditional expression of a floxed allele (Doyle et al., 2008; Stanley et al., 2013).

While providing detailed information about the molecular identity of populations of neurons, TRAP does not provide neuroanatomical information. Given that the function of a defined population of neurons is inextricably linked to its circuit connectivity, we sought to adapt TRAP technology to molecularly profile and identify subsets of neurons that project into specific brain regions. We focused first on the nucleus accumbens, which plays an important role in diverse behaviors such as feeding, addiction, and depression (Chaudhury et al., 2013; Lim et al., 2012; Luscher and Malenka, 2011; Tye et al., 2013).

To profile neurons based on their site of projection, we set out to functionalize GFP (Tsien, 1998), such that it could tag ribosomes and allow their precipitation in a manner analogous to that of TRAP. Since GFP is commonly encoded in retrograde tracing viruses, such as canine adenovirus type 2 (CAV; Bru et al., 2010), this approach would allow us to precipitate ribosomes from only those neurons that project to a defined region. To achieve this, we utilized camelid nanobodies, which are small, genetically-encoded, intracellularly stable and bind their antigens with high specificity and avidity (Muyldermans, 2013). Camelid nanobodies have recently been used in a number of applications, such as intracellular localization of proteins (Ries et al., 2012), live cell antigen targeting (Rothbauer et al., 2006), and modulation of gene expression (Tang et al., 2013).

We hypothesized that an anti-GFP nanobody fused to a ribosomal protein could stably bind GFP intracellularly and allow for ribosome precipitation. Moreover, if

used in combination with GFP expressed from a retrograde tracing virus such as CAV-GFP, this approach would allow for immunoprecipitation of ribosomes specifically from projective neurons.

In the current work, we generated transgenic mice that express an N-terminal fusion protein consisting of the V_HH fragment of a camelid antibody raised against GFP (Rothbauer et al., 2006), fused to large ribosomal subunit protein Rpl10a under the control of the synapsin promoter. By injecting the retrogradely transported CAV-GFP virus (Bru et al., 2010) into the nucleus accumbens shell, we were able to capture ribosomes from presynaptic neurons in the ventral midbrain and hypothalamus, and identify markers delineating cell-types that project to this region. Furthermore, using a Cre-conditional AAV encoding the NBL10 fusion, we were able to molecularly profile VTA dopamine neurons projecting to the nucleus accumbens. This work provides a general means for molecularly profiling presynaptic cell-types based on their projection pattern, and identifies marker genes for neuronal populations that are potentially relevant to a variety of behaviors including feeding, and neuropsychiatric diseases, such as addiction and depression.

CHAPTER 2: MATERIALS AND METHODS

2.1 Mice

All experiments were approved by The Rockefeller University Institutional Animal Care and Use Committee (IACUC) and were in accordance with the National Institutes of Health guidelines. Mice were all housed on a 12 hr light-dark cycle with *ad libitum* access to food and water (unless stated otherwise). All behaviors and molecular assays were performed in the light cycle. The following mouse lines were used in the current work:

2.1.1 CreMdriver lines. *Slc32a16IRES6Cre* (Vgat-IRES-Cre, Jackson Labs Stock 016962), *Slc17a86IRES6Cre* (VGluT3-IRES-Cre, Lou et al., 2013), *ePet6Cre* (Jackson Labs Stock 012712), *Pmch6Cre* (Knight et al., 2012; Jego et al., 2013), *Slc6a36IRES6 Cre* (-AT-IRES-Cre, Backman et al., 2006), *Slc6a46Cre* (SERT-Cre, MMRRC Stock 031028-UC-), *Ntsr16Cre*, *GRP6IRES6Cre* (Krashes et al., 2014).

2.1.2 Conditional knockouts. *Tph2 lox/lox* (Wu et al., 2012), *Slc17a8 lox/lox* (provided by Robert Edwards, unpublished), *Tfam lox/lox* (Ekstrand et al., 2007).

2.1.3 Transgenics. *SYN6NBL10* (Ekstrand et al., 2014), *Ntsr16GFPL10* (provided by Eric Schmidt).

2.1.4 Reporters. *Ef1a6LSL6GFPL10R* (Stanley et al., 2013), *p116EGFP* (Oh et al., 2013).

2.1.5 WildMtype mice. *C57BL/6J* (Jackson Labs Stock 000664).

2.2 Viral vectors

Viral vectors were used throughout the numerous studies described within this thesis. These viruses can be classified by their utility: molecular profiling, circuit mapping, and optogenetic control.

2.2.1 Molecular profiling. AAV5-FLEX-GFPL10 (Nectow et al., submitted; produced at UNC Vector Core), AAV2-FLEX-GFPL10 (Nectow et al., submitted), AAV9-FLEX-GFPL10 (Nectow et al., submitted), AAV5-FLEX-NBL10 (Ekstrand et al., 2014**;** produced at UNC Vector Core), AAV5-IV-GFPL10 (Nectow et al., submitted; produced at UNC Vector Core), AAV5-IV-NBL10 (Nectow et al., unpublished; produced at UNC Vector Core), CAV-GFP (provided by Eric Kremer, Kremer et al., 2000).

2.2.2 Circuit mapping. AAV9-FLEX-GFP (from the Allen Brain Institute, produced by the Penn Vector Core), Rabies(ΔG)-GFP(EnvA) (provided by the Salk Vector Core, Wall et al., 2010), AAV8-FLEX-TC^B (provided by Brady Weissbourd/ Liqun Luo, Weissbourd et al., 2014), PRV-mCherry (Ekstrand et al., 2014).

2.2.3 Optogenetic control. AAV5-EF1a--IO-hChR2(H134R)-EYFP (activation), AAV5-EF1a--IO-EYFP (control), AAV5-EF1a--IO-Arch3.0-EYFP (inhibition). All AAVs used for optogenetic control were obtained from the UNC Vector Core (these viruses were all originally developed by Karl -eisseroth's group).

2.3 Generation of novel viral vectors

The plasmids pAAV-FLEX-GFPL10 and pAAV-FLEX-NBL10 were generated as previously reported (see Ekstrand et al., 2014; Nectow et al., submitted). Briefly, we PCR amplified GFPL10 or NBL10 adding 5' NheI and 3' AscI cut sites for subcloning

into pAAV-EF1a-DIO-hChR2(H134R)-mCherry-WPRE-HGHpA (Addgene plasmid #20297). GFPL10 or NBL10 was subcloned into the AAV vector in the reverse orientation using NheI and AscI cut sites, replacing ChR2-mCherry, and resulting in pAAV-FLEX-GFPL10 or pAAV-FLEX-NBL10. pAAV-IV-GFPL10 and pAAV-IV-NBL10 were generated by synthesizing a ~1-2 kb fragments with 3' lox sites between EGFP or 3x-FLAG-HA-Nanobody and Rpl10a coding sequence and 5' AscI and 3' EcoRI cut sites (Genewiz). The fragment was then subcloned into the ChR2-mCherry vector with AscI and EcoRI cut sites, replacing ChR2-mCherry and the 3' lox sites. All plasmids were then sent to the University of North Carolina Vector Core for AAV packaging with serotype 5, as described above.

2.4 Tissue culture

For Retro-TRAP studies, Hepa 1-6 cells were mock infected or infected with CAV-GFP at 1000 particles/cell for 2 hrs in DMEM+2% FBS. After 2 hrs, the inoculum was removed and replaced with DMEM+10% FBS. After 48 hrs, the cells were lysed in 250 µl 0.15 M KCl buffer with RNase inhibitors and protease inhibitors. Input RNA was prepared and GFP IPs were performed as with the brain lysates. For vTRAP studies, HEK293T cells were transfected with pAAV-IV-GFPL10 and either pCMV-Cre or vehicle. After sufficient expression of GFPL10 (2-3 d), cells were lysed and both DNA and RNA were collected. PCR was used to assess presence of GFPL10 DNA, and Taqman qPCR was used to quantitate both DNA and RNA abundance in the presence or absence of Cre recombinase.

2.5 Stereotaxic surgeries

Mice age 6-20 weeks were induced and maintained on isofluorane anesthesia before stereotaxic injection of fiber optic placement (see below for details on viral injections, locations, and fiber placement). After injections, the needle was left in place for 5-10 min before slowly retracting. The skin was either closed with a surgical clip (after injection) or suturing (after fiber optic implantation). Dorsal raphe ML and AP coordinates are relative to lambda. All other ML and AP coordinates are relative to bregma. DV coordinates are all relative to the pial surface.

2.5.1 Retro-TRAP studies. For initial Retro-TRAP studies (Ekstrand et al., 2014), SYN-NBL10 transgenic, p11-EGFP, or wild type mice were injected bilaterally in the nucleus accumbens shell (NAc, coordinates: ±1.0 mm ML, +1.35 mm AP, -4.2 mm DV). SYN-NBL10 and WT mice were injected with CAV-GFP. p11-EGFP mice were injected with PRV-mCherry. DAT-IRES-Cre mice were injected bilaterally in both the NAc with CAV-GFP, as well as the VTA with AAV-FLEX-NBL10 (coordinates: ±0.5 mm ML, -3.15 mm AP, -4.2 mm DV).

2.5.2 Cell-type-specific Retro-TRAP studies. For mesolimbic dopamine neuron profiling, DAT-IRES-Cre mice were injected bilaterally in both the NAc (±1.44 mm ML, +1.35 mm AP, -4.25 mm DV:6°) with CAV-GFP and VTA (±1.02 mm ML, -3.15 mm AP, -4.23 mm DV:7°) with AAV-IV-GFPL10. For nigrostriatal dopamine neuron profiling, DAT-IRES-Cre mice were injected bilaterally in both the CPu (±1.76 mm ML, +0.5 mm AP, -2.5 mm DV:6°) with CAV-GFP and SNc (±1.52 mm ML, -2.8 mm AP, -4.23 mm DV:7°) with AAV-IV-GFPL10.

2.5.3 Molecular profiling of dorsal raphe cell types. VGluT3-IRES-Cre, Vgat-IRES-Cre, or ePet-Cre mice were injected into the DRN with 1.0 µl AAV-IV-GFPL10 (0 mm ML, 0 mm AP, -2.8 mm DV). The skin was then closed with a surgical clip, and mice were allowed to recover for at least three weeks prior to performing GFP immunoprecipitations.

2.5.4 Molecular profiling using viral TRAP (vTRAP). Injections of 1.0 µl AAV5-FLEX-GFPL10 were made in the lateral hypothalamus (LH, ±1.56 mm ML, -1.5 mm AP, 4.75 mm DV:8°) of Pmch-Cre mice, ventral tegmental area (VTA, ±0.5 mm ML, -3.15 mm AP, -4.2 mm DV) of DAT-IRES-Cre mice, and the dorsal raphe nucleus (DRN, 0 mm ML, 0 mm AP, -2.8 mm DV) of SERT-Cre mice.

2.5.5 Optogenetic implantation for behavior and electrophysiology. ePet-Cre, VGluT3-IRES-Cre, or Vgat-IRES-Cre mice were injected with 1.0 µl AAV5-Ef1a-DIO-ChR2(H134R)-EYFP or AAV5-Ef1a-DIO-eArch3.0-EYFP in the DRN (coordinates, relative to lambda: +0.8 mm ML, 0 mm AP, -3.0 mm DV:15°) followed by implantation of a fiber optic ferrule (Thor Labs) above the DRN (coordinates, relative to lambda: +0.8 mm ML, 0 mm AP, -2.4 mm DV:15°). The skin was then closed by suturing around the implanted fiber optic/ferrule. Mice were allowed at least 2.5 weeks to recover from surgery before performing behavioral studies.

2.5.6 Drug infusion studies. Mice were anesthetized with ketamine (100 mg/kg/10 ml) and xylazine (10 mg/kg/10 ml) in sterile saline. For gastrin-releasing peptide (GRP, R&D systems) infusions, bilateral guide cannulae (26-gauge, 5 mm length) were implanted above the NAc (±0.75 mm ML, +1.5 mm AP,–3.9 mm DV). Mice were given 1 wk to recover prior to conditioned place preference (CPP)

experiments. GRP (0.125, 0.25, or 0.50 µg/0.5 µl/side) or vehicle (PBS) was delivered through an injector needle at a rate of 0.1 µl/min. After the 5 min infusion, injector needles remained in place for 5 min to prevent backflow of the injection until each CPP training session started.

2.6 Polysome purification

Streptavidin MyOne T1 Dynabeads (300 µl per IP, Invitrogen) were washed twice on a magnetic rack with PBS and loaded with biotinylated Protein L (120 µg, Thermo Scientific) for 35 min at room temperature. The Protein L loaded beads were blocked by five washes in PBS with 3% IgG-free and protease-free BSA (Jackson ImmunoResearch). After the final block was removed, beads were resuspended in Buffer A (10 mM HEPES [pH 7.4], 150 mM KCl, 5 mM $MgCl_2$, 1% NP40) and loaded with 2x50 µg monoclonal GFP antibodies (clones 19C8 and 19F7; Doyle et al., 2008) at room temperature. Mice were sacrificed by cervical dislocation and a ventral piece including the hypothalamus and midbrain was rapidly dissected in ice-cold Buffer B (1xHBSS, 4 mM $NaHCO_3$, 2.5 mM HEPES [pH 7.4], 35 mM Glucose) with 100 mg/ml cycloheximide (Sigma). The dissected pieces were pooled in 3 groups of 6 brains each and transferred to a glass homogenizer (Kimble Kontes 20), and homogenized in 1.5 ml ice-cold Buffer C (10 mM HEPES [pH 7.4], 150 mM KCl, 5 mM $MgCl_2$) with 0.5 mM DTT (Sigma), 80 U/ml RNasin Plus (Promega), 40U/ml Superase-In (Life Technologies), 100 mg/ml cycloheximide, protease inhibitor cocktail (Roche) and 100 ng/ml GFP-Trap Protein (ChromoTek). Tissue samples were homogenized three times at 250 rpm and ten times at 750 rpm on a variable-

speed homogenizer (Glas-Col) at 4°C. Homogenates were transferred to microcentrifuge tubes and clarified at 2,000xg for 10 min at 4°C. 140 µl each of 10% IGEPAL CA-630 (NP-40; Sigma) and 1,2-diheptanoyl-sn-glycero-3-phospho-choline (DHPC at 100 mg/0.69 ml; Avanti Polar Lipids) was added to the supernatant. The solutions were mixed and centrifuged again at 17,000xg for 15 min at 4°C. The resulting supernatants were transferred to new tubes and 50 µl of each cleared lysate was mixed with 50 µl Lysis Buffer (0.7 µl β-mercaptoethanol/100 µl Lysis Buffer; Agilent Absolutely RNA Nanoprep Kit) and stored at -80° for later preparation as input RNA. The remaining lysates (approximately 1.5 ml) were used for immunoprecipitation. The beads incubating with GFP antibodies were washed twice in Buffer A with 0.5 mM DTT, 80 U/ml RNasin Plus and 100 mg/ml cycloheximide before the cleared brain lysates were added. The immunoprecipitation was allowed to run at 4°C for 40 min. Beads were washed four times with Buffer D (10 mM HEPES [pH 7.4], 350 mM KCl, 5 mM $MgCl_2$, 1% NP40) with 0.5 mM DTT, 80 U/ml RNasin Plus and 100 mg/ml cycloheximide. Before removing the last wash solution the beads were moved to a new tube. After the final wash, RNA was eluted by adding 100 µl Lysis Buffer and purified using the Absolutely RNA Nanoprep Kit (Agilent). For qPCR analysis cDNA was prepared with the QuantiTect Reverse Transcription Kit (Qiagen). For RNA-seq cDNA libraries were prepared with the SMARTer Ultralow Input RNA for Illumina Sequencing Kit (Clontech). For FLAG IPs (in the case of AAV-IV-NBL10 for cell-type-specific Retro-TRAP), Protein G Dynabeads (300 µl per IP, Life Technologies) were washed 2 times in 1 ml 0.15 M KCl buffer. The beads were then resuspended in 930 µl 0.15 M KCl

buffer, 10 µl 10% BSA, and 60 µl FLAG antibody (Sigma) and placed on a rotating rack overnight at 4°C. On the day of IPs (the next morning) these beads were then resuspended in the supernatant from the GFP IPs and allowed to incubate on a rotating rack for 1 hr at 4°C. FLAG IP beads were treated exactly as GFP IP beads after the immunoprecipitations.

2.7 High-throughput RNA sequencing (RNA-seq)

Sequencing was performed on an Illumina HiSeq 2500 sequencer using 100 bp single-reads. Samples were sequenced in triplicate (3 biological replicates per group). Tophat2 (v2.0.3) was used to align the reads using the Bowtie1 (v0.12.7) option. Segment size was 25 bp, allowing for 2 mismatches. Anchor size for splices was set to 10 bp allowing for 0 mismatches. Cufflinks (v2.1.1) was used for transcript abundance estimation and differential expression testing. The gene annotation was from Ensembl NCBIM37 (mm9 build).

2.8 Immunohistochemistry (IHC)

Mice were transcardially perfused with PBS, followed by 4% PFA. Brains were then postfixed for 12-24 hrs at 4°C. Fixed brains were vibratome (Leica) sectioned to a thickness of 50 µm. Primary antibodies used were: rabbit anti-HA (1:1000, Cell Signaling), mouse anti-NeuN (1:1000, EMD Millipore), chicken anti-GFP (1:1000, Abcam), rabbit anti-TH (1:1000, Pel-Freeze), chicken anti-TH (1:1,000, Aves Labs), rabbit anti-MCH (1:1000, Phoenix Pharmaceuticals), rabbit anti-Hypocretin (1:1000, Phoenix Pharmaceuticals), rabbit anti-Tph2 (1:500, Novus Biologicals). Secondary

antibodies were Alexa Fluor-conjugated (Invitrogen). All images were captured on a Zeiss LSM780 confocal microscope.

2.9 Fluorescence in situ hybridization (FISH)

FISH probe sequences were PCR amplified using the primers specified for each gene in the Allen Brain Atlas and subsequently cloned into a pCRII dual promoter plasmid (Invitrogen). The orientation of the cloned probe sequence in relation to the SP6 and T7 promoters of pCRII was determined by sequencing. The linear DNA fragment necessary for *in vitro* transcription was produced by PCR amplification using M13 primers. Antisense digoxigenin-labeled probes were generated by *in vitro* transcription using SP6 or T7 RNA polymerase (Roche) and M13 PCR product template. RNA probes were purified using the Absolutely RNA Nanoprep Kit (Agilent) and yield was quantified on a Nanodrop (usually 100-400 ng/µl). Mice were transcardially perfused with 10 ml PBS followed by 50 ml ice-cold 4% PFA. Brains were dissected, postfixed in 4% PFA for 24 hrs and equilibrated in 30% sucrose for 24-48 hrs. Brains were frozen and 30 µm sections were collected in cold PBS. To quench endogenous peroxidase activity, brain sections were incubated in 3% H_2O_2 for 1 hr. Sections were rinsed 3x5 min in PBS and acetylated for 30 min (9.83 ml H20; 134 µl triethanolamine; 13 µl HCl; 19 µl acetic anhydride). After acetylation the sections were permeabilized in PBS + 0.1% Triton X-100 for 1 hr and washed 3x5 min in PBS. Prehybridization in hybridization buffer (50% formamide; 5xSSC; 5xDenhardts; 250µg/ml Baker's yeast tRNA; and 500 µg/ml sheared salmon DNA) was performed for 1 hr at 37°C. Approximately 500 ng DIG-labeled antisense

probe was added to the hybridization buffer and the sections were incubated shaking slowly at 65°C overnight. On day 2, sections were washed 3 times at 55°C (5 min in 5xSSC and 2x15 min in 0.2xSSC) followed by a 5 min wash in 0.2xSSC at room temperature. The sections were then incubated for 5 min in Buffer 1 (B1; 0.1M Tris pH 7.5; 0.15M NaCl) and blocked for 1 hr in TNB (B1 + 0.5% blocking reagent; Roche). The blocked sections were incubated with primary antibodies diluted in TNB: anti-digoxigenin-PO- Fab fragments (1:100; Roche); chicken anti-GFP (1:500; Abcam) and rabbit anti-TH (1:500; Pel-Freeze), and incubated overnight at 4°C. On day 3, sections were washed 3x5 min in TNT (B1 + 0.05% Tween), incubated with Alexa Fluor conjugated secondary antibodies against chicken and rabbit IgG (1:500 in TNB; Invitrogen) and washed again 3x5 min in TNT. The FISH signal was then developed for 10 min using the TSA Plus Cy3 Fluorescence System (Perkin Elmer) and the sections were washed 3x5 min in TNT.

2.10 Optogenetic stimulation

For all behavioral assays using optogenetic activation, mice received blue light laser stimulation (473 nm, OEM Lasers/OptoEngine) of 10-15 mW with a 10-ms pulse width (see text for frequency: either 10 or 20 Hz pulse trains). Stimulation paradigms were programmed into an arbitrary waveform generator (Agilent Technologies, no. 33220A).

2.11 Behavioral studies

Studies were performed to assess reward/valence (real-time place preference, conditioned place preference), locomotion (open field test), and feeding (food intake assay). Prior to behavioral assays, mice were handled for four days for approximately 5 min. On the fourth and final day of handling, the mice were tethered to the fiber optic cable and allowed to freely roam their home cage for approximately 5 minutes.

2.11.1 Real-time place preference (RTPP). RTPP was assessed using an online stimulation protocol programmed using EthoVision XT 9 (Noldus). A custom, two-compartment black plastic chamber (50 cm x 50 cm x 25 cm) with a ~8 cm opening for the mouse to move freely between compartments was used. RTPP was run for 20 min. When the mice enter the stimulation-paired chamber, continuous stimulation is delivered to the animal (frequency is defined in the text). The difference score (DS) was calculated as time spent in the stimulation-paired chamber minus time spent in the non-stimulation-paired chamber.

2.11.2 Conditioned place preference (CPP). An unbiased CPP paradigm was used as previously described (Koo et al., 2012; Lobo et al., 2010). Mice were evaluated for GRP or GRP/cocaine CPP in a 3-chamber CPP box using Med Associates software. The box consisted of a smaller middle chamber (12 cm width × 15 cm length × 33 cm height) and two conditioning larger chambers (24.5 cm width × 15 cm length × 33 cm height) with different contextual clues including a gray verses stripe chamber, different floor mesh, and different lighting. On day 1, mice were placed in the CPP box for 20 min to ensure no chamber bias. One week later, mice were conditioned to one chamber for 30 min in the morning (saline) and to the opposite

chamber in the afternoon (0.125 or 0.50 μg/side GRP; 5 or 10 mg/kg cocaine, ip) over two days. The GRP and cocaine dose was chosen based on a dose-response analysis of GRP CPP in the current study and of cocaine CPP in a previous study (Koo et al., 2012). On day 4, the CPP test day, mice were allowed to freely explore all three chambers for 20 min. CPP scores represent time spent in the paired – time spent in the unpaired chamber.

2.11.3 Open field test (OFT). Locomotor function was assayed over a 15 min period for optogenetic manipulations and a 20 min period for genetic lesion studies. For optogenetic OFT, mice were placed in the open field and locomotor function was measured over three 5-min epochs (Laser Off, Laser On, Laser Off) using EthoVision XT 9. During the Laser On epoch, mice received constant optogenetic stimulation (frequency is defined in the text).

2.11.4 Food intake assay. The food intake assay was performed in the home cage. A weigh boat containing standard mouse chow was placed in the corner of the home cage, and food intake was measured over three 20-min epochs (Laser Off, Laser On, Laser Off), respectively. During the Laser On epoch, mice received constant optogenetic stimulation (frequency is defined in the text). For 5-HT and VGluT3 neuron stimulation studies, mice were food deprived through their entire previous dark cycle. For GABA neuron stimulation studies, mice were given *ad libitum* access to food.

2.12 Slice electrophysiology

Mice were perfused with cold artificial cerebrospinal fluid (aCSF) composed of (in mM): 128 NaCl, 3 KCl, 1.25 NaH_2PO_4, 10 D-glucose, 24 $NaHCO_3$, 2 $CaCl_2$, and 2 $MgCl_2$ (oxygenated with 95% O_2 and 5% CO_2, pH 7.35, 295–305 mOsm). Acute brain slices containing the dorsal raphe or ventral tegmental area were cut using a microslicer (DTK-1000, Ted Pella) in 95% O_2 and 5% CO_2 saturated sucrose-aCSF, which was derived by fully replacing NaCl with 254 mM sucrose. Slices were maintained in the holding chamber containing aCSF for 1 h at 37°C. Slices were transferred into a recording chamber fitted with a constant flow rate of aCSF equilibrated with 95/5% O_2/CO_2 (2.5 ml/min) maintained at 35 °C. Glass recording pipettes were filled with an internal solution composed of (in mM): 115 potassium gluconate, 20 KCl, 1.5 $MgCl_2$, 10 phosphocreatine, 10 HEPES, 2 magnesium ATP, and 0.5 GTP (pH 7.2, 285 mOsm). Neurons were identified by their location fluorescence. Whole-cell or cell-attached recordings were performed to record neuronal firing activity (Multiclamp 700B; Molecular Devices). Optical fibers (Thor Labs, BFL37-200) were connected using an FC/PC adaptor to a 473-nm blue laser diode (Crystal Laser, BCL-473-050-M), and a stimulator (Agilent Technologies, no. 33220A) was used to generate light pulses. Data acquisition was collected using a Digidata 1440A digitizer and pClamp 10.2 (Axon Instruments). For electrophysiological validation of cell body or terminal ChR2 activation we tested stimulation protocols at 0, 10, 20, 30 and 40 Hz.

2.13 Data analysis and statistics

Data analysis and statistics were performed using a number of modalities: Matlab, R, Microsoft Excel, Graphpad Prism, and Noldus EthoVision XT 9. RNA-seq data was processed offline in Matlab R, and Excel. Comparative analysis was performed between mesolimbic and nigrostriatal dopamine neurons using *post hoc* 2-way ANOVA to evaluate expression level differences in the immunoprecipitations. Taqman analyses were performed using Excel and Prism. All Taqman values obtained were normalized to ribosomal protein Rpl23. Fold-enrichments were obtained by dividing the IP RNA value for each gene by the Input/Total RNA value (IP/Input). All behavioral data were analyzed using Excel, Prism, and EthoVision XT 9. Animal tracking was implemented through EthoVision, while offline analyses were performed to quantitate behavioral data. To assess the effect of behavior as a function of stimulation epoch (for feeding and locomotion), a 2-way ANOVA was used. To assess the effect of stimulation on valence (in the RTPP assay), an unpaired Student's t-test was performed to compare the two treatments (Control vs. Cre+:ChR2).

CHAPTER 3: DORSAL RAPHE CONTROL OF INNATE BEHAVIORS

3.1 DRN(5-HT) neurons do not acutely affect survival-related function

The dorsal raphe nucleus (DRN) has been implicated in a number of survival-related behaviors (Heisler et al., 2006; Warden et al., 2012). To directly assess the contribution of serotonin (5-HT) to the functional output of the dorsal raphe, we asked whether acute manipulation of DRN 5-HT neurons could influence survival-related function. To acutely manipulate serotonin neuron activity, we selectively transduced DRN 5-HT neurons with a Cre-dependent AAV expressing a Channelrhodopsin-2/enhanced yellow fluorescent protein fusion (AAV-DIO-ChR2-EYFP) in ePet-Cre transgenic mice (Figure 3.1A), which selectively express the enzyme Cre recombinase in raphe serotonin neurons (Scott et al., 2005). *In vitro* recordings demonstrated that DRN(5-HT) neurons can follow 10 Hz spike trains with high fidelity (Figure 3.1B). We first assessed the effect of optogenetic stimulation on general locomotor function, as previous reports have suggested that the raphe may play a role in arousal and locomotion-related behaviors (Jacobs and Fornal, 1993; Waterhouse et al., 2004). Using an open field test (OFT), we found no observable effect on mouse velocity (Figure 3.1C). Previous work has also suggested that serotonin plays a critical role in food intake (Heisler et al., 2006). Surprisingly, when we acutely manipulated DRN(5-HT) neurons, we found no overall acute effect on food intake (Figure 3.1D). This does not, however, preclude the likely possibility that DRN(5-HT) neurons are controlling food intake over longer time scales (Heisler et al., 2006).

Another critical aspect of survival-related function is its connection to reward. A number of groups have suggested various roles for DRN(5-HT) neurons in controlling reward-related behaviors (Liu et al., 2014). We set out to test whether or not acute stimulation of these neurons was rewarding. When we stimulated the mice in a real-time place preference paradigm (RTPP), we found the stimulation had no effect on the animal's preference for the stimulation-paired or unpaired chamber (Figure 3.1E). These data, together, suggest a limited role for dorsal raphe serotonin neurons in controlling acute behaviors, consistent with the idea that these neurons play more of a long-term modulatory role. A significant subset of DRN(5-HT) neurons have also been found to partially overlap with a population within the DRN expressing the glutamate transporter VGluT3 (*Slc17a8*), which is often co-opted for glutamate co-release (Fremeau et al., 2004; Nelson et al., 2014; Seal and Edwards, 2006). We thus set out to see if DRN(VGluT3) neurons could control any survival-related functions on a rapid timescale.

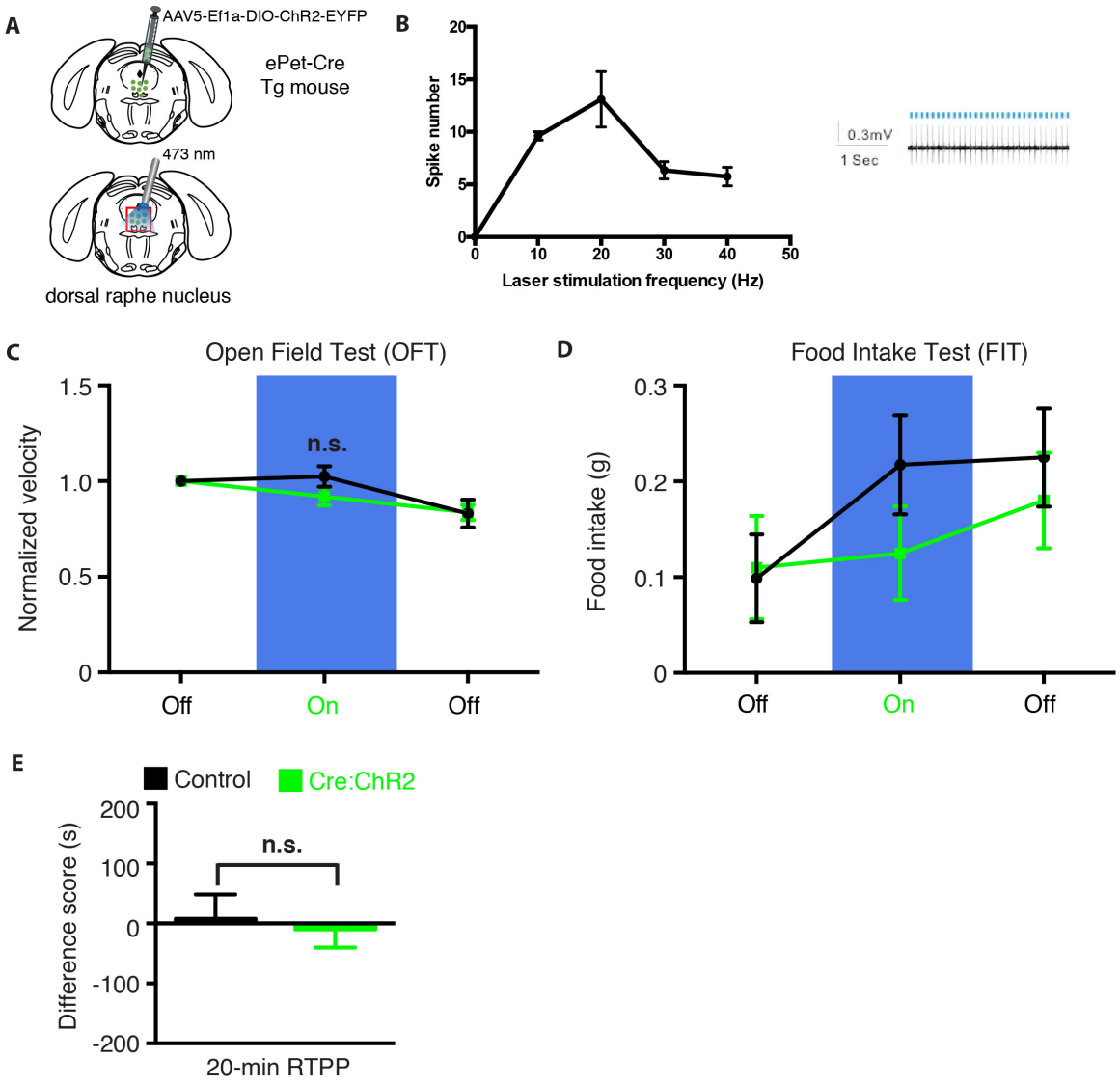

Figure 3.1. Dorsal Raphe Nucleus 5-HT Neurons Do Not Acutely Modify Survival-Related Behaviors. (A) AAV-EF1a-DIO-ChR2-EYFP is injected into the dorsal raphe nucleus of ePet-Cre transgenic mice and an optical fiber is placed above the DRN. (B) Frequency-dependent stimulus response (left) and sample cell-attached trace (right) of DRN(5-HT) neurons in response to optical stimulation. (C) DRN(5-HT) neurons do not acutely alter locomotion. (D) DRN(5-HT) neurons do not acutely effect feeding behavior after starvation. (E) Stimulation of DRN(5-HT) neurons is not rewarding. All data are displayed as mean ± SEM. n.s., not significant.

3.2 DRN(VGluT3) neurons acutely modulate survival-related behaviors

To first confirm the co-expression of serotonergic transcripts in DRN(VGluT3) neurons, we utilized a viral approach to translating ribosome affinity purification (vTRAP, Nectow et al., in preparation). Briefly, we cloned the GFP/large ribosomal subunit protein fusion construct into a Cre-dependent (FLEX'd) AAV vector, enabling rapid molecular profiling of *a priori* anatomically- and molecularly-defined populations of neurons. We then utilized this virus to investigate enrichment for the serotonin lineage-specific marker gene ePet (Scott et al., 2005), which is also the driver gene for serotonin-specific Cre-recombinase expression. When we assayed for expression of ePet mRNA in DRN(VGluT3) neurons, we found significant enrichment for the marker gene (Figure 3.2A). Importantly, when we performed profiling in DRN(Vgat) neurons, a population with limited to no overlap with DRN(5-HT) neurons, we found significant depletion of ePet transcript (Figure 3.2A; $p < 0.05$), demonstrating the sensitivity and specificity of vTRAP for these different dorsal raphe populations. Having demonstrated co-expression of ePet and VGluT3 transcripts, we set out to identify the behavioral role of DRN(VGluT3) neurons.

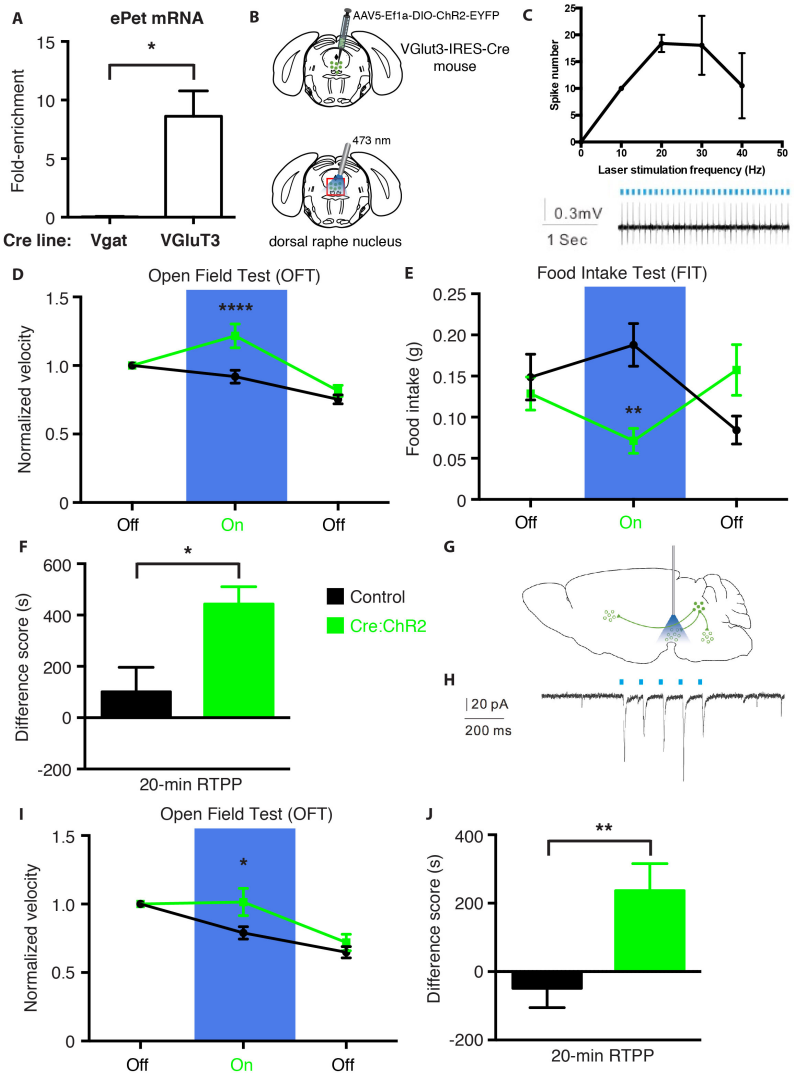

Figure 3.2. Dorsal Raphe Nucleus VGluT3 Neurons Partially Overlap with 5-HT Neurons and Acutely Modulate Survival-Related Behaviors. (A) Serotonin marker gene ePet is enriched in DRN(VGluT3) neurons but not DRN(Vgat) neurons. (B) AAV-EF1a-DIO-ChR2-EYFP is injected into the dorsal raphe nucleus of VGluT3-IRES-Cre knock-in mice and an optical fiber is placed above the DRN. (C) Frequency-dependent stimulus response (top) and sample cell-attached trace (bottom) of DRN(VGluT3) neurons in response to optical stimulation *in vitro*. (D) Stimulation of DRN(VGluT3) neurons induces locomotor activity. (E) DRN(VGluT3) neurons suppress food intake after starvation. (F) Stimulation of DRN(VGluT3) neurons is rewarding. (G) Schema for stimulation of DRN(VGluT3) neurons projecting to the ventral tegmental area. (H) Excitatory postsynaptic currents (ePSCs) evoked from electrophysiologically identified VTA dopamine neurons during stimulation of DRN(VGluT3) projections. (I) Increased locomotor activity after stimulation of the projections. (J) Stimulation of DRN(VGluT3) projections to VTA elicits reward-related behavior. All data are displayed as mean ± SEM. *p < 0.05, **p < 0.01, ****p < 0.0001.

As with DRN(5-HT) neurons, we injected the dorsal raphe with AAV-DIO-ChR2-EYFP, but in this case utilizing VGluT3-IRES-Cre knock-in mice (Figure 3.2B). These neurons were also able to follow 10 Hz spike trains with high fidelity (Figure 3.2C). However, when we tested DRN(VGluT3) neurons for their effect on locomotor function, we found that their stimulation significantly enhances locomotion (Figure 3.2D). Furthermore, stimulation of these neurons acutely suppresses food intake (Figure 3.2E). Previous work has also suggested that stimulation of non-serotonergic neurons in the DRN is rewarded (McDevitt et al., 2014). Consistent with these observations, we found that stimulation of DRN(VGluT3) neurons is appetitive (Figure 3.2F). Together, these data suggest a critical role for DRN(VGluT3) neurons in rapidly modifying survival-related functions. To identify a potential circuit mechanism for these effects, we turned our focus to the ventral tegmental area (VTA), which receives significant input from DRN non-5-HT neurons (McDevitt et al., 2014).

To test the behavioral effect of the DRN(VGluT3) → VTA projection, we injected Cre-dependent ChR2 in the DRN of VGluT3-IRES-Cre mice, followed by implantation of a fiber optic unilaterally over the VTA (Figure 3.2G). Stimulation of this projection was able to elicit spike trains and ePSCs in putative VTA dopamine neurons (Figure 3.2H). When we assayed for the effect of this projection on locomotion, we found a small but significant increase in locomotor function (Figure 3.2I). DRN(VGluT3) neurons are known to significantly collateralize (Gagnon and Parent, 2014), so it is possible that stimulation of this projection led to antidromic activation of a separate

motor-related structure (Jennings et al., 2013). Additionally, to confirm that this projection plays a critical role in modulating reward-related behaviors (Qi et al., 2014), we found that stimulation of this projection was able to elicit real-time place preference for the stimulation-paired chamber (Figure 3.2J; McDevitt et al., 2014; Qi et al., 2014). These data suggest a downstream mechanism through which DRN(VGluT3) neurons rapidly modify locomotor and reward-related behaviors.

3.3 DRN(GABA) neurons control certain aspects of survival functions

Within the DRN, there also exists a significant GABAergic population of neurons, which we hypothesized might functionally oppose the role of DRN(VGluT3) neurons. We first confirmed that these neurons are a molecularly-distinct population with the DRN by demonstrating depletion of *Vgat* mRNA from both DRN(5-HT) and DRN(VGluT3) neurons using vTRAP (Figure 3.3A). We then performed optogenetic activation studies on this population to further understand its role in controlling behavior.

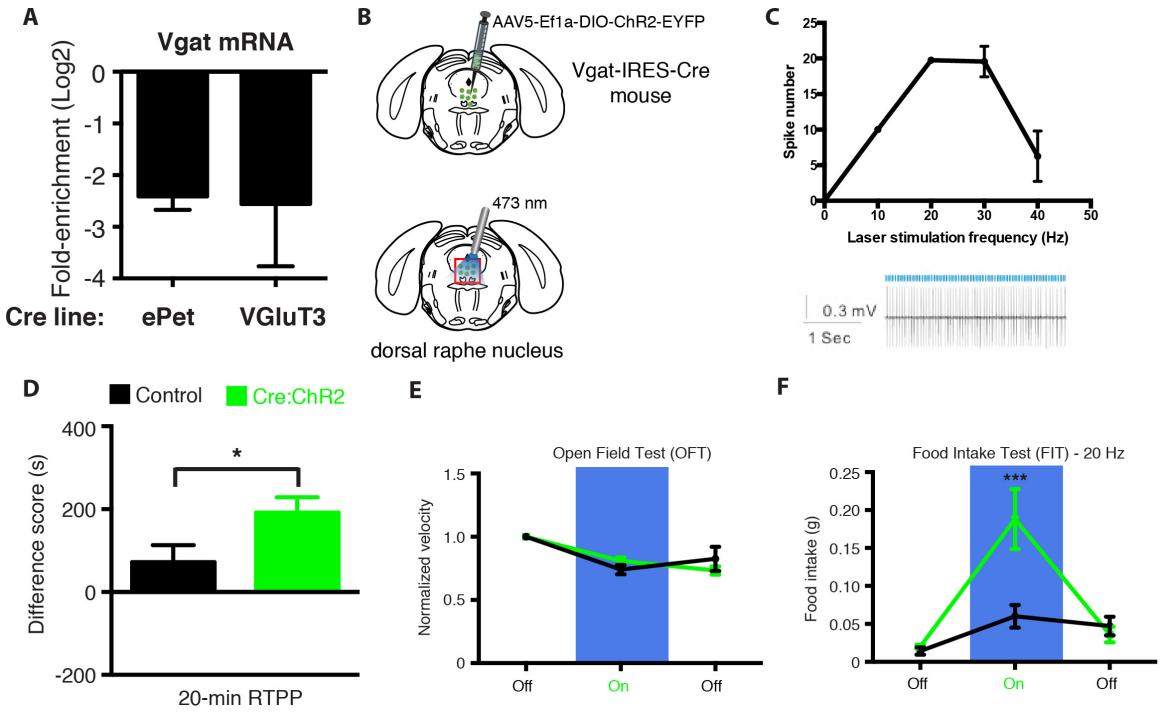

Figure 3.3. Dorsal Raphe Nucleus GABA Neurons Represent a Unique Population Within the DRN that Acutely Modulates Survival-Related Behaviors. (A) Vgat mRNA is depleted from both 5-HT and VGluT3 neural populations within the DRN, suggesting that it represents a unique population. (B) AAV-EF1a-DIO-ChR2-EYFP is injected into the dorsal raphe nucleus of Vgat-IRES-Cre knock-in mice and an optical fiber is placed above the DRN. (C) Frequency-dependent stimulus response (top) and sample cell-attached trace at 20 Hz (bottom) of DRN(Vgat) neurons in response to optical stimulation *in vitro*. (D) Stimulation of DRN(Vgat) neurons induces a real-time place preference. (E) DRN(Vgat) neurons do not alter locomotion. (F) Stimulation of DRN(Vgat) neurons elicits robust food intake when mice are fed *ab libitum*. All data are displayed as mean ± SEM. *$p < 0.05$, **$p < 0.01$.

We utilized Vgat-IRES-Cre mice to selectively express ChR2 within DRN(GABA) neurons (Figure 3.3B). Additionally, these neurons were able to robustly follow spike trains at 10 and 20 Hz (Figure 3.3C). We first confirmed that these neurons can influence reward-related behaviors through RTPP (McDevitt et al., 2014), finding that 10 Hz stimulation of these neurons is sufficient to elicit a rewarding effect, despite the high basal firing rate of these neurons (Figure 3.3D). We then investigated the role of these neurons in modifying locomotor function. Stimulation of these neurons at 10 Hz had no effect on locomotion (Figure 3.3E). Additionally, we found that higher frequency stimulation (20 Hz) had no effect on locomotor function (data not shown). We then set out to see if these neurons could modify feeding-related behaviors.

Previous work has suggested that the DRN/vlPAG receives inputs from the paraventricular hypothalamic nucleus (PVH) that can elicit robust food intake (Stachniak et al., 2014). In stimulating DRN(GABA) neurons at a lower frequency (10 Hz), we found no effect on food intake (data not shown); however, at a higher stimulation frequency of 20 Hz, we found that stimulation of DRN(GABA) neurons could robustly elicit food intake on a rapid timescale (20 minutes; Figure 3.3F). Taken together with previously published data on the PVH-DRN/vlPAG projection, this work suggests a potential GABA-GABA synapse in the DRN that rapidly controls food intake.

This work suggests a novel circuit-level and cell-type-specific mechanism through which different populations of dorsal raphe neurons can modify survival-related behaviors. Further work will focus on identifying the downstream targets of each of these cell types to determine how each population controls different aspects of behavior.

CHAPTER 4: RAPID MOLECULAR PROFILING WITH VIRUSES

4.1 Development of viruses capable of rapid molecular profiling

Molecular profiling in the brain is exceptionally difficult. Unlike many peripheral organs and organ systems, separating individual neurons from one another is laborious work that often results in low-quality sample output. An alternative solution to this problem was developed by directly accessing translating mRNAs from cell types expressing a principal marker gene. This technology, termed translating ribosome affinity purification (TRAP, Doyle et al., 2008; Heiman et al., 2008) enabled cell-type-specific access to neuronal ribosomes through driving cell-specific expression of EGFP N-terminally fused to large ribosomal subunit protein RPL10a (hereafter GFPL10, Heiman et al., 2008). The original implementation of this approach drove the cell-specific expression of GFPL10 utilizing BAC transgenesis (bacTRAP, Heiman et al., 2008). While effective, this technique is rather slow, requiring the generation of new BAC transgenic mouse lines for each new cell type to be profiled. We set out to simplify and expedite this approach using viral methodologies.

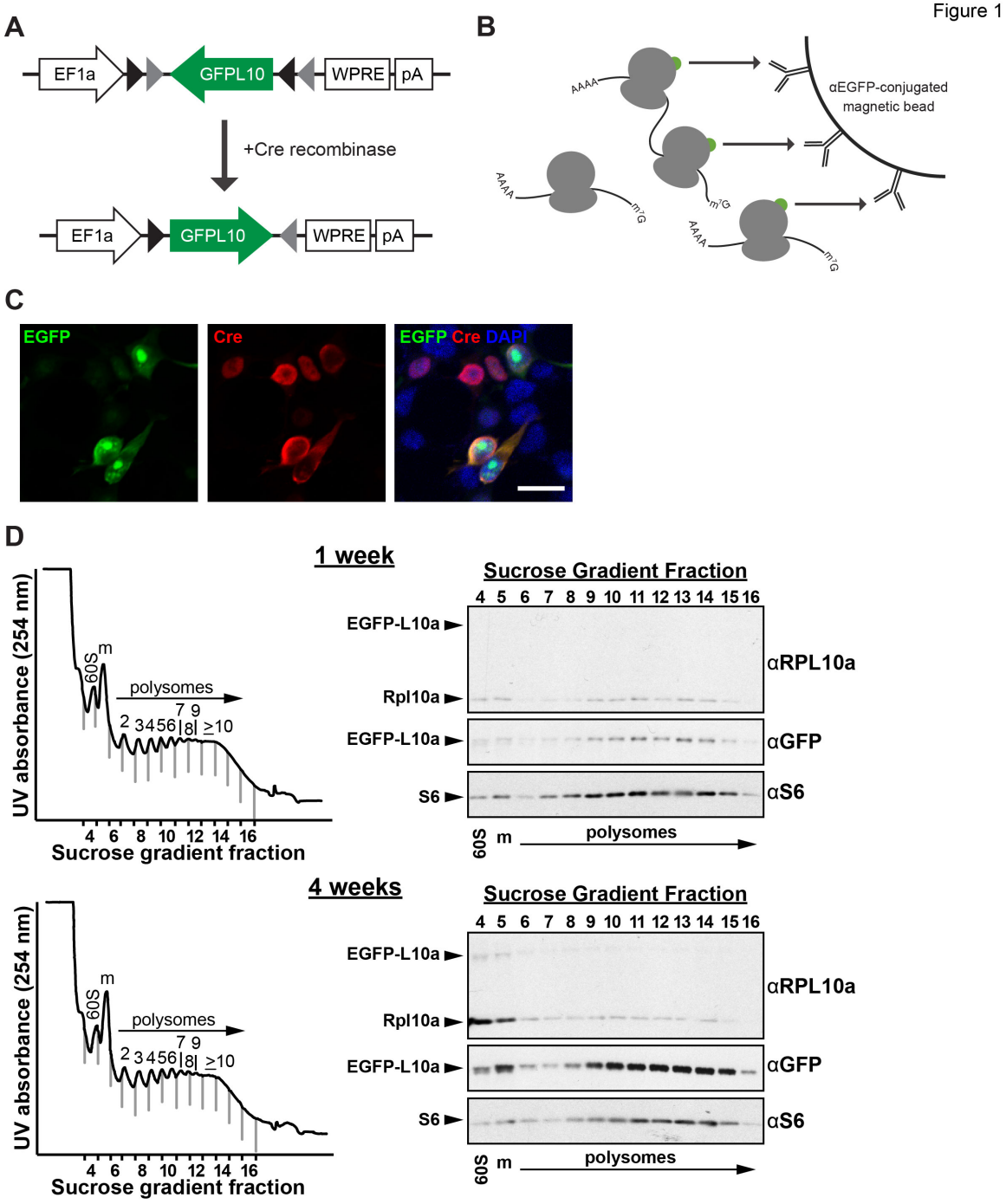

Figure 4.1. vTRAP Concept and Demonstration of Expression and Functional Integration of GFPL10. (A) AAV-FLEX-GFPL10 is activated solely when in the presence of the enzyme Cre recombinase. (B) Molecular schema of a GFP IP, which results in immunopurification of translating mRNAs from Cre-expressing neurons. (C) Tissue culture studies demonstrating nucleolar puncta in GFPL10-expressing cells. (D) Polysome fractionation, demonstrating integration of virally-expressed GFPL10 into neuronal ribosomes.

Given the broad availability of Cre-driver lines, FLEX'd AAVs (Atasoy et al., 2008) expressing a Cre-conditional GFPL10 construct would serve as an effective technique for profiling *a priori* genetically-defined cell populations. This approach also adds in the extra dimension of anatomic specificity, rendering the approach far more selective for given anatomic loci (through stereotaxic injection), as compared with traditional bacTRAP, which relies on crude manual dissection by hand. A schema for this approach is depicted in Figure 4.1A-B. We then performed *in vitro* tissue culture studies to demonstrate successful Cre-dependent expression of the GFPL10 construct. Co-transfection of the Cre-conditional pAAV-FLEX-GFPL10 plasmid with a plasmid expressing myc-tagged Cre recombinase demonstrated the Cre-dependent (and restricted) expression of GFPL10 (Figure 4.1C). Of note, cells that are DAPI-positive but do not contain Cre are also negative for GFPL10 expression. Additionally, cells expressing GFPL10 have notable nucleolar puncta, indicative of ribosomal integration (Figure 4.1C; Kriaucionis and Heintz, 2009).

To demonstrate successful integration of the GFPL10 fusion protein *in vivo*, we then injected Emx1-IRES-Cre transgenic mice with AAV-FLEX-GFPL10 in the cortex and took two time points, 1 and 4 weeks post-injection. Given the expression dynamics of AAVs, which often take 5-10 days to fully express (Kaspar et al., 2002), we expected a minimal degree of expression after 1 week, followed by a robust expression 4 weeks later. In line with this hypothesis, we observed a limited expression of GFPL10 after 1 week, as demonstrated with staining against both RPL10a, as well as GFP (Figure 4.1D). After 4 weeks, we observed persistent and

enhanced expression of the GFPL10 fusion with what appears to be significant displacement of the endogenous copies of RPL10a from the polysomal fractions (Figure 4.1D). Together, these data display a time-dependent dynamic of GFPL10 expression and subsequent integration into polysomes. We thus set out to perform simultaneous region- and cell-type-specific molecular profiling studies.

We accomplished this aim by first confirming restricted expression of AAV-FLEX-GFPL10 in a variety of different Cre-driver lines representing regions from throughout the brain, such as the cortex, thalamus, midbrain, and hypothalamus. Indeed, using cortex- and thalamus-specific Cre-driver lines, we were able to see expectedly sparse labeling within these regions (Figure 4.2A). Furthermore, in these lines (and as with the prior *in vitro* studies), we were able to observe nucleolar puncta (Figure 4.2B) suggesting successful integration of the virally-expressed construct into the host ribosomes. We then injected Cre-driver lines specific for dopaminergic neurons of the ventral tegmental area (DAT-IRES-Cre), serotonergic neurons of the dorsal raphe nucleus (SERT-Cre), and MCH neurons of the lateral hypothalamus (Pmch-Cre). We then performed IHC, confirming cell-type-specific expression of the GFPL10 fusion protein within each of these cell types (Figure 4.2C).

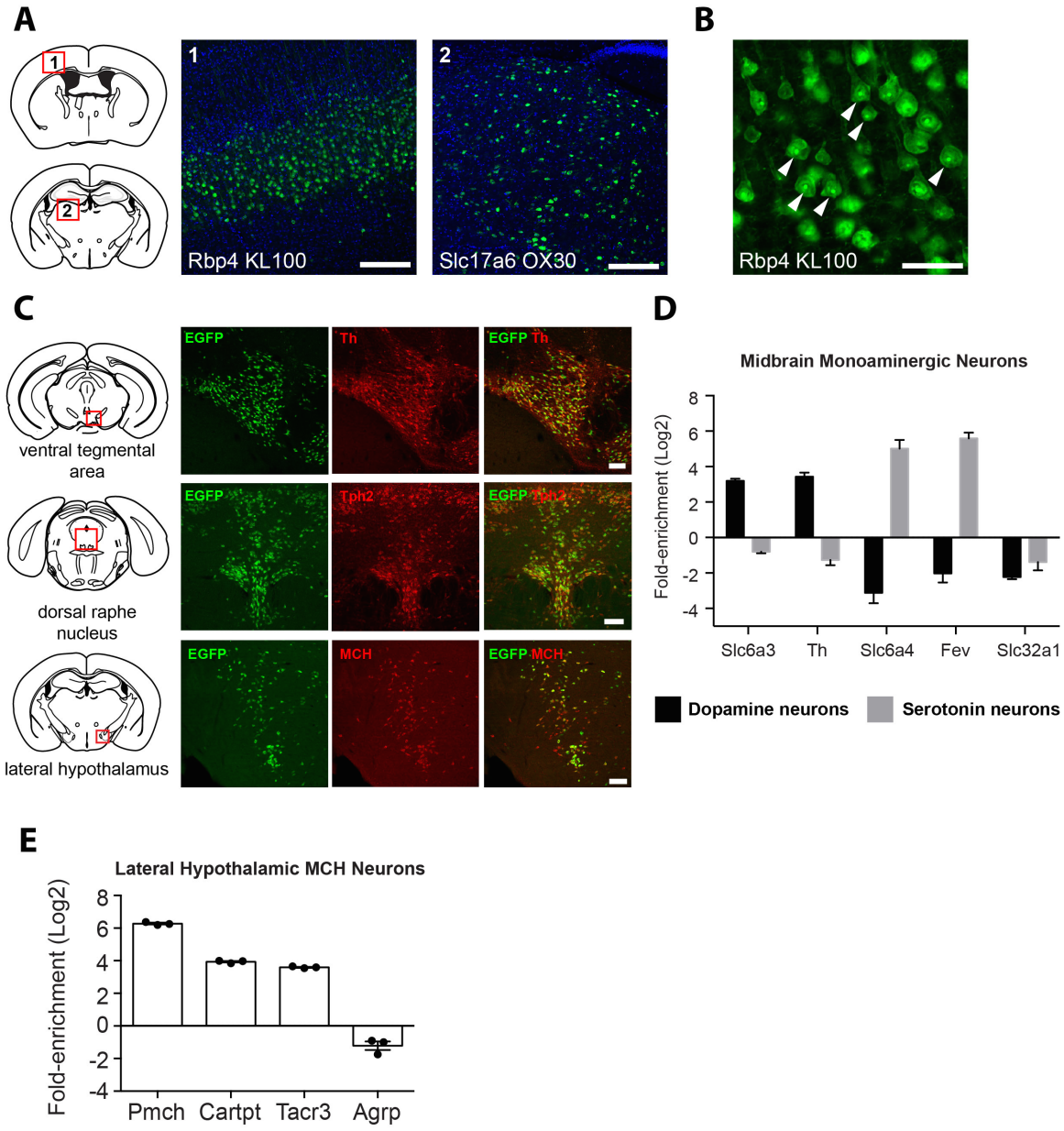

Figure 4.2. Testing of AAV-FLEX-GFPL10 in Multiple Cre-driver Lines. (A) Immunostaining of sparse GFPL10 staining in Cre-driver lines specific to cortex (1) and thalamus (2). (B) Apparent nucleolar puncta are observed in neurons expressing GFPL10, suggesting ribosomal integration of the fusion protein. (C) Expression of AAV-FLEX-GFPL10 in Cre-driver lines representative of the midbrain and hypothalamic populations: ventral tegmental area dopamine neurons (DAT-IRES-Cre), dorsal raphe nucleus serotonin neurons (SERT-Cre), and lateral hypothalamic MCH neurons (Pmch-Cre). (D) Enrichments for dopaminergic and serotonergic marker genes in the respective populations. (E) Enrichments for MCH neuron marker genes, with concomitant depletion of non-MCH neuron marker genes. Scale bars, 200 μm for low magnification of cortex and thalamus, 50 μm for high magnification of cortex, and 100 μm for images of VTA, DRN, and LH.

To molecularly profile each of these cell types, we performed immunoprecipitations (IPs) from the Cre-driver mice injected with AAV-FLEX-GFPL10, hypothesizing that three weeks post-infection was sufficient time to observe substantial enrichments. We first focused on two well-characterized populations of neurons, with a number of unique marker genes: ventral tegmental area (VTA) dopamine (DA) and dorsal raphe nucleus (DRN) serotonin (5-HT) neurons. After performing IPs from these two regions, we observed substantial RNA yields (average of > 9 ng total yield per IP, data not shown), suggesting successful incorporation of GFPL10 into the translating ribosome in each of these cell-types. We then assessed enrichment for control marker genes: positive control *Gfp* (from *Gfp-Rpl10a* mRNA), which should have expression restricted to only Cre-positive, AAV-infected neurons, and negative control glial genes *Gfap*, *Mal*, and *Mbp*. In both cases, we observed significant enrichment for *Gfp* (10-fold for VTA, 27.3-fold for DRN; $p < 0.01$), while depleting for all three tested glial genes (data not shown), demonstrating that the current method has a sufficient dynamic range to detect cell-type marker genes. We then compared cell type marker gene enrichment between VTA DA and DRN 5-HT neurons.

4.2 Molecular profiling of midbrain monoaminergic cell types

The ventral tegmental area plays an important role in reward processing (Schultz, 1998), as well as in mood disorders and addiction (Russo and Nestler, 2013), and the dorsal raphe has also been implicated in a variety of mood disorders, due to its association with the neurotransmitter serotonin. Indeed, the DRN has been implicated in the response to stressor controllability (Amat et al., 2005), as well as

behavioral challenge (Warden et al., 2012) and social defeat stress (Challis et al., 2013). Given the importance of these molecularly distinct cell types in governing a diverse array of behaviors, we set out to see if we could differentially enrich for transcripts that are specific to each of these neural populations. The following transcripts were chosen for comparative analysis: *Slc6a3* (DAT, the dopamine transporter) and *Th* (the rate-limiting enzyme in dopamine synthesis), *Slc6a4* (SERT, the serotonin transporter) and *Fev* (Pet-1, the serotonin lineage marker; Jensen et al., 2008), and *Slc32a1* (Vgat, the transporter for GABA), which is expressed at very low or negligible levels in either of the studied cell-types.

In comparing these two cell-types, we observed significant specificity for each of the markers tested between treatments (Treatment: $p < 0.05$, Interaction: $p < 0.0001$; Figure 4.2D). Dopaminergic marker genes *Slc6a4* (16.1-fold) and *Th* (25.6-fold) were significantly differentially enriched in dopaminergic neurons ($p < 0.0001$), while serotonergic marker genes *Slc6a4* (267.6-fold) and *Fev* (182.6-fold) were significantly differentially enriched in serotonergic neurons ($p < 0.0001$). Notably, there was no significant difference observed in *Vgat* enrichment. Additionally, a subset of serotonergic neurons within the DRN express the vesicular glutamate transporter 3, *Slc17a8* (VGluT3), which enables glutamate co-release in the principal cells (Johnson, 1994; Fremeau et al., 2002) and may play a role in modulating anxiety-related behaviors (Amilhon et al., 2010). Indeed, we observed significant enrichment for *Slc17a8* mRNA (10.4-fold, $p < 0.05$).

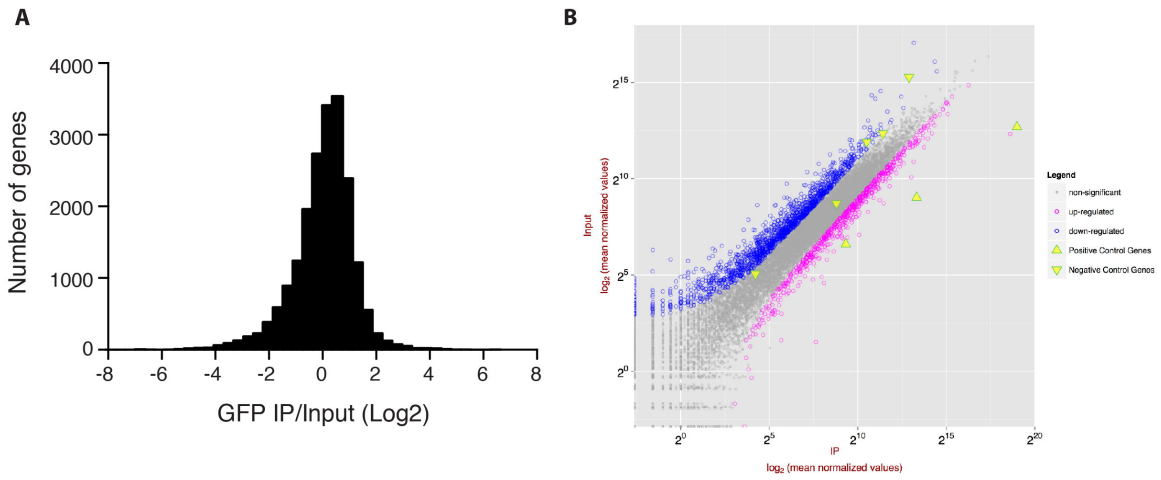

Figure 4.3. High-throughput RNA-sequencing for Molecular Profiling of Lateral Hypothalamic MCH Neurons. (A) Histogram displaying normal distribution of gene enrichments for MCH neurons. (B) Scatter plot displaying input versus IP.

4.3 Molecular profiling of lateral hypothalamic MCH neurons

We then set out to profile MCH neurons of the lateral hypothalamus. Melanin-concentrating hormone neurons comprise a significant population within the lateral hypothalamus (LH) and are causally implicated in feeding behaviors (Shimada et al., 1998). We selected MCH neurons for comprehensive molecular profiling, as they play a key role in numerous feeding- and sleep-related behaviors (Jego et al., 2013; Shimada et al., 1998), yet there is surprisingly little known about their molecular composition. Additionally, these neurons comprise a sparse population within the LH, which would test the sensitivity and specificity of the current viral approach to translational profiling. We profiled these neurons, finding significant enrichment for cell-type marker *Pmch* (77.7-fold, $p < 0.01$), as well as *Cartpt* (15.3-fold, $p < 0.01$) and *Tacr3* (12.1-fold, $p < 0.05$) (Figure 4.2E), two other genes which are co-expressed in MCH neurons (Croizier et al., 2010; Knight et al., 2012). Importantly, when we assessed enrichment of *Agrp*, a marker for the arcuate nucleus, we observed significant depletion (2.4-fold, $p < 0.05$). After enriching for known MCH cell-type marker genes, we then set out to profile these neurons in an unbiased, high-throughput fashion.

To profile LH MCH neurons, we performed high-throughput RNA sequencing (RNA-seq; Figure 4.3A). The data are also displayed as a scatter plot to represent the individual normalized mapped reads for both the Input and IP samples (Figure 4.3B). Notably, the most significantly enriched gene in the entire data set is *Pmch* (99-fold). Additionally, *Cartpt* (23.7-fold) and *Tacr3* (8.2-fold) are in the top 20 most

significantly enriched genes in the entire data set. The ability to maximally enrich for these control transcripts is essential, and this unbiased metric demonstrates the specificity of vTRAP. Furthermore, in recent work utilizing the Retro-TRAP methodology (Ekstrand et al., 2014), we identified a number of transcripts as enriched in projections from the midbrain and hypothalamus to the nucleus accumbens (NAc); however, for many of the marker genes, we did not attempt to colocalize gene expression, making us unsure of the anatomic localization or cell-type responsible for the observed enrichment.

In the current RNA-seq study, we've identified a number of novel marker genes that are putatively expressed in MCH neurons. By identifying transcripts that are enriched in both the current data set (MCH neurons) and that of midbrain/hypothalamic projections to NAc, we can begin to assign cell-type-specific information to connectivity data observed with Retro-TRAP. A number of transcripts are enriched in both data sets, such as *Ache* (6.2-fold), *Crhbp* (6.9-fold), *Dmrtb1* (12.2-fold), *Grin1* (5-fold, and *Mup6* (77.1-fold) (all genes $q < 0.05$ in both data sets, data not shown). Thus, this work has enabled us to cell-type-specifically assign the origin of transcript enrichment for a number of genes in neurons projecting to the nucleus accumbens, a major projection target of LH MCH neurons (Haemmerle et al., 2015). Taken together, these data suggest that we can utilize the intersection of Retro-TRAP and vTRAP studies to comprehensively profile neural circuitry in a projection- and cell-type-specific fashion.

The above studies utilizing vTRAP enabled molecular profiling of two principal monoaminergic neurons, as well as high-throughput analysis of a neuromodulatory neural population, MCH neurons of the lateral hypothalamus. In the latter case, in tandem with results previously published by our group (Ekstrand et al., 2014), we were able to identify transcripts specific to MCH neurons of the lateral hypothalamus, that also happen to project to the nucleus accumbens. While these studies were rather successful in cell-type-specific transcript enrichment, we asked whether we could extend the dynamic range of our enrichment profiles through the generation of a tighter Cre-dependent molecular switch.

4.4 Development of 'Invtroverted' GFPL10 virus

Though not commonly reported in the literature, FLEX constructs are known to exhibit a degree of leakiness independent of Cre recombinase (Miyamichi et al., 2013). Two mechanisms are likely to be responsible for this adventitious Cre-independent expression: a) aberrant recombination of lox sites during bacterial propagation of the AAV plasmid (A.R.N., unpublished data), and b) read-through in the antisense direction *in vivo* (due to either cryptic promoters in the 3' UTR or bidirectional activity of the EF1a promoter after episomal head-to-tail concatemerization). To eliminate the latter possibility, we implemented 'Introvert' technology, which was originally developed to eliminate leaky antisense transcription in pseudorabies viral vectors (M.I.E., unpublished data).

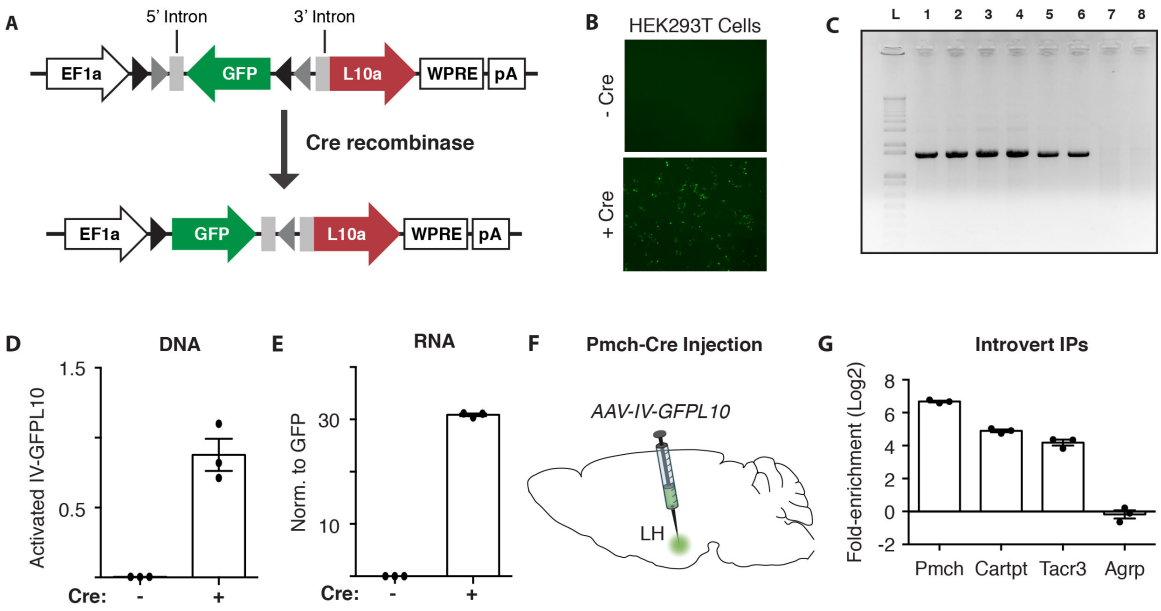

Figure 4.4. Development of 'Introvert' Constructs for Molecular Profiling. (A) Design of AAV-IV-GFPL10. In the presence of the enzyme Cre recombinase, IV-GFPL10 will be activated, and splicing will result in a contiguous GFPL10 fusion protein. (B) *In vitro* studies where HEK293T cells are cotransfected with pAAV-IV-GFPL10 and pCMV-Cre. Only cells in the Cre-positive cultures express GFPL10. (C) PCR of DNA made from transfected HEK293T cell lysate from (B). Activated form of GFPL10 (bottom panel of (A)) is detected only in the Cre-positive treatments. Rows 1-4: Inactive GFPL10 (Cre+: 1-2, Cre-: 3-4); Rows 5-8: Active GFPL10 (Cre+: 5-6, Cre-: 7-8). (D and E) qPCR for activated form of GFPL10 at the level of DNA ($p < 0.05$, D) and RNA ($p < 0.01$, E). (F) Schema for injection of AAV-IV-GFPL10 injected into the LH of Pmch-Cre transgenic mice. (G) Enrichments of hypothalamic marker genes *Pmch* ($p < 0.001$), *Cartpt* ($p < 0.01$), *Tacr3* ($p < 0.05$), and *Agrp* (n.s.) after IPs from the hypothalamus. qPCR data are normalized to Rpl23 expression. Data are presented as mean ± SEM.

Introvert technology is based on the FLEX construct, though when combined with intron sequences can enable the Cre-dependent expression of a fusion protein due to splicing (see also Fenno et al., 2014). We therefore decoupled expression of GFP from Rpl10a expression in the absence of Cre recombinase; only in the presence of Cre would GFP be able to be expressed as a fusion, epitope-tagging RPL10A (for schema, see Figure 4.4A). Briefly, this sequence was synthesized and subcloned into pAAV-FLEX-GFPL10 to generate pAAV-IV-GFPL10. When we tested this construct in HEK293T cells, GFP expression was observed selectively in the presence of Cre recombinase co-transfection (Figure 4.4B). Furthermore, when we assayed for 'inactivated' and 'activated' forms of Introverted GFPL10 DNA, we observed the inactivated variant in both treatments, while the activated variant was only detected in the Cre-containing treatment (Figure 4.4C). These observations were then confirmed with quantitative PCR, at the level of DNA (Figure 4.4D) and mRNA (Figure 4.4E). After observation of successful recombination and concomitant expression of GFPL10 protein, pAAV-IV-GFPL10 was packaged into an AAV, serotype 5.

To test the dynamic range of AAV-Introvert-GFPL10, we injected the virus into Pmch-Cre transgenic mice (Figure 4.4F) exactly as above, and assayed for enrichment of MCH neuron marker genes. As expected, all marker genes were significantly enriched: *Pmch* (102.5-fold, $p < 0.001$), *Cartpt* (29.9-fold, $p < 0.01$), and *Tacr3* (18.4-fold, $p < 0.05$) (Figure 4.4G). Importantly, in comparing overall expression trends between the data sets generated by 'FLEXed' and 'Introverted'

GFPL10, we found a significant difference between the two treatments (Treatment: $p < 0.01$, Interaction: $p < 0.01$, 2-way ANOVA), suggesting that Introverting the GFPL10 construct resulted in an increase in signal-to-noise (improved dynamic range).

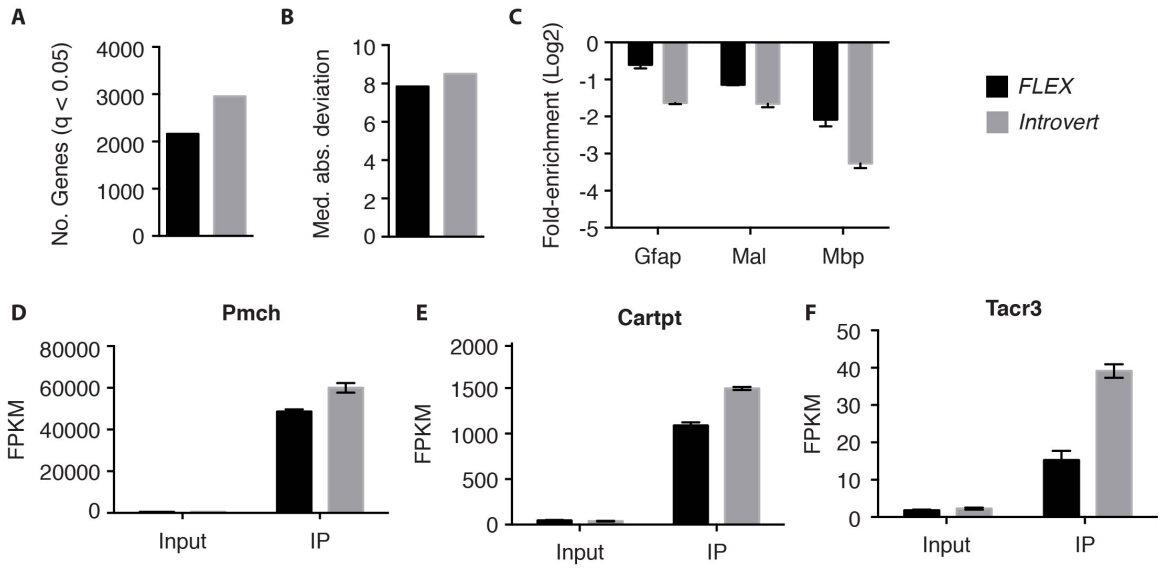

Figure 4.5. Comparison of AAV-FLEX-GFPL10 and AAV-IV-GFPL10. (A) Comparison of number of q-value significant genes for FLEX (2160 genes) versus Introvert (2954 genes) treatments. (B) Median absolute deviation (MAD) of FLEX and Introvert treatments. (C) Differential enrichments for glial marker genes *Gfap* ($p < 0.0001$), *Mal* ($p < 0.05$), and *Mbp* ($p < 0.0001$). Introverted GFPL10 results in overall greater depletion for negative control marker genes (Treatment: $p < 0.001$, Interaction: $p < 0.05$). (D to F) Introverted GFPL10 results in greater enrichment for MCH neuron marker genes *Pmch* ($p < 0.001$, D), *Cartpt* ($p < 0.0001$, E), and *Tacr3* ($p < 0.0001$). RNA-seq data are normalized as fragments per kilobase of transcript per million mapped reads (FPKM). Data are presented as mean ± SEM.

The data presented above suggest that Introvert represents a significant improvement over the currently utilized FLEX technology. To confirm these results in a high-throughput, unbiased fashion, we performed RNA-seq on the Introvert data set for a comparison between Introvert- and FLEX-based translational profiling. Upon sequencing, we assessed the total number of q-value significant genes detected (FLEX: 2160, Introvert: 2954; Figure 4.5A). We also used an unbiased metric for robust measures of scale, the median absolute deviation (MAD), which was also greater in the Introvert treatment (Figure 4.5B), suggesting that Introvert has a superior dynamic range to FLEX-based vTRAP.

To confirm the superior dynamic range of Introvert-based vTRAP, we then looked at negative control glial genes, as well as known MCH neuron marker genes from the RNA-seq data sets. Glial genes *Gfap* (1.5-fold versus 3.1-fold, $p < 0.0001$), *Mal* (2.2-fold versus 3.2-fold, $p < 0.05$), and *Mbp* (4.3-fold versus 9.7-fold, $p < 0.0001$) were all significantly more depleted in the Introvert treatments (Figure 4.5C). Additionally, all MCH neuron marker genes (*Pmch*, $p < 0.001$; *Cartpt*, $p < 0.0001$; *Tacr3*, $p < 0.0001$) were significantly more enriched using Introvert-based vTRAP (Figure 4.5D-F). Taken together, these data demonstrate that Introvert-based vTRAP improves dynamic range by both increasing enrichment of cell-type marker genes, while reducing enrichment (increasing depletion) for negative control marker genes. Thus, Introvert represents a step forward in reducing Cre-independent background generated by FLEX/DIO-based constructs.

CHAPTER 5: PROJECTION-SPECIFIC MOLECULAR PROFILING

5.1 Outline of the Retro-TRAP approach

Retro-TRAP (whether solely projection-specific or also simultaneously cell-type-specific) utilizes a two-component GFP-Nanobody system (discussed further below). An outline of the schema for successful Retro-TRAP studies including timing of injections and immunoprecipitations is displayed in Figure 5.1.

5.2 Generation of SYN-NBL10 transgenic mice

GFP is commonly used to visualize restricted subsets of neurons within the brain, but means for directly profiling these neurons are limited (Sugino et al., 2006). In order to profile neurons expressing GFP, we first set out to tag ribosomes with a camelid nanobody raised against GFP (Figure 5.2A). Previous work has demonstrated that it is possible to create N-terminal fusions of the large ribosomal subunit protein Rpl10a with small epitope tags such as GFP that do not interfere with ribosome function (Heiman et al., 2008). We thus generated a transgenic mouse that expresses an anti-GFP nanobody fused to the N terminus of ribosomal subunit protein Rpl10a (NBL10) under the control of the neuron-specific human synapsin promoter (hereafter SYN-NBL10). In addition, we engineered the NBL10 fusion protein with an HA tag, allowing us to visualize the sites of expression using immunohistochemistry (Figure 5.2B).

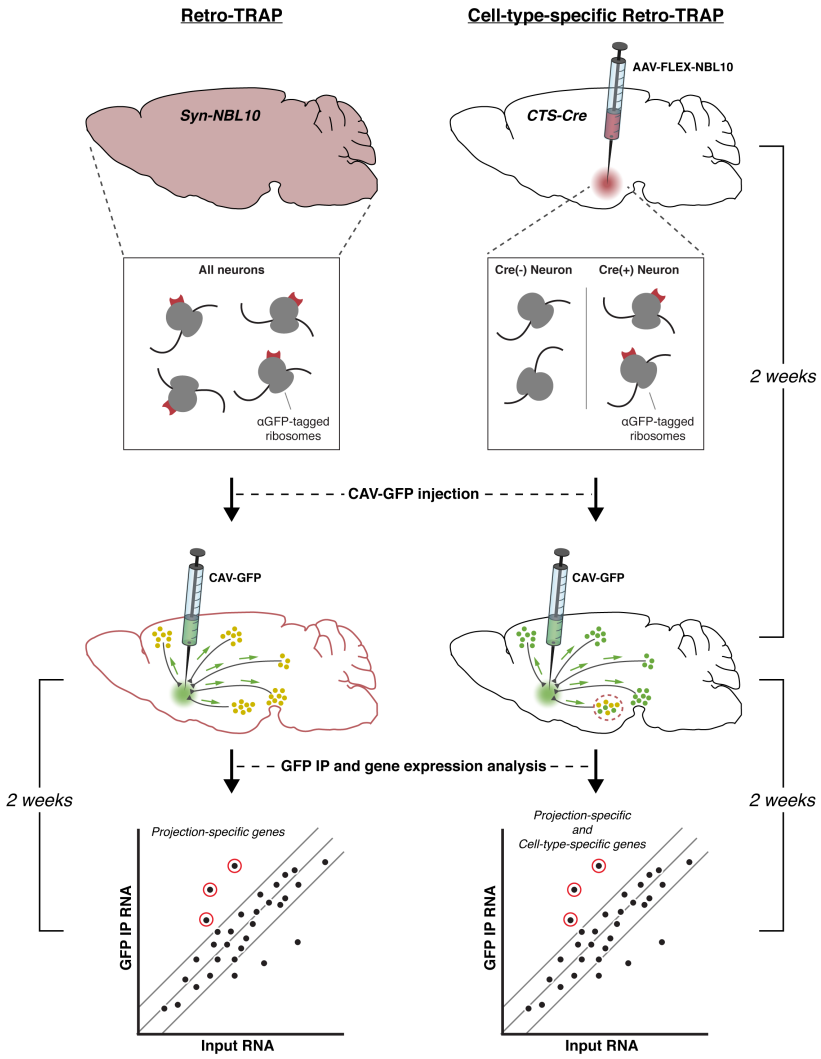

Figure 5.1. Retro-TRAP Strategy and Experimental Design. Experimental design for Retro-TRAP and cell-type-specific Retro-TRAP proceeds top to bottom, in parallel. Retro-TRAP uses SYN-NBL10 mice, whereas cell-type-specific Retro-TRAP uses cell-type-specific Cre-driver lines (CTS-Cre). **Top**: SYN-NBL10 mice have constitutive expression of the NBL10 construct in all neurons. Cell-type-specific Retro-TRAP requires the stereotaxic injection of AAV-FLEX-NBL10 into the desired region, followed by a 2-week incubation period allowing for expression and incorporation of the NBL10 fusion into ribosomes of Cre-positive neurons. **Middle**: CAV-GFP injection into a target retrogradely labels all neurons projecting to that region. In Retro-TRAP, all neurons labeled with GFP are accessible to GFP immunoprecipitation (GFP IP). In cell-type-specific Retro-TRAP, only the double-positive neurons (expressing both GFP and the NBL10 fusion) are accessible to a GFP IP. A 2-week incubation period enables stable expression of GFP. **Bottom**: After dissection of the desired brain region, GFP IP, and gene expression analysis, projection-specific (Retro-TRAP) or projection- and cell-type-specific (cell-type-specific Retro-TRAP) marker genes can be successfully identified using high-throughput RNA sequencing.

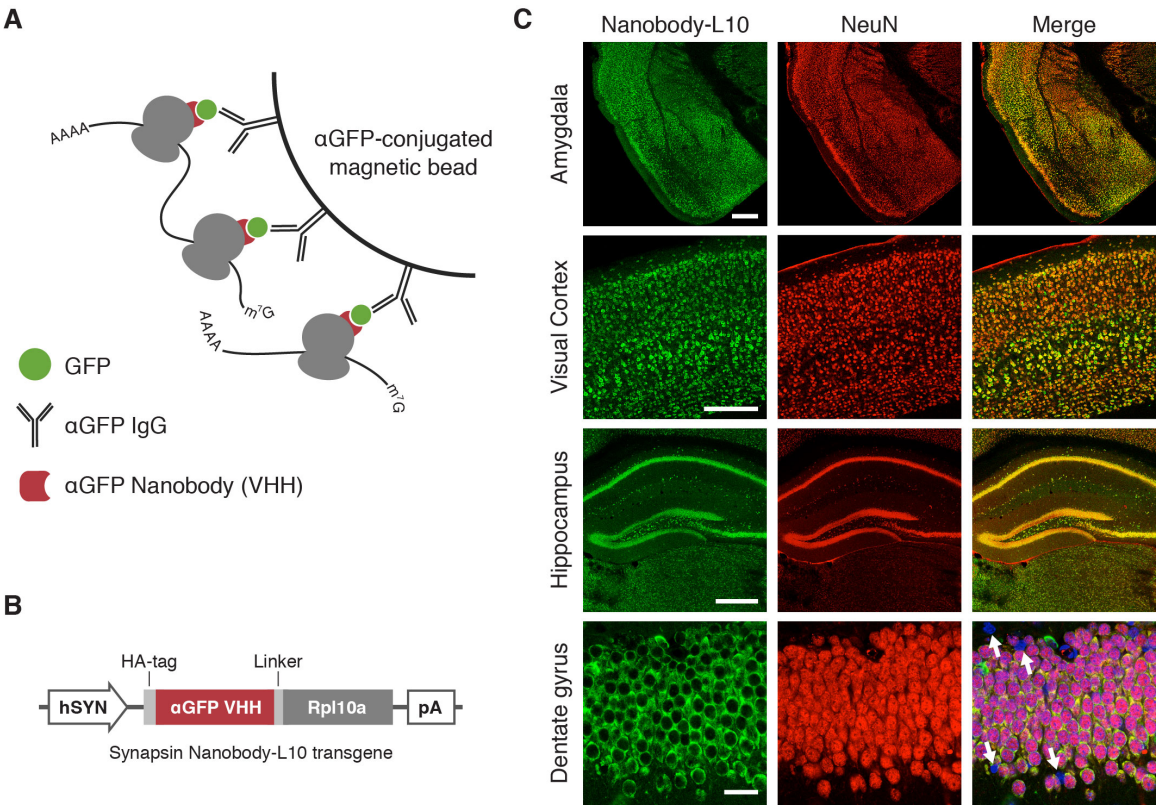

Figure 5.2. Neuron-Specific Expression of a Nanobody-L10 Fusion Protein. (A) Heterologous expression of an anti-GFP camelid nanobody fused to a ribosomal protein allows for immunoprecipitation of translating mRNAs in the presence of GFP. (B) Transgene used to generate SYN-NBL10 mice. A neuron-specific human synapsin promoter (SYN) drives the expression of an HA-tagged anti-GFP camelid VHH domain (nanobody) fused to ribosomal protein L10a. (C) Colocalization between HA-tagged NBL10 (green) and neuronal marker NeuN (red) in various brain regions. Dentate gyrus merge also displays Hoechst staining to show the presence of HA-/NeuN- glial cell-types (white arrows). Scale bars, 500 μm for amygdala and hippocampus, 250 μm for visual cortex, and 25 μm for dentate gyrus.

To confirm that expression of the NBL10 transgene was neuron-specific, we performed immunohistochemistry for HA and NeuN, a commonly used neuronal marker (Figure 5.2C). We then counted more than 4000 cells (n = 3 mice) and found only 4 cells that were not double-labeled, demonstrating that NBL10 expression is neuron-specific in these mice (Figure 5.3). Moreover, upon counterstaining with Hoechst to mark all nuclei in the brain, we found large numbers of HA-/NeuN- cells, further indicating that NBL10 is not expressed in non-neuronal cell-types (Figure 5.2C, white arrows).

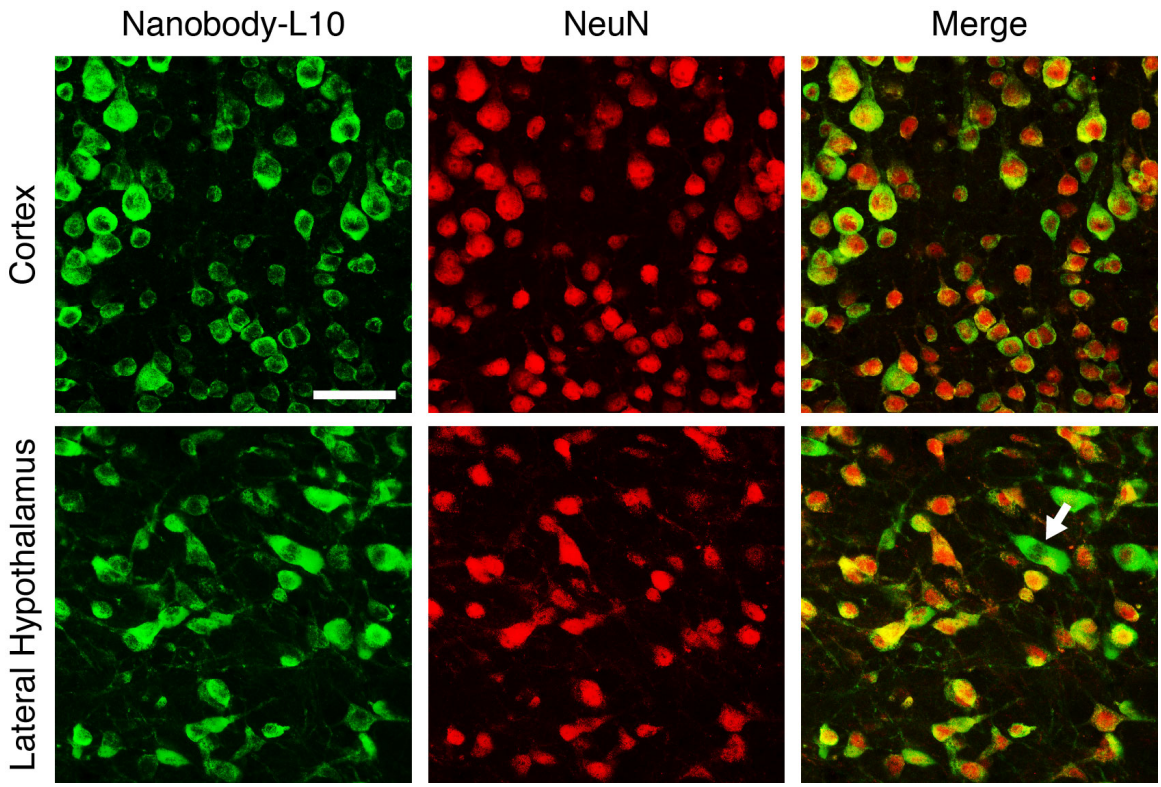

Figure 5.3. Histology for SYN-NBL10 Mouse. Cortex (top row) and lateral hypothalamus (bottom row) double-stained for NBL10 (green) and NeuN (red). White arrow indicates a NBL10+/NeuN- cell. Scale bar, 50 μm.

5.3 Nanobody-tagged ribosomes can be precipitated using GFP

We next set out to selectively immunoprecipitate (IP) neuronal ribosomes from SYN-NBL10 transgenic mice using GFP. Magnetic beads were coated with anti-GFP monoclonal antibodies that bind different epitopes on GFP than the one recognized by the nanobody. We then compared the ability of beads loaded with recombinant GFP versus control beads to immunoprecipitate ribosomes from whole brain lysate of SYN-NBL10 transgenic mice (Figure 5.4A). In our immunoprecipitate, we obtained yields of 2.0 ng/µl RNA for GFP-loaded beads and 0.004 ng/µl RNA for control beads ($p < 0.01$; Figure 5.4B). Similarly, 18S and 28S rRNA peaks were only detected in IPs using GFP-coated beads demonstrating that GFP is required for immunoprecipitation of RNA (Figure 5.4C). If the IP is specific to neuronal ribosomes, we would also expect to substantially deplete for glial markers, while not depleting for neuronal markers in the precipitated RNA. We found that RNA for all tested glial markers were indeed depleted in the IP relative to total (Input) RNA: *Gfap* (38.8-fold), *Mal* (49.1-fold), and *Mbp* (55.1-fold) ($p < 0.0001$ for all genes; Figure 5.4D). As expected, the neuronal markers *Kcc2*, *Nefl*, and *Snap25*, were present in similar amounts in the IP relative to Input RNA. All enrichments were determined by dividing IP over Input values for each gene after normalization to Rpl23. These experiments confirmed that nanobody-tagged neuronal ribosomes can be selectively immunoprecipitated from SYN-NBL10 transgenic mice in the presence of GFP, while immunoprecipitation of glial ribosomes is markedly reduced.

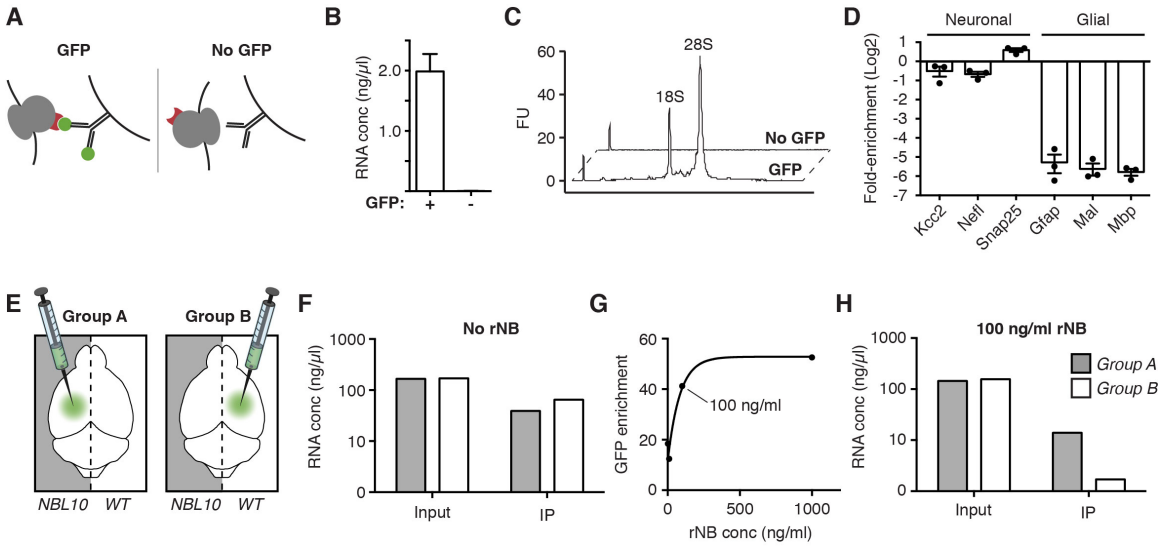

Figure 5.4. Optimization of Immunoprecipitation for GFP. (A) Schematic of immunoprecipitation with and without GFP. (B) Quantification of RNA yield after immunoprecipitation from SYN-NBL10 mice using GFP-coated or uncoated magnetic beads ($p < 0.01$). (C) Bioanalyzer trace of immunoprecipitated RNA with and without GFP. FU, fluorescence units. (D) Taqman analysis of neuronal and glial marker genes in RNA immunoprecipitated with recombinant GFP ($p < 0.0001$ for glial markers). (E) Mixing experiment illustration. CAV-GFP is injected into a SYN-NBL10 (grey background) or wild-type (white background) mouse. Injected brains are homogenized together with a non-injected brain of the complementary genotype to assay GFP-nanobody binding in lysates during the IP. (F) RNA yield after immunoprecipitation of mixed lysates with no recombinant nanobody (rNB) added to the homogenization buffer. (G) GFP enrichment in IP RNA from SYN-NBL10 mice injected with CAV-GFP. Data is plotted as GFP fold-enrichment (IP/Input) against buffer rNB concentration. (H) RNA yield after immunoprecipitation of mixed lysates with 100 ng/ml rNB in the buffer. Data are presented as mean ± SEM.

5.4 Selective immunoprecipitation of ribosomes bound to virally-encoded GFP

The finding that GFP can be used to immunoprecipitate NBL10-decorated ribosomes suggested that this approach could be used to precipitate ribosomes after infection of neurons with a virus expressing GFP. Canine adenovirus expressing GFP (CAV-GFP) was injected bilaterally into the nucleus accumbens (Figure 5.5A), and the region surrounding the injection site was dissected. Immunohistological staining revealed that the vast majority of cells that were infected were neurons (Figure 5.5D). We then lysed tissue from the infected region and performed a GFP IP. Consistent with the previous data, glial markers were depleted: *Gfap* (11.1-fold), *Mal* (14.8-fold), and *Mbp* (21.2-fold). In addition, *Gfp* was enriched (11.5-fold; Figure 5.5B-C). To test the possibility that GFP enrichment might be artificially increased by directly pulling down the nascent translating strand, we infected Hepa 1-6 cells with CAV-GFP (Figure 5.5E) and performed IPs. In this case, we were not able to detect any RNA in our IPs (Figures 5.5F-G), demonstrating that nascent strand contamination of our IPs is negligible. Additionally, we observed no substantial alterations in endogenous gene expression relative to mock infected cells, further confirming that CAV-GFP is a suitable virus for translational profiling (Figure 5.5H).

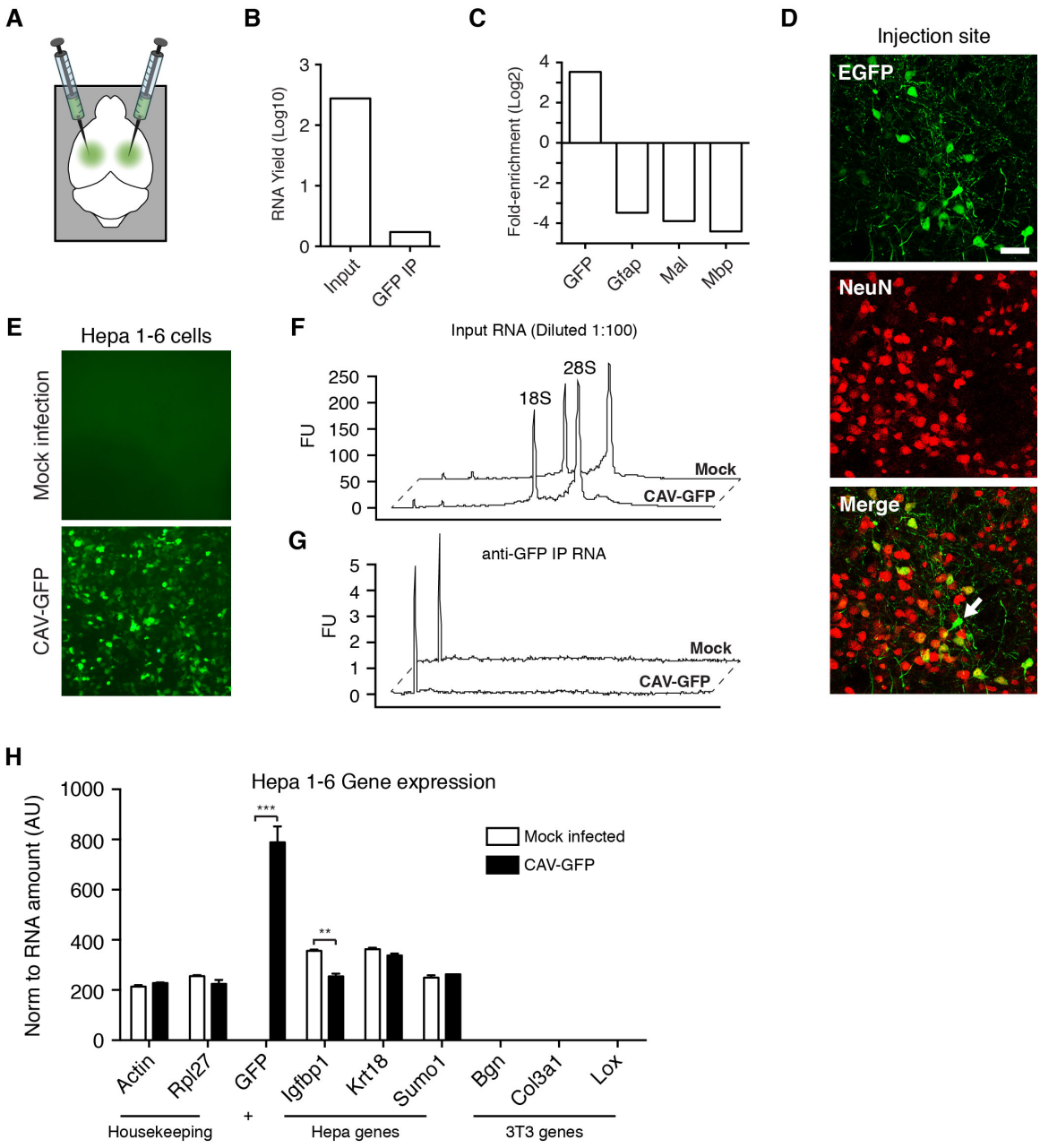

Figure 5.5. Virally-Targeted GFP Expression for Translational Profiling. (A) Schematic for bilateral CAV-GFP injections into the striatum. (B) RNA yield from Input and IP of striatum on a Log10 scale. (C) Fold-enrichments (IP/Input) of positive control *Gfp*, and glial markers on a Log2 scale. (D) Colocalization between CAV-GFP (green) and NeuN (red). White arrow indicates a GFP+/NeuN- cell. Scale bar, 50 µm. (E) Hepa 1-6 cells mock infected (top) or infected with CAV-GFP (bottom). (F and G) Bioanalyzer traces of Input (F) and IP (G) RNA with and without CAV-GFP. Input RNA diluted 1:100, IP RNA undiluted. (H) TaqMan analysis on Hepa 1-6 RNA for various housekeeping genes and cell-type markers. **p < 0.01, ***p < 0.001.

However, since only virally-infected cells should express GFP mRNA, we had expected to obtain a substantially higher enrichment for GFP above the 11.5-fold that was observed. We thus considered the possibility that *Gfp* enrichment might be lower than expected due to viral overexpression of GFP. Excess GFP would likely have a high stoichiometry relative to the NBL10 fusion protein, in which case there might not be enough nanobody to sequester all soluble GFP protein in infected cells, leading to GFP spillover in the lysate. Spillover would potentially cause promiscuous GFP binding to free NBL10-labeled ribosomes from nearby but uninfected neurons. This would, in turn, lead to a decrease in the relative amount of GFP RNA in our IPs and consequently reduce enrichment of GFP RNA as well as other mRNAs expressed in the infected neurons. We addressed this possibility by designing a mixing experiment to test whether GFP spillover was a significant source of background.

The mixing experiment was designed to assess the extent to which excess GFP could bind to nanobody-tagged ribosomes after tissue homogenization. In a first experiment, tissue from wild type (WT) mice infected with CAV-GFP was combined with tissue from uninfected SYN-NBL10 transgenic mice and homogenized together (hereafter Group B; Figure 5.4E, right). If RNA was precipitated after incubation of the mixed lysate with magnetic beads coated with anti-GFP antibodies, it would confirm that free GFP was binding to nanobody-labeled ribosomes after tissue homogenization. The data were compared to that in which tissue from CAV-GFP-infected SYN-NBL10 transgenic mice was mixed with tissue from WT mice (Group A; Figure 5.5E, left). We found that equivalent amounts of RNA were precipitated in

Groups A and B thus confirming that free GFP can bind to nanobody-labeled ribosomes in the lysate (Figure 5.5F). This suggested that a robust experiment would require the elimination of this binding.

We reasoned that by adding recombinant nanobody (rNB) to the lysate, we could sequester free GFP and render it unavailable for binding to the NBL10 fusion protein. This would reduce the background in our immunoprecipitate and thus augment GFP enrichment. To test this, we analyzed the fold-enrichment for GFP RNA in immunoprecipitations from brains of CAV-GFP-infected SYN-NBL10 mice in the presence of increasing amounts of rNB in the homogenization buffer. We found that the addition of rNB markedly increased the fold-enrichment for GFP RNA to more than 41-fold, compared to the previously observed 11.5-fold enrichment without the addition of rNB (Figure 5.5G). We also found that the increased enrichment of GFP RNA was near maximal at 100 ng/ml of added rNB (Figure 5.5G).

We then repeated the mixing experiment described above, now adding 100 ng/ml of rNB prior to tissue homogenization. In this case, substantially more RNA was recovered from Group A (~14 ng/µl), as compared to Group B (1.7 ng/µl; Figure 5.5H). These data demonstrate that the addition of 100 ng/ml of free rNB is sufficient to reduce promiscuous binding of GFP to ribosomes from uninfected neurons, while also maximizing the enrichment of GFP. Thus, the addition of recombinant nanobody prior to tissue homogenization greatly improves the specificity of the GFP immunoprecipitation.

5.5 Translational profiling of neurons projecting to the nucleus accumbens

The previous experiments demonstrated that we are able to immunoprecipitate ribosomes specifically from CAV-GFP-infected neurons in SYN-NBL10 transgenic mice. We next set out to molecularly profile neurons that project from one region to another by exploiting the retrograde transport of CAV-GFP from nerve terminals to soma. This virus is replication-deficient, so when it reaches the soma of the presynaptic neuron, it is incapable of traversing synapses and will not infect any other upstream neurons. Thus by infecting nerve terminals with CAV-GFP in SYN-NBL10 transgenic mice, ribosomes in the soma will be labeled with GFP. We next assessed whether we could isolate ribosomes and mRNA from neurons that project into the nucleus accumbens (NAc).

The nucleus accumbens integrates inputs from diverse regions throughout the brain, including the raphe nuclei in the brainstem, the medial prefrontal cortex, and hippocampus. Additionally, the NAc receives heavy input from dopaminergic neurons of the ventral tegmental area (VTA), as well as inputs from melanin-concentrating hormone (MCH) neurons of the lateral hypothalamus (LH; Georgescu et al., 2005). These populations are known to play important roles in reward-related behaviors and feeding, respectively. We were especially interested in these circuits because dysfunction of the NAc can contribute to a variety of disorders, such as obesity, addiction, and depression. Importantly, the VTA and LH inputs are anatomically segregated (i.e. sufficiently distant) from the accumbens shell, making it possible to dissect the brain regions from which these presynaptic populations

originate without contaminating our IP with CAV-GFP-infected neurons at the site of injection (Figure 5.6A). While subsets of MCH neurons of the LH and dopaminergic neurons of the VTA project to regions other than the NAc, the current methodology would allow us to selectively profile only the subpopulations of MCH and DA neurons that project directly to the accumbens shell. Neurons that do not project to the NAc will not express GFP, and their ribosomes will therefore not be precipitated (Figure 5.6B).

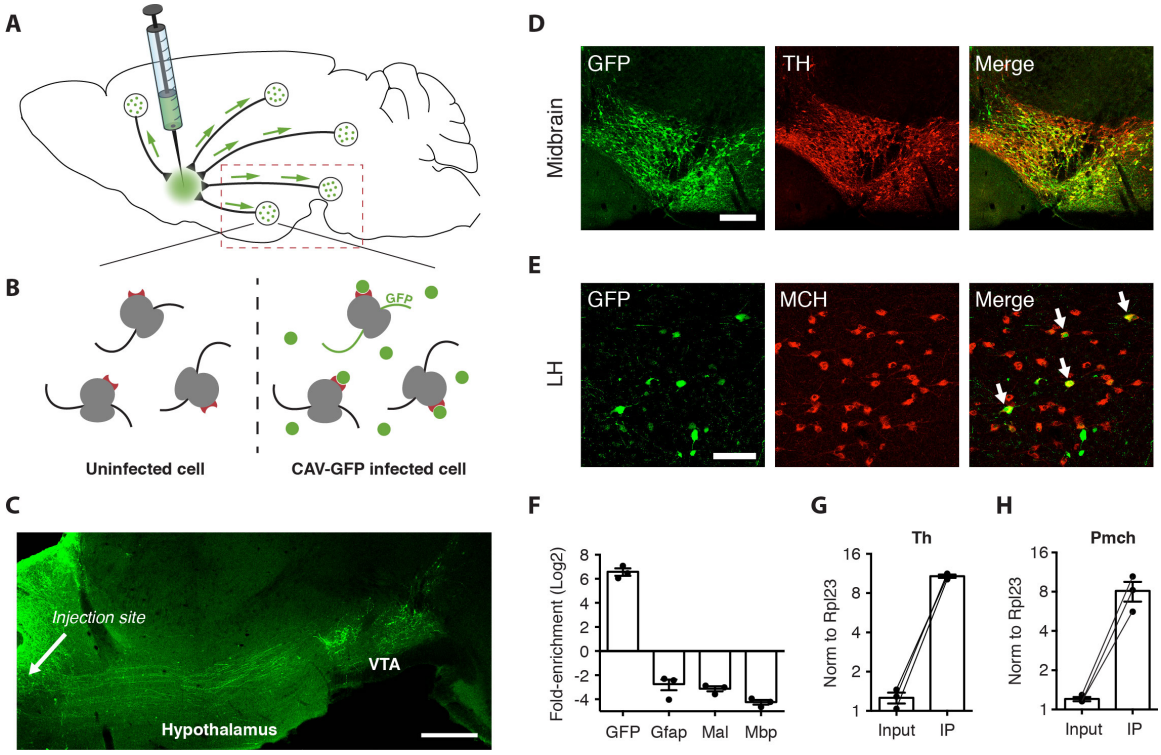

Figure 5.6. Projection-Specific Translational Profiling After CAV-GFP Injections into Nucleus Accumbens. (A) CAV-GFP injected into the nucleus accumbens is retrogradely transported to brain regions that send projections to the injection site. Only projective neurons will express GFP, as the virus is unable to replicate or cross synapses. Dashed red box indicates dissection for immunoprecipitation. (B) Infected neurons contain GFP mRNA and protein (green circles) that can bind nanobody-tagged (red) ribosomes. Interspersed uninfected cells will not contain GFP mRNA or protein. (C) Sagittal image showing retrograde spread of CAV-GFP through the hypothalamus and ventral midbrain. (D) Colocalization between GFP and TH in the ventral midbrain. (E) Colocalization between GFP and MCH in the lateral hypothalamus. White arrows indicate double-positive cells. (F) qPCR for GFP and glial transcripts after IP ($p < 0.05$ for all genes). Data is expressed as fold-enrichment (IP RNA/Input RNA). (G and H) qPCR results for tyrosine hydroxylase ($p < 0.001$) and pro-melanin-concentrating hormone ($p < 0.05$) transcripts. Scale bars, 500 μm in (C), 250 μm in (D), and 100 μm in (E). qPCR data is normalized to Rpl23 expression. Data are presented as mean ± SEM.

We injected mice with CAV-GFP in the nucleus accumbens and mapped the regions that were labeled with GFP to visualize neurons that project to the NAc. We observed a large number of GFP-positive neurons throughout the midbrain and hypothalamus (Figure 5.6C), as well as in the medial prefrontal cortex, amygdala, hippocampus, and dorsal raphe nucleus (Figure 5.7). Consistent with previous reports (Lammel et al., 2011), we also found that the majority of VTA neurons retrogradely labeled from the nucleus accumbens expressed tyrosine hydroxylase (TH; Figure 5.6D), a marker for dopaminergic neurons. We observed substantial numbers of GFP-positive neurons in the hypothalamus and confirmed that GFP co-localized with MCH in a subset of neurons in the LH (Figure 5.6E).

To purify ribosomes from neurons projecting to the NAc, we dissected a 3-mm piece of tissue distant from the site of injection that included the hypothalamus and the midbrain after bilateral injections of CAV-GFP in the NAc of SYN-NBL10 mice. We performed GFP IPs in the presence of 100 ng/ml rNB (Figure 5.6A, red dashed box). We observed highly significant enrichment for *Gfp* RNA (96.4-fold), while depleting for all glial markers tested: *Gfap* (6.7-fold), *Mal* (8.7-fold), and *Mbp* (18.8-fold) ($p < 0.05$ for all genes; Figure 5.6F). Importantly, we found significant enrichment for *Th* RNA (8.7-fold, $p < 0.001$; Figure 5.6G) and *Pmch* RNA (6.7-fold, $p < 0.05$; Figure 5.6H). These data validate that the current method can identify marker genes for neurons that project to the NAc.

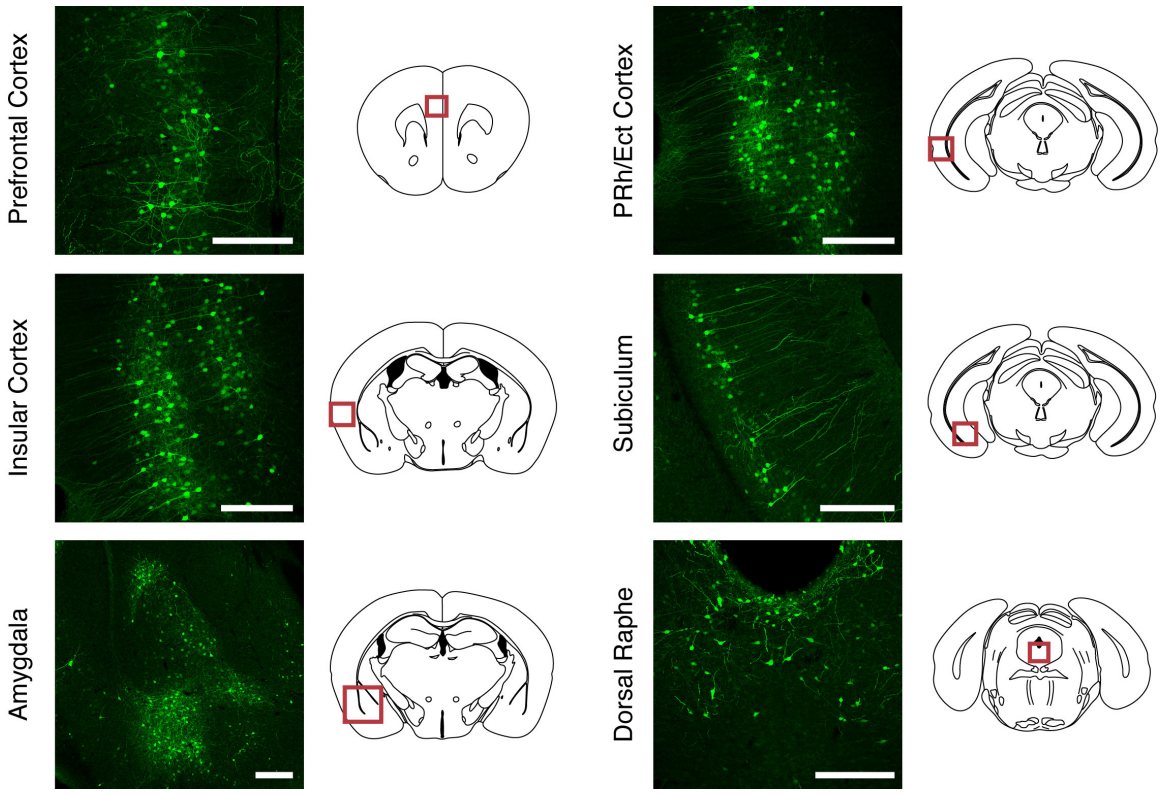

Figure 5.7. Projections to the Nucleus Accumbens Identified by CAV-GFP Retrograde Tracing. Various loci targeted by CAV-GFP through injection into the nucleus accumbens shell. Red boxes indicate region of interest. All scale bars, 250 μm.

5.6 Identification of marker genes for neurons projecting to the nucleus accumbens

Dopaminergic neurons of the VTA (Sesack and Grace, 2010) and MCH neurons of the LH (Georgescu et al., 2005) are known to project to the nucleus accumbens. However, the molecular profile of the specific subsets of these neurons that project to the NAc has not been explored, nor have markers for additional neural populations that project to this region been systematically identified. To address this, we performed high-throughput RNA sequencing (RNA-seq) on the IP RNA, as well as on the Input RNA from the midbrain and hypothalamus after injection of CAV-GFP into the NAc of SYN-NBL10 mice (Figures 5.8A-B). The total number of mapped reads was similar between the Input and IP RNA samples. Analysis of the sequencing data showed significant enrichment (IP/Input) of greater than 100-fold for GFP (Figure 5.8A), suggesting that the IP was highly specific for CAV-GFP-infected neurons that project from the dissected region to the NAc.

We plotted the IP RNA and Input RNA FPKM (Fragment Per Kilobase of transcript per Million mapped reads) values on a log-log scale (Figure 5.8C). The top 75 genes that were enriched in the IP RNA samples after RNA-seq analysis are also listed in Table 5.1. As seen previously with qPCR, RNA-seq data showed enrichment for *Pmch* (6.9-fold), as well as *Tacr3* (6.5-fold) and *Cartpt* (5.1-fold), and transcription factors *Foxa1* (5.7-fold) and *Foxa2* (4.9-fold). All of these genes have been reported to be co-expressed in MCH neurons (Croizier et al., 2010; Knight et al., 2012; Silva et al., 2009).

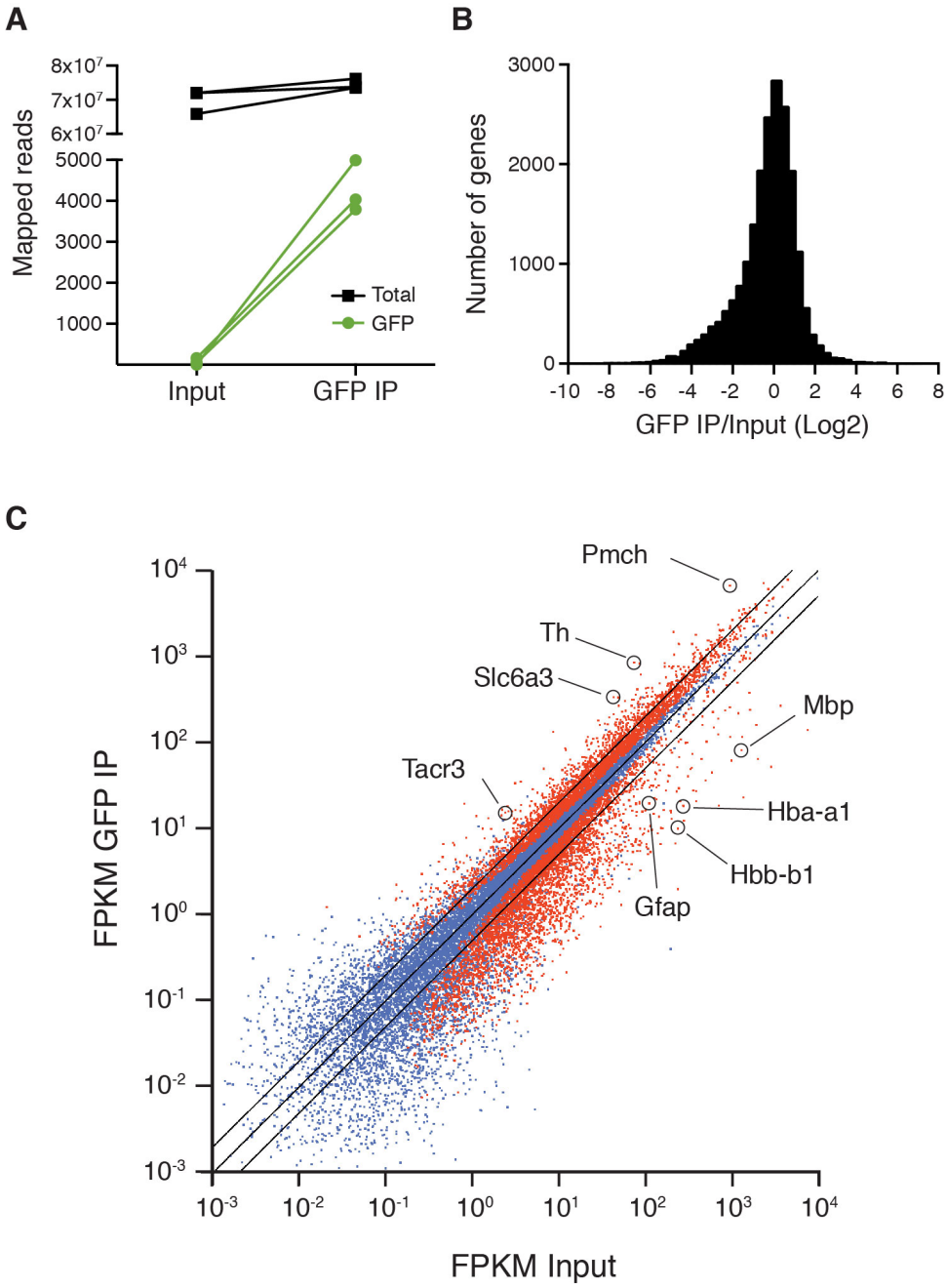

Figure 5.8. Identification of Differentially Expressed Marker Genes by RNA-Seq. (A) RNA-seq analysis of total reads mapped to the mouse genome (black) and EGFP coding sequence (green) plotted on a linear scale. (B) Histogram display of number of differentially enriched genes (IP/Input). (C) FPKM GFP IP plotted against FPKM Input on a log-log scale. Outer lines are 2-fold enriched/depleted genes. A subset of differentially-enriched marker genes are highlighted. Red dots indicate genes that are significantly different ($q < 0.05$) in Input versus IP. Blue dots indicate non-significant genes.

Table 5.1. Annotated Enrichments of Top 75 Genes as Identified by RNA-Seq. Table is sorted by fold-change. All genes listed are q-value significant ($q < 0.05$). Genes related to dopaminergic, MCH, and hypocretin neurons are highlighted.

Gene	Fold-change	Note
Pdzk1	59.3	
Theg	16.8	
Alkbh6	15.5	
Gkn1	14.3	
En1	**12.6**	**Dopamine neuron development**
Sprr1a	11.6	
Th	**11.4**	**Dopamine neurons**
Thop1	11.4	
Tmem207	11.4	
Gtsf1	11.3	
Slc10a4	**10.8**	**Monoaminergic and cholinergic neurons**
Slc39a4	10.4	
Cndp1	10.3	
Nol3	10.1	
Grp	9.7	Gastrin-releasing peptide
Hcrt	**9.6**	**Hypocretin neurons**
Mup6	9.2	
Cox6a1	9.1	Mitochondrial complex IV subunit
Pgls	8.7	
Slc6a3	**7.8**	**Dopamine neurons**
Hist3h2ba	7.6	
Syt5	7.4	
Rps4y2	7.3	
Ntf3	7.1	Neurotrophin 3
Ooep	7.1	
Pmch	**6.9**	**MCH neurons**
Mib2	6.9	
Chrna6	6.8	Nicotinic cholinergic receptor subunit
Cisd1	6.8	
Rln3	6.6	Relaxin 3 neurons
Tacr3	**6.5**	**MCH neurons**
Med28	6.3	
Tpo	6.2	
Ptpn20	6.2	
Fam179a	6.1	
Ntsr1	6.1	Neurotensin receptor 1
Gch1	5.9	
Htr5b	5.8	Serotonin receptor subunit
Eif1	5.8	
Cldn26	5.8	
Ccdc106	5.8	
Uts2r	5.7	Urotensin receptor 2
Fam159b	5.7	

Table 5.1 (continued)

Gene	Fold-change	Note
Foxa1	**5.7**	**MCH/Hypocretin neurons**
Hist1h4c	5.6	
Bex2	5.6	
Twist2	5.6	
Lypla2	5.6	
Uncx	5.5	
Krt18	5.5	
Cps1	5.4	
Penk	5.4	Preproenkephalin
Sncb	**5.4**	**Synuclein (beta)**
Wnt2	5.3	
Mmp12	5.3	
Ddc	**5.2**	**Dopamine neurons**
Nurr1	**5.2**	**Dopamine neuron development**
Exoc3l	5.2	
Zar1	5.2	
Mrpl12	5.1	Mitochondrial ribosomal protein
Gtf2h4	5.1	
Cartpt	**5.1**	**Pomc and MCH neurons**
Txnl4a	5.1	
Aldh1a7	5.1	
Dkkl1	5.1	
Ntn1	5.1	
Dmrtb1	5.0	
Cox8a	5.0	Mitochondrial complex IV subunit
Plvap	5.0	
Ndc80	4.9	
Foxa2	**4.9**	**MCH/Hypocretin neurons**
Chchd6	4.9	
Ap2s1	4.9	
Elovl3	4.9	
Snca	**4.9**	**Synuclein (alpha)**

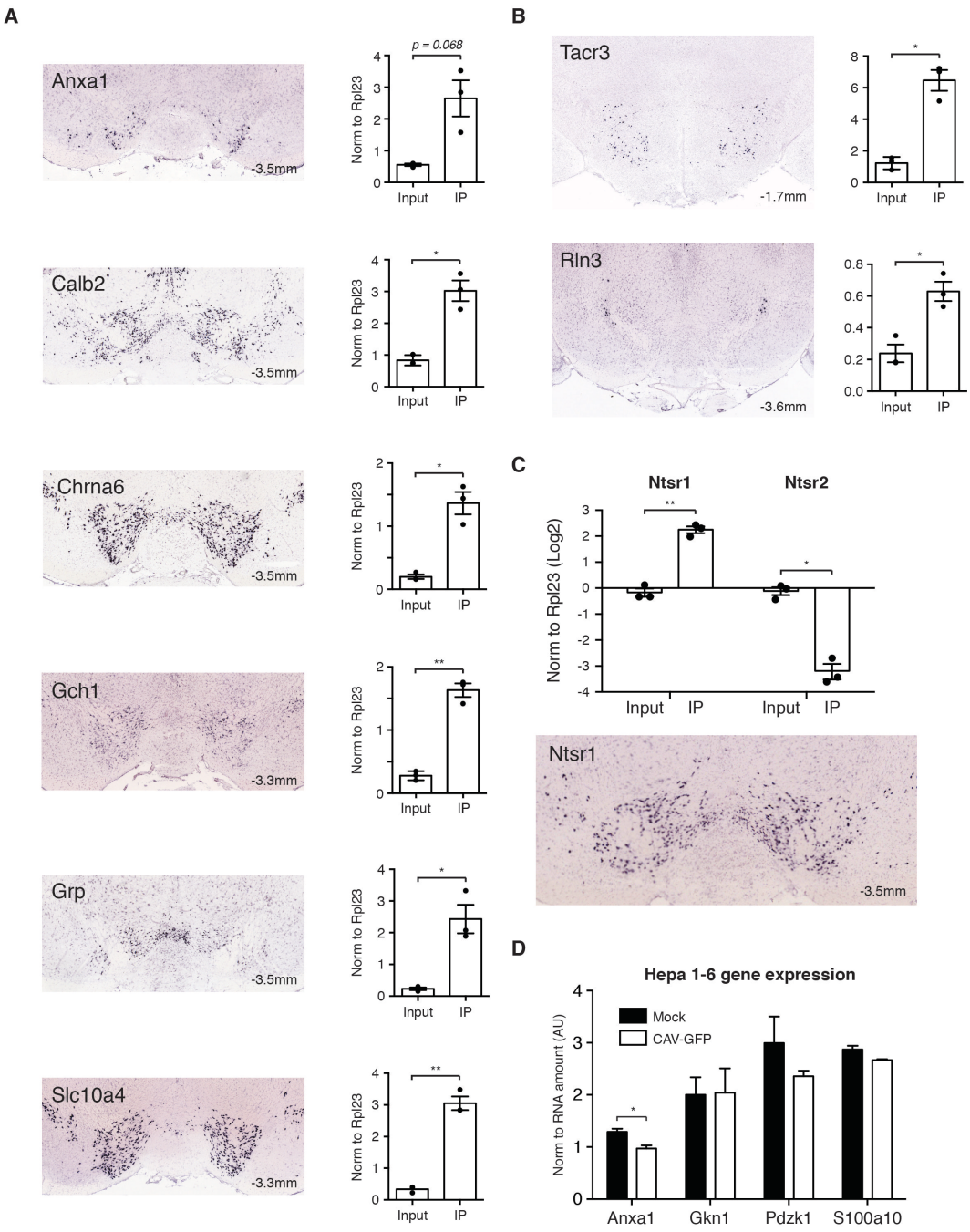

Figure 5.9. Confirmation of Marker Genes Revealed by RNA-seq. (A) Allen Brain Atlas (ABA) images for ventral midbrain genes with corresponding Taqman confirmation. (B) ABA images for *Tacr3* and *Rln3* with corresponding Taqman confirmation. (C) Differential expression of neurotensin receptor isoforms *Ntsr1* and *Ntsr2* as confirmed by Taqman, alongside ABA image for *Ntsr1*. (D) *In vitro* effects of CAV-GFP infection on expression of cell-type marker genes identified in RNA-seq study. qPCR data is normalized to *Rpl23*, except in (D). Data is plotted on a linear scale, except in (C) where it is Log2. ABA AP coordinates are in the bottom right of each image. *p < 0.05, **p < 0.01.

Similarly, marker genes co-expressed with *Th* (11.4-fold enriched) in dopaminergic neurons of the ventral midbrain were also enriched including, *Slc6a3* (7.8-fold), *Ddc* (5.2-fold), and *Nurr1* (5.2-fold), as well as α-synuclein (*Snca*, 4.9-fold; Mosharov et al., 2009). These genes were then re-confirmed with qPCR: *Slc6a3* (10.1-fold, $p < 0.05$), *Ddc* (5.7-fold, $p < 0.01$), *Nurr1* (2.8-fold, $p < 0.01$), and *Snca* (4.6-fold, $p < 0.01$). Another subset of highly-enriched genes not commonly associated with midbrain dopamine neurons, such as *Anxa1*, *Calb2*, *Chrna6*, *Gch1*, *Grp*, and *Slc10a4* were further analyzed by qPCR, and paired with their Allen Brain Atlas expression profiles (Figure 5.9A**;** Lein et al., 2007). These data confirmed their expression in the ventral midbrain and further validate the ability of this approach to identify transcripts expressed in specific subsets of projection neurons.

We also found differential expression of the neurotensin receptor isoforms Ntsr1 and Ntsr2, with significant enrichment of *Ntsr1* (6.1-fold) and depletion of *Ntsr2* (7.4-fold) in the immunoprecipitated RNA. Ntsr1 has been shown previously to play an important role in signaling from the LH to the VTA as part of a reward circuit (Kempadoo et al., 2013). The expression of these isoforms was confirmed by qPCR, with *Ntsr1* enriched 5.4-fold ($p < 0.01$) and *Ntsr2* depleted 8.3-fold ($p < 0.05$; Figure 5.9C). RNAs for numerous additional genes were significantly enriched in the IP RNA and many of these genes are likely to be markers for populations of neurons projecting to the NAc (Figure 5.9B). Importantly, when we tested the effect of CAV-GFP infection on expression of a subset of identified marker genes in tissue culture, no substantial alterations were observed (Figure 5.9D).

5.7 Identification of novel projection markers

In our analysis of the RNA-seq data, we observed that a subclass of S100A genes (7 out of 8) were substantially depleted from our immunoprecipitation. However, *S100a10* was significantly enriched (2.1-fold; Figure 5.10A), and this was confirmed by qPCR (2.1-fold, $p < 0.01$; Figure 5.10B). *S100a10* expression was not significantly altered by infection with CAV-GFP *in vitro* (Figure 5.9D). *S100a10*, also known as p11, is known to interact with serotonin receptors and has been causally implicated in depressive disorders (Svenningsson et al., 2006). Indeed, p11-containing cortical projection neurons have recently been identified as being responsible for mediating the response to antidepressants (Schmidt et al., 2012); however, data suggesting a possible role for p11 neurons projecting from hypothalamus to NAc are lacking.

To validate the finding that hypothalamic neurons expressing p11 project to the NAc using a different neural tracer, we generated a replication-deficient pseudorabies virus expressing mCherry (PRV-mCherry). PRV is another well-characterized virus that is retrogradely transported after injection, and similar to CAV-GFP, this strain is incapable of traversing synapses. We injected PRV-mCherry bilaterally into the nucleus accumbens of p11-EGFP transgenic mice (Oh et al., 2013) and observed substantial overlap between cells expressing p11 (EGFP) and mCherry in the lateral hypothalamus (Figure 5.10C), confirming these neurons project to the NAc.

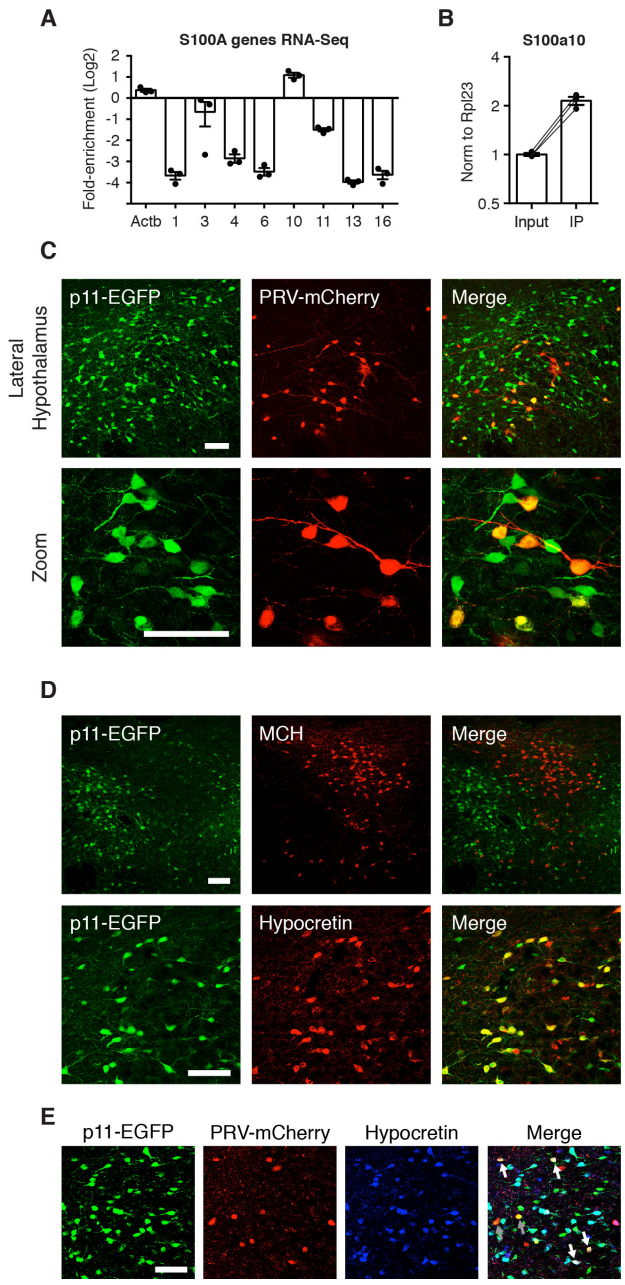

Figure 5.10. A Subset of Hypothalamic Projection Neurons Express p11. (A) Differential enrichment (IP/Input) of the S100A family of genes in neurons projecting to the nucleus accumbens assessed by RNA-seq, on a Log2 scale. Actin (*Actb*) is shown for reference. (B) qPCR confirmation of S100a10 (p11) enrichment ($p < 0.01$). (C) Colocalization between p11-EGFP and PRV-mCherry in the lateral hypothalamus. (D) Top panel, colocalization between p11-EGFP and MCH. Bottom panel, colocalization between p11-EGFP and hypocretin. (E) Colocalization between p11-EGFP, PRV-mCherry, and hypocretin. White arrows indicate triple-stained cells. Grey arrows indicate p11-positive projection neurons that do not colocalize with hypocretin. qPCR data is normalized to Rpl23. Data are presented as mean ± SEM. All scale bars, 100 μm.

We additionally wanted to know if there was any overlap between the p11 projection neurons and other markers for cell-types in the lateral hypothalamus that project to the NAc. Co-staining for MCH and p11-EGFP revealed clear anatomical segregation between the two cell-types (Figure 5.10D, top panel). Furthermore, we were not able to colocalize p11 and MCH in any neurons of the p11-EGFP mouse. These data suggest that the p11 neurons in the LH that project to the NAc comprise a subset of LH neurons distinct from MCH neurons. We noted, however, in the RNA-seq data that there was significant enrichment for hypocretin RNA (9.6-fold; Table 5.1). Hypocretin expression defines a distinct subpopulation of lateral hypothalamic neurons that does not overlap with MCH neurons. We thus performed immunohistochemistry for p11 and hypocretin and observed significant overlap and cellular colocalization between the two cell-types (Figure 5.10D, bottom panel). We found that p11 was expressed in three different regions of the hypothalamus (the arcuate nucleus, LH, and paraventricular hypothalamus), and overlaps substantially with hypocretin in the LH (Figure 5.11A). The overlap between p11 and hypocretin in the LH ranged between 39-52%, depending on the relative position along the AP axis (Figure 5.11B).

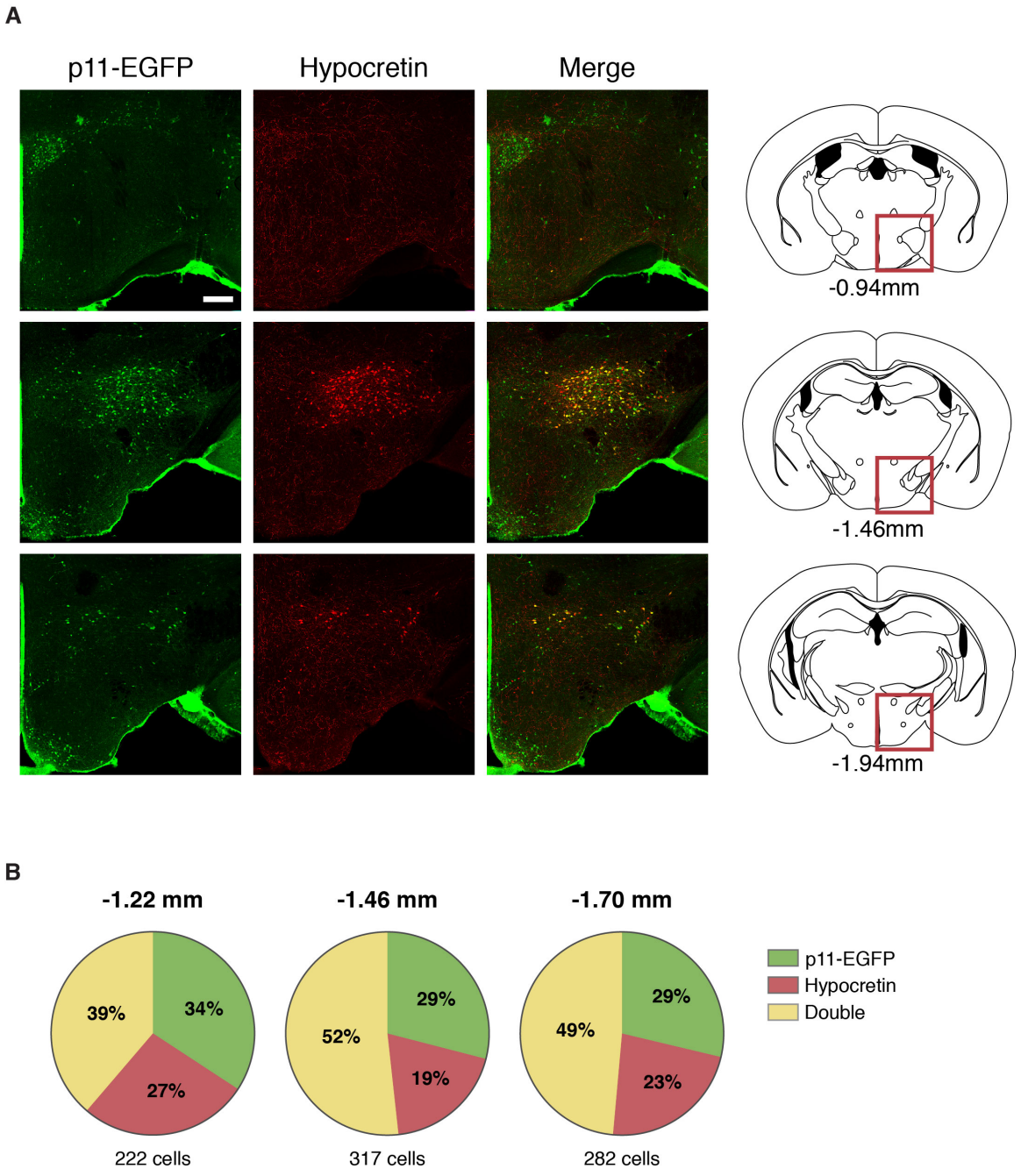

Figure 5.11. Histology for p11 Neurons of the Lateral Hypothalamus. (A) Colocalization between p11-EGFP and hypocretin in the lateral hypothalamus. Red boxes indicate region of interest. Scale bar, 250 μm. (B) Quantification of p11/hypocretin overlap in the lateral hypothalamus at 3 different AP levels.

We then injected PRV-mCherry into the nucleus accumbens of p11-EGFP mice and co-stained for hypocretin. Triple staining for GFP, mCherry, and hypocretin revealed that p11 neurons projecting to the nucleus accumbens partially overlap with the LH hypocretin neurons (Figure 5.10E). Overall, this study identifies a subpopulation of p11 neurons in the LH that project to the NAc, and demonstrates that most but not all of these projection neurons co-express hypocretin.

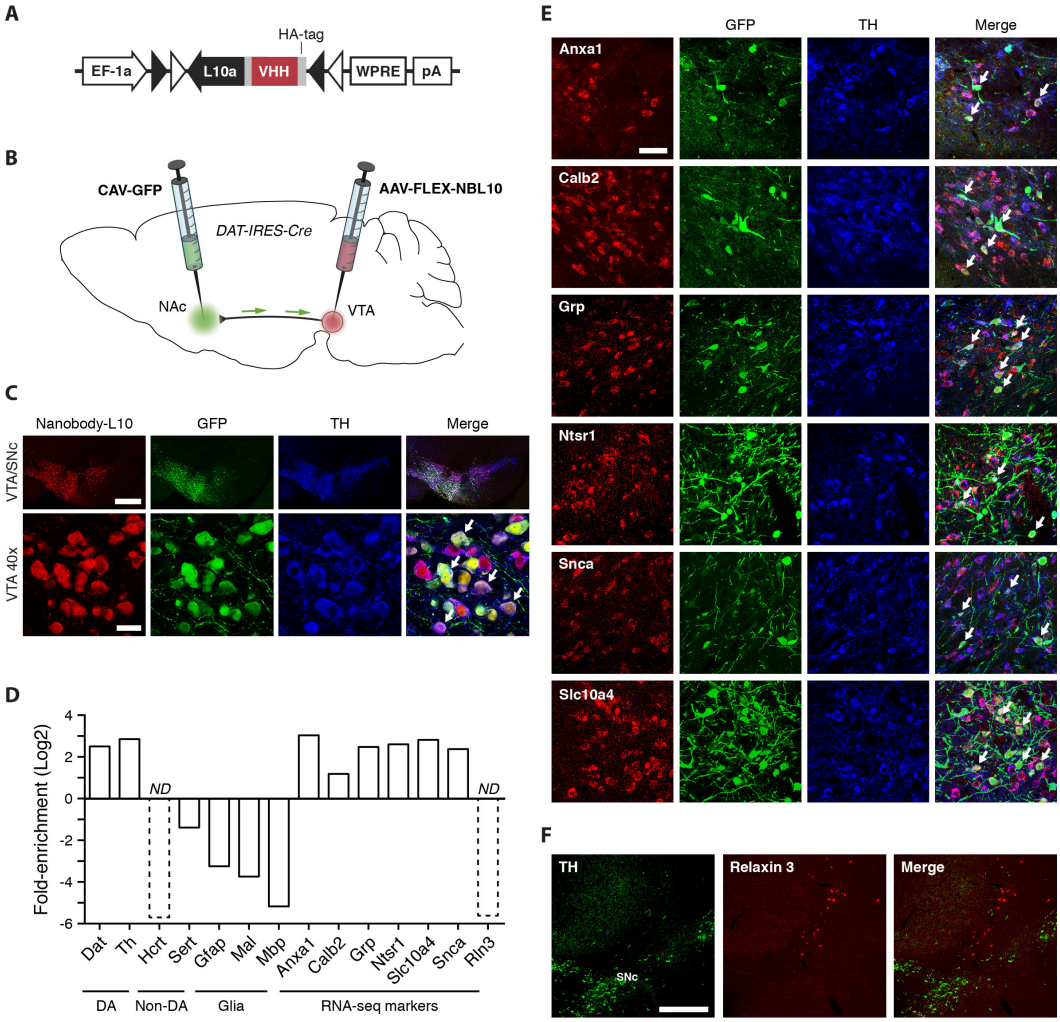

Figure 5.12. Molecular Profiling of VTA Dopamine Neurons Projecting to the Nucleus Accumbens. (A) AAV-FLEX-NBL10 construct developed to conditionally express NBL10 in the presence of Cre recombinase. (B) AAV-FLEX-NBL10 is injected into the VTA and CAV-GFP into the NAc of DAT-IRES-Cre mice. NBL10 is restricted to VTA dopamine neurons, and CAV-GFP to NAc-projecting neurons. Only ribosomes from double-labeled cells (VTA dopamine neurons projecting to the NAc) can be immunoprecipitated. (C) Colocalization between NBL10, GFP (from CAV), and TH in the VTA. (D) qPCR after cell-type-/projection-specific IPs. Data is expressed as fold-enrichment (IP RNA/Input RNA). 'ND' means that IP RNA is not detected. (E) Enriched marker genes from (D) labeled using FISH. Colocalization between enriched genes, GFP (from CAV), and TH. Colocalization between Relaxin 3 and TH. qPCR data is normalized to Rpl23. Scale bars, 500 μm for top panel and 25 μm for bottom panel in (C), and 50 μm for (E). White arrows in (C) and (E) indicate triple-stained cells.

5.8 Molecular profiling of VTA dopamine neurons projecting to nucleus accumbens

In our earlier studies, we identified a number of markers that are expressed in ventral midbrain neurons projecting to the nucleus accumbens (see Figure 5.9). The data did not distinguish whether these markers were expressed in dopaminergic neurons of the VTA or in a different population. To test whether these markers are expressed in VTA dopamine neurons projecting to the nucleus accumbens, we set out to extend the current approach to make it cell-type-specific. To accomplish this, we took advantage of the fact that our technique utilizes a two-component system; namely, both GFP and NBL10 are required to immunoprecipitate RNA from a given cell. Furthermore, the NBL10 construct is relatively small (~1 kb), which makes it amenable to cloning into a Cre-dependent (FLEXed) AAV (Atasoy et al., 2008). We thus cloned the Nanobody-L10 fusion protein (NBL10) into a Cre-conditional AAV (AAV-FLEX-NBL10; Figure 5.12A). We then injected CAV-GFP into the nucleus accumbens, and AAV-FLEX-NBL10 into the VTA of DAT-IRES-Cre mice (Figure 5.12B; Backman et al., 2006). Immunohistochemistry against NBL10 and TH demonstrated that NBL10 expression was restricted to midbrain dopamine neurons. Furthermore, we noted that a subset of these neurons were also labeled with GFP, confirming that we had targeted a substantial number of VTA dopamine neurons that project to the NAc (Figure 5.12C).

To purify ribosomes from only those VTA dopamine neurons that project to the NAc, we dissected a 2-mm piece of tissue that included the midbrain and performed IPs

as described above. In this case, we precipitated RNA only from VTA dopamine neurons that project to the NAc, as only they will express both GFP and NBL10. Importantly, ribosomes from cells expressing only GFP (non-dopamine neurons that project to the NAc) or only NBL10 (VTA dopamine neurons that do not project to the NAc) will not be precipitated, as both components are required. We substantially enriched for midbrain dopamine markers including *Slc6a3* (5.7-fold) and *Th* (7.2-fold), while depleting for non-dopaminergic marker genes *Hcrt* (IP RNA did not amplify) and *Slc6a4* (2.6-fold), as well as glial markers *Gfap* (9.5-fold), *Mal* (13.3-fold), and *Mbp* (36-fold) (Figure 5.12D).

A number of genes identified by our RNA-seq study are expressed in the ventral midbrain (see Allen Brain Atlas and Figure 5.9), suggesting that these are markers for VTA dopamine neurons projecting to the nucleus accumbens. We assessed the enrichment of seven of these different marker genes by qPCR. Six of the genes were substantially enriched: *Anxa1* (8.2-fold), *Calb2* (2.3-fold), *Grp* (5.6-fold), *Ntsr1* (6.1-fold), *Slc10a4* (7.1-fold), and *Snca* (5.2-fold) (Figure 5.12D). To further validate that the enriched subset of genes are expressed in VTA dopamine neurons projecting to the NAc, we injected the NAc with CAV-GFP. We then performed fluorescence *in situ* hybridization (FISH) against each one of these marker genes in tandem with immunohistochemistry against GFP and TH (Figure 5.12E). In each case, we observed substantial numbers of triple-labeled cells (white arrows), confirming that we were able to profile projective VTA dopamine neurons. Of note, previous studies have shown expression of *Grp* in midbrain dopamine neurons (Chung et al., 2005),

though localization to the nucleus accumbens-projecting dopamine neurons has not been demonstrated. Conversely, we did not enrich for relaxin-3 (*Rln3*), which was identified in the RNA-seq study (Figure 5.12D). Upon co-staining for relaxin-3 mRNA and TH, we found that this marker was not expressed in midbrain dopamine neurons, but rather in a discrete population dorsal to the posterior substantia nigra (Figure 5.12F). Thus, by systematically comparing data generated using AAV-FLEX-NBL10 to the region-specific approach, we were able to identify markers for VTA dopamine neurons, as well as markers for non-dopaminergic cell-types.

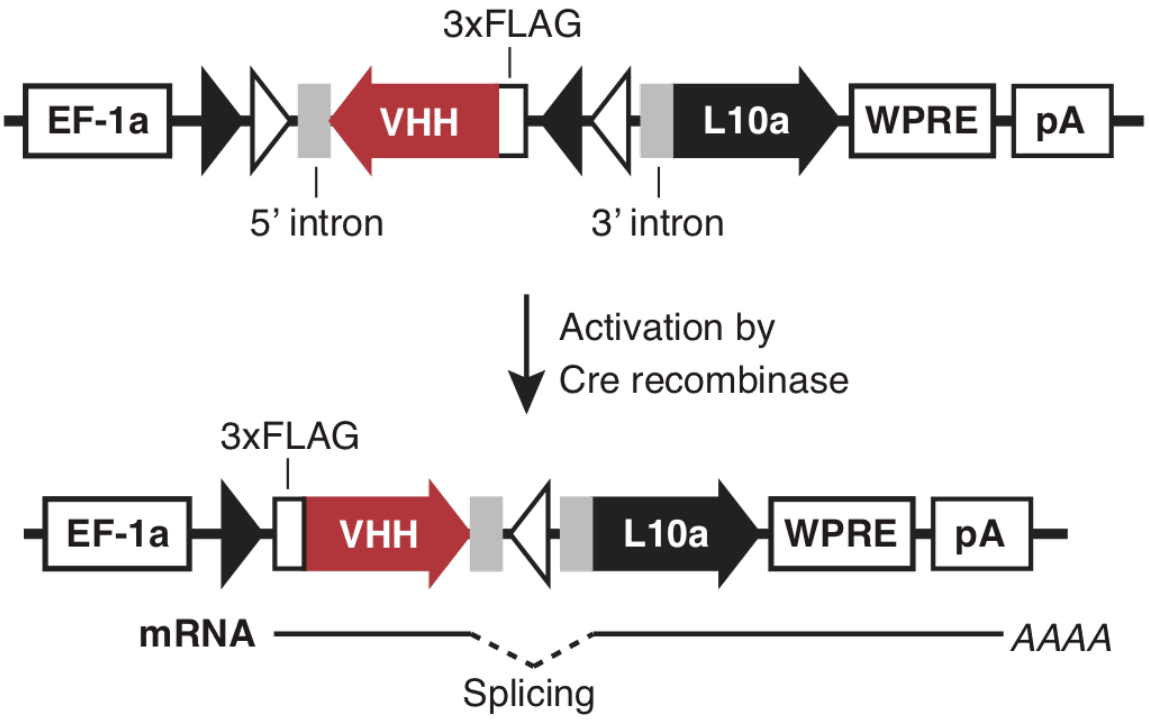

Figure 5.13. AAV-IV-NBL10 for Cell-Type-Specific Retro-TRAP Profiling. AAV-IV-NBL10 is based off of 'Introvert' (IV) technology, which is a Cre-dependent construct that combines the FLEX switch with flanking introns to enable gene splitting, which still results in the same contiguous fusion protein (M.I.E., unpublished data). We adapted the IV strategy for Cre-dependent expression of the NBL10 fusion, with an added 5' 3xFLAG tag that enables simultaneous molecular profiling of the targeted cell type (to normalize to the projection target). Solely in the presence of Cre recombinase, IV-NBL10 is activated to form the fusion construct, which is then expressed and integrated into the large ribosomal subunit.

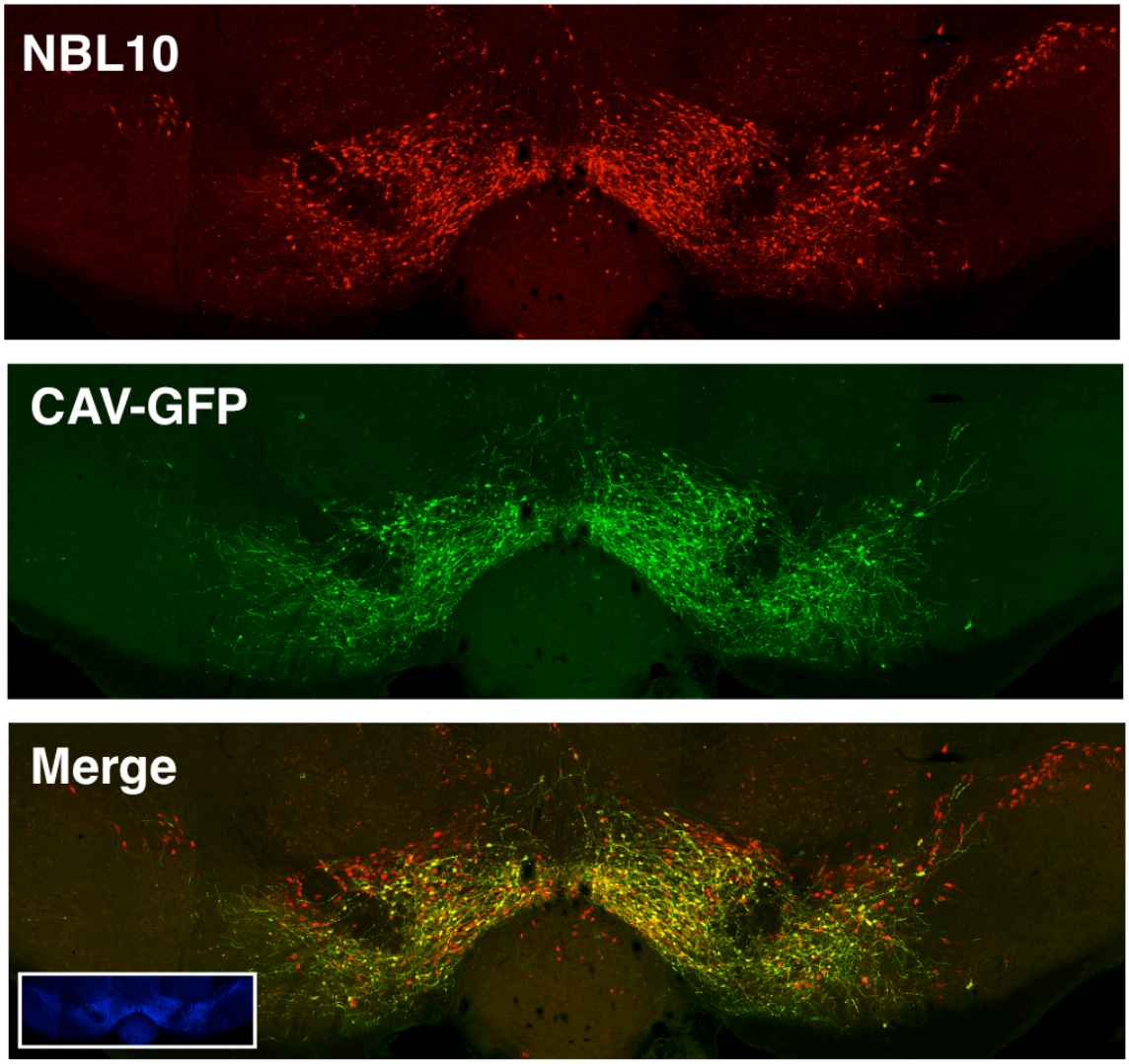

Figure 5.14. Ventral Tegmental Area Staining of NBL10 and GFP After Viral Injections. Immunohistochemistry in the ventral midbrain. AAV-IV-NBL10 was injected into the VTA (**top**), followed by CAV-GFP injection (**middle**) into the nucleus accumbens. Inset displays tyrosine hydroxylase (TH) counterstain.

5.9 Cell-type-specific Retro-TRAP for comparative analysis of mesolimbic and nigrostriatal dopamine neurons

We then set out to systematically compare midbrain dopaminergic projections to the striatum using cell-type-specific Retro-TRAP. In these studies, we generated another Cre-dependent AAV engineered to conditionally express the NBL10 construct. In this case, we utilized 'Introvert' technology (Mats Ekstrand, unpublished data and see above), with the hope that this switch would provide tighter Cre-dependent regulation of gene expression, as compared to the 'FLEX' construct. Briefly, Introvert technology enables one to split a gene in half and then 'FLEX' one half to make it Cre-dependent regardless of reading frame or orientation (see Figure 5.13). We then synthesized an 'Introverted' form of NBL10 and cloned it into an AAV plasmid, thus creating AAV-IV-NBL0. Importantly, AAV-IV-NBL10 also carries N-terminal HA and FLAG tags for IHC and cell-type-specific (but not projection-specific) profiling (Figure 5.14), respectively. We then utilized a similar approach as described above to perform simultaneous cell-type- and projection-specific molecular profiling of dopaminergic neurons targeting the striatum.

We achieved this aim by first injecting AAV-IV-NBL10 into the ventral midbrain of DAT-IRES-Cre mice. After waiting two weeks for sufficient expression of NBL10, we then injected CAV-GFP into either the ventral or dorsal striatum (nucleus accumbens and caudate putamen, respectively) (Figure 5.15). Two weeks later, we performed IPs first against GFP to profile the mesolimbic/nigrostriatal projections, and then against FLAG as a control for selective expression of the NBL10 construct

in midbrain dopamine neurons. We then performed high-throughput RNA sequencing (RNA-seq) on the RNA samples obtained, so we could perform comparative analyses between the dopaminergic projections.

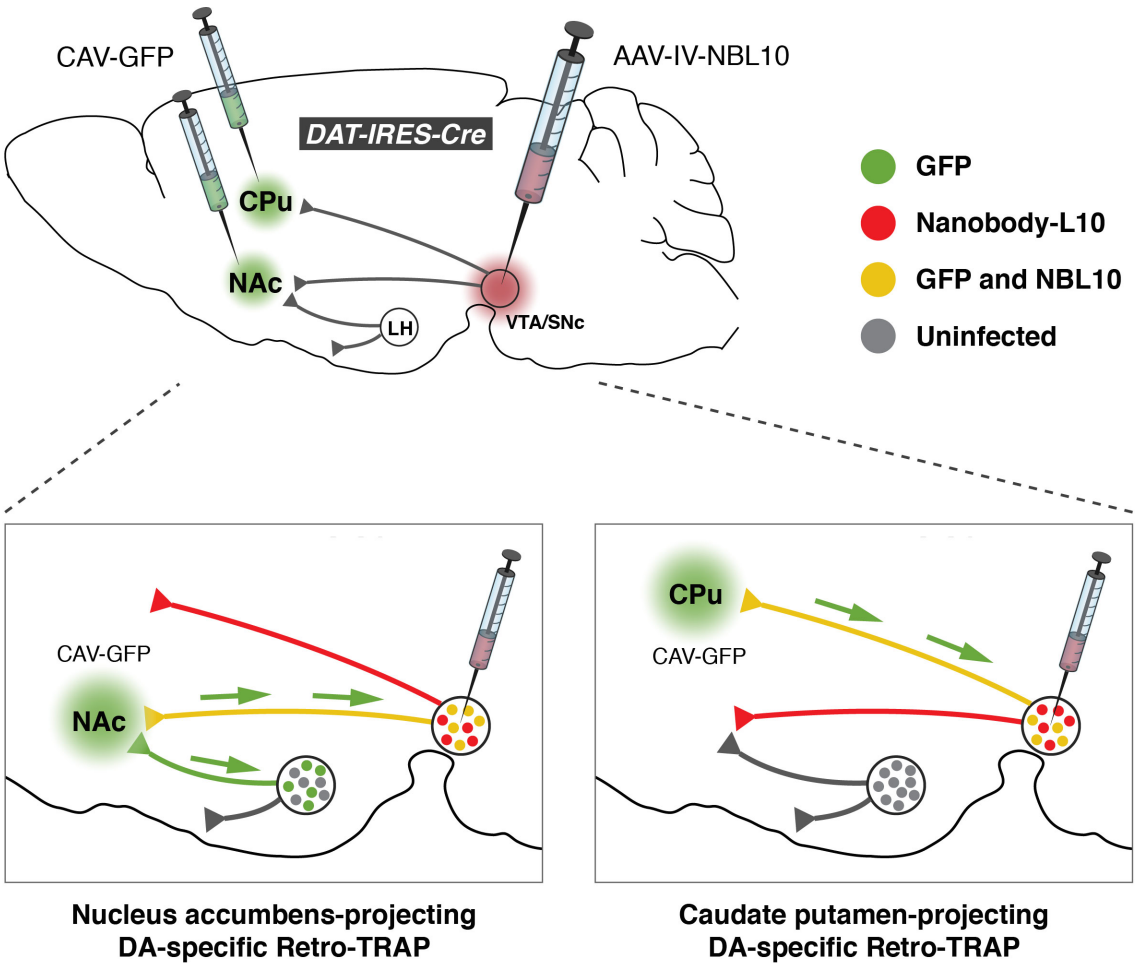

Figure 5.15. Differential Targeting of the Mesolimbic and Nigrostriatal Dopaminergic Projections using Cell-type-specific Retro-TRAP. (**Top**) AAV-IV-NBL10 is injected into the ventral midbrain of DAT-IRES-Cre mice, while the retrograde tracing, replication-deficient canine adenovirus expressing GFP (CAV-GFP) is injected into either the nucleus accumbens (NAc) or caudate putamen (CPu). (**Bottom**) Molecular profiling of NAc-projecting VTA DA neurons (mesolimbic, **bottom left**) and CPu-projecting SNc DA neurons (nigrostriatal, **bottom right**). Note that in each case only the yellow neurons (containing both GFP and NBL10) are accessible for IP.

Before performing comparative analysis, we first confirmed the specificity of the cell-type-specific approach over the original Retro-TRAP strategy. Because AAV-IV-NBL10 is selectively expressed only within dopaminergic neurons of the ventral midbrain, we should be able to significantly boost our enrichment for dopaminergic transcripts as compared to the original Retro-TRAP approach, which non-selectively targeted all neurons projecting to the NAc from the midbrain and hypothalamus. Indeed, when we compared enrichments for known and newly-identified dopaminergic transcripts, we found significant enrichment in the cell-type-specific approach across the board (Figure 5.16). Known dopaminergic transcripts in the cell-type-specific approach were all enriched 13.1-34.9-fold, as compared with the original Retro-TRAP approach, which yielded enrichments on the order of 3.9-12.2-fold. In particular, these differentially enriched transcripts (and their comparative enrichments) are: *Th* (12.2 versus 34.9, $p < 0.01$), *Slc6a3* (7.7 versus 20.8, $p < 0.01$), *Slc18a2* (3.9 versus 15.6, $p < 0.0001$), *Ddc* (5.2 versus 20.6, $p < 0.0001$), and *Nr4a2* (5.4 versus 13.1, $p < 0.05$). For other and newly-identified dopaminergic transcripts, increased degree of enrichment was similar to traditional dopaminergic genes: *Anxa1* (4.3 versus 19.6, $p < 0.001$), *Chrna6* (6.8 versus 20.9, $p < 0.001$), *En1* (12.8 versus 26.4, $p < 0.01$), *Grp* (11.3 versus 38.4, $p < 0.01$), *Ntsr1* (6.1 versus 18, $p < 0.0001$), *Slc10a4* (10.9 versus 29.7, $p < 0.001$), and *Snca* (4.9 versus 13, $p < 0.01$). Having sufficiently demonstrated the cell-type-specificity of the current approach, we continued with comparative studies to identify molecular markers distinguishing the mesolimbic and nigrostriatal dopaminergic projections.

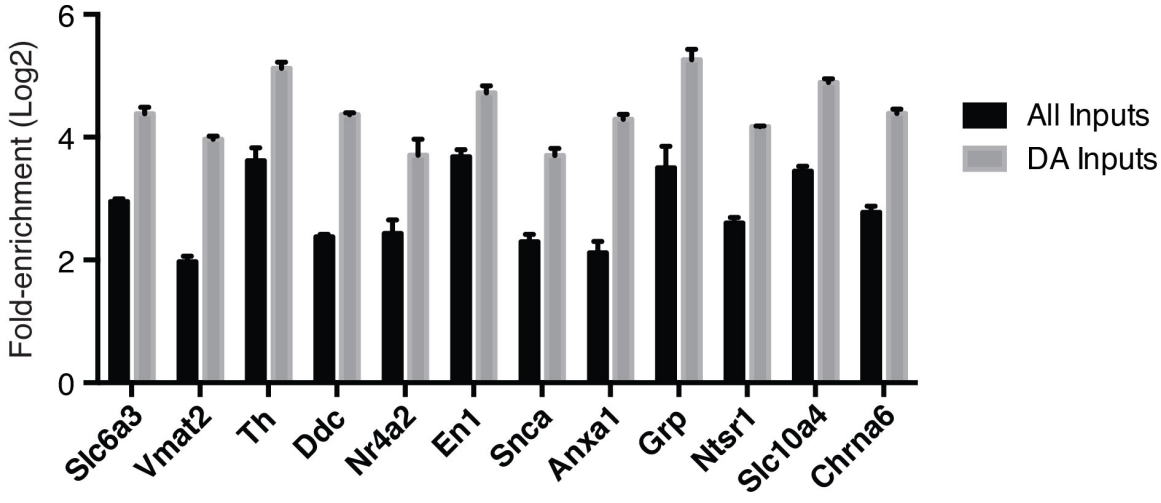

Figure 5.16. Dopamine Neuron Markers are Highly Enriched in Cell-type-specific Retro-TRAP of the Mesolimbic Dopamine Circuit. Comparative analysis between original Retro-TRAP strategy (black bars, 'All Inputs') and cell-type-specific Retro-TRAP (grey bars, 'DA Inputs'). Enrichments for known/newly-identified mesolimbic DA marker genes. All genes are significantly more enriched in the DA Inputs group. *Nr4a2* and *Snca*, $p < 0.05$; all other genes, $p < 0.0001$. All data are displayed as mean ± SEM.

The mesolimbic and nigrostriatal dopaminergic projections play somewhat divergent roles in the behaving animal, the former more responsible for motivational state and the latter for locomotor function/action selection, despite the fact that they have remarkable similarities: they appear cytochemically similar (Lammel et al., 2008), and occupy adjacent, blending loci within the ventral midbrain (Wise, 2009). Additionally, these cell types send parallel projections into the striatum (the ventral tegmental area targets the nucleus accumbens, while the substantia nigra pars compacta targets the caudate putamen). Efforts to molecularly distinguish these two populations have been limited to patch clamp aspiration (Lammel et al., 2008), laser-capture microdissection (Li et al., 2013), and crude co-labeling with immunohistochemistry, which often result in low mRNA yields. However, an approach such as Retro-TRAP should be able to simply parse out these two populations by virtue of cell-type-specificity and connectivity.

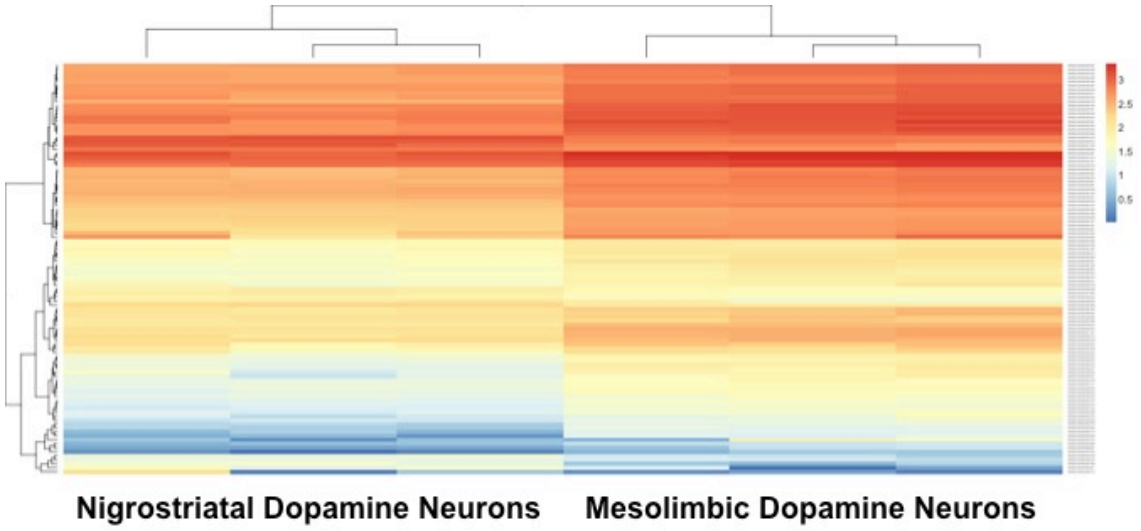

Figure 5.17. Heat Map Comparison of Mesolimbic and Nigrostriatal Dopamine Neurons. Data generated from high-throughput RNA-sequencing. All genes are significant ($q < 0.05$). Red is indicative of enrichment, and blue is indicative of depletion.

We first visualized the RNA-seq data using a heat map, demonstrating all significant genes ($q < 0.05$) in either the mesolimbic or nigrostriatal projection (Figure 5.17). It is immediately clear that these two projections share much in common, as expected for two populations of dopamine neurons. For example, we would expect to see similarities of enrichment for all dopaminergic marker genes. Indeed, there is a significant degree of similarity between these two populations in dopamine-specific marker gene enrichment (data not shown). Of note, it has previously been reported that *Drd2* and *Slc6a3* are heterogeneously expressed in the ventral midbrain (Haber et al., 1995). When we compared the two marker genes, we were able to observe increased enrichment within the nigrostriatal (nst) projection, as compared with the mesolimbic (msl) projection: *Drd2* (94 msl vs. 131 nst FPKM, $p < 0.01$) and *Slc6a3* (816 msl vs. 1253 nst FPKM, $p < 0.0001$). Additionally, upon closer inspection, we observed marked differences in the molecular profiles of each of these projective cell types, as demonstrated using principal component analysis (PCA, Figure 5.18). It then remained to determine which marker genes were differentially enriched between these two populations.

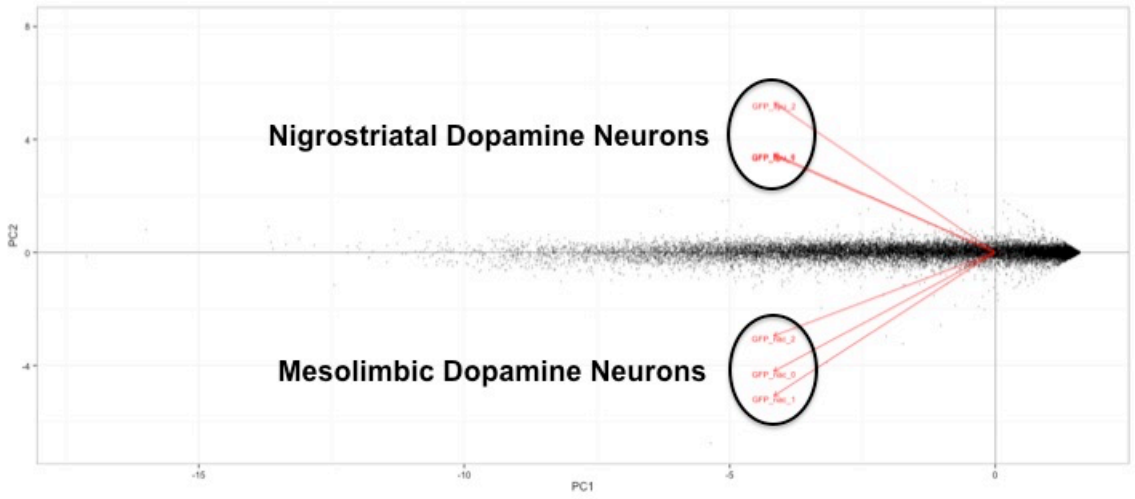

Figure 5.18. Principal Component Analysis of Mesolimbic and Nigrostriatal Dopamine Neurons. PCA segregates the two populations into two distinct clusters, demonstrating that these populations are molecularly distinguishable.

Identifying selectively expressed marker genes within these two projections is a critical goal, as these two populations of dopamine neurons are differentially susceptible to Parkinson's disease. In the disease state, the nigrostriatal dopamine neurons selectively degenerate with a relative preservation of the mesolimbic projection. The mechanisms underlying the privileged state of mesolimbic dopamine neurons are currently unknown; however there is some evidence suggesting that this has to do with molecular differences that exist between the two populations (Damier et al., 1999a, b). These initial molecular differences could give rise to a population of dopamine neurons predisposed to degeneration, a so-called 'multiple hit' hypothesis (Sulzer, 2007). We first set out to see if a simpler hypothesis underlying the differential susceptibility of these cell types to Parkinson's disease.

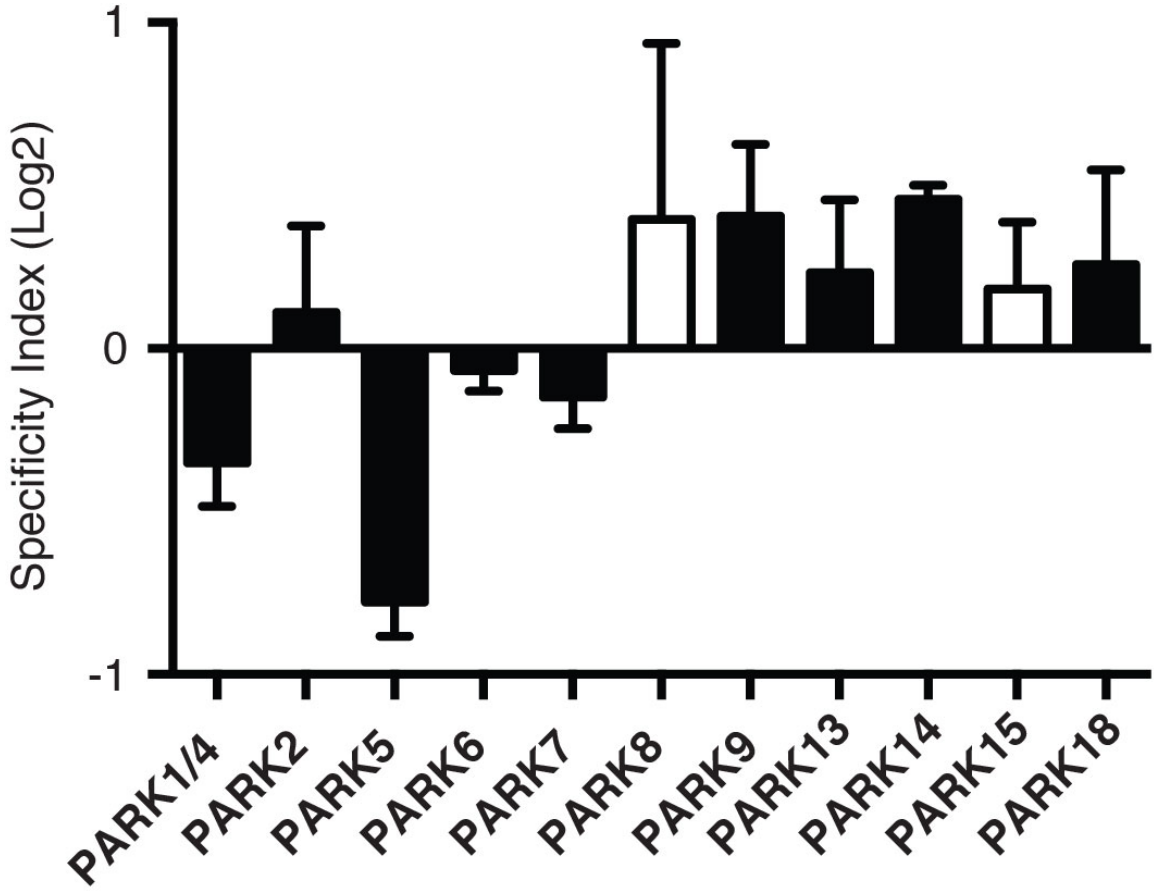

Figure 5.19. Similar Enrichment for Parkinson's Disease Marker Genes in Mesolimbic and Nigrostriatal Dopamine Neurons. Expression specificity (nigrostriatal/mesolimbic) for Parkinson's disease-associated (PARK) genes. Differentially expressed genes: PARK1/4 (Snca, $p < 0.05$), PARK5 (Uchl1, $p < 0.0001$), PARK14 (Pla2g6, $p < 0.0001$). Closed bars (9/11 genes) indicate enrichment in both projections, open bars (2/11 genes) are indicative of differential enrichment. All other genes are not significantly differentially enriched. All data are displayed as mean ± SEM.

One (overly) simple hypothesis underlying this differential susceptibility could be the differential expression of the known genetic variants associated with Parkinson's disease (the PARK gene family). If these genes were preferentially enriched/depleted from these two populations, it could possibly hint at a mechanism for which mutations would serve to the significant detriment of one population but not necessarily the other. However, when we looked at relative enrichment of the PARK genes (by generating a specificity index: nigrostriatal/mesolimbic enrichment), we found similar enrichment for the PARK genes between the treatments (Figure 5.19), with only three differentially expressed: *PARK1/4* (*Snca*, mesolimbic-specific, $p < 0.05$), *PARK5* (*Uchl1*, mesolimbic-specific, $p < 0.0001$), and *PARK14* (*Pla2g6*, nigrostriatal-specific, $p < 0.0001$). However, we did notice that most of the PARK genes were enriched within dopamine neurons regardless of mesolimbic/nigrostriatal projection-specificity (Figure 5.19, black bars, 9/11 genes). These data suggest a potential role for dopamine neuron function (or dysfunction), but alone are insufficient to suggest a potential mechanism for the differential susceptibility to a disease state. We thus turned our investigations to other potential mechanisms by which these cell types differentially respond to insult.

One popular hypothesis underlying the selective degeneration of nigrostriatal dopamine neurons is that these neurons are more readily susceptible to excitotoxicity (due to their inability to proper handle calcium load through buffering). Previous cytochemical reports have suggested that there is a relatively

reduced expression of calbdindin (*Calb1*) in the nigrostriatal projection neurons that degenerate in Parkinson's disease (Damier et al., 1999a, b). When we looked at calcium buffering proteins calbindin (*Calb1*) and calretinin (*Calb2*), we found that these two genes were increasingly enriched in the mesolimbic projection (Figure 5.20): *Calb1* (mesolimbic-specific, $p < 0.01$) and *Calb2* (mesolimbic-specific, $p < 0.0001$). Interestingly, we also found selective enrichment within the mesolimbic projection for a marker gene not previously associated with dopamine neurons, *Casr*. Calcium-sensing receptor (CaSR) is a G-protein coupled receptor (GPCR) responsible for sensing extracellular levels of calcium. We found significant enrichment for *Casr* within the mesolimbic projection, as compared with the nigrostriatal projection ($p < 0.0001$). One possibility for this gene not having previously been detected in these neurons is its very low expression level, on the order of 0.5-1 FPKM in our IPs, as compared with an even lower amount in the input; this is more remarkable when contrasted with marker genes like *Calb1* and *Calb2*, which have expression levels 2-3 orders of magnitude larger (Figure 5.20). These data further demonstrate the importance of utilizing approaches such as Retro-TRAP that yield higher levels of quality mRNA in a high-throughput fashion. Together, these data suggest a potential mechanism by which nigrostriatal dopamine neurons are selective susceptible excitotoxicity, through their inability to buffer and sense calcium.

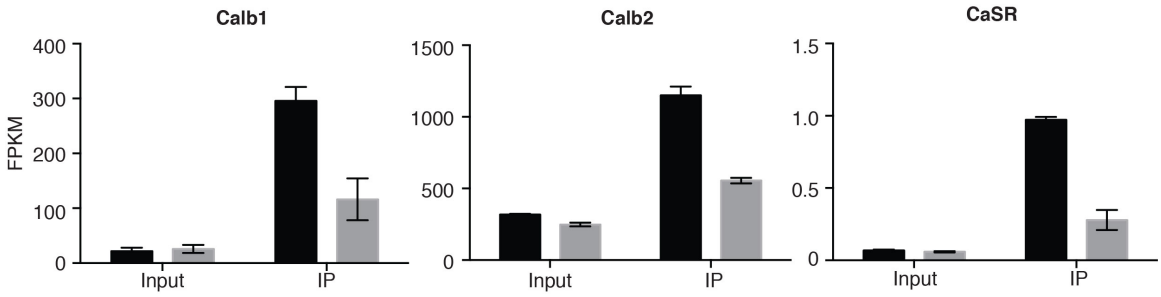

Figure 5.20. Differential Expression of Calcium Buffering and Sensing Proteins within the Mesolimbic and Nigrostriatal Dopamine Circuitry. The mesolimbic (msl, black bars) and nigrostriatal (nst, grey bars) dopaminergic projections have calcium buffering and sensing protein expression heavily biased towards the mesolimbic circuit. This is reflected in the differential enrichments observed with calcium buffering proteins *Calb1* (left, 296 msl vs. 116 nst FPKM, $p < 0.01$) and *Calb2* (middle, 1151 msl vs. 555 nst FPKM, $p < 0.0001$), and calcium sensing protein *Casr* (right, 0.9715 msl vs. 0.2787 nst FPKM, $p < 0.0001$). All data are displayed as mean ± SEM.

5.10 Molecular characterization of the nigrostriatal dopaminergic projection in health and disease states

While we were able to perform high-throughput molecular profiling to compare the mesolimbic and nigrostriatal projections, another desirable aim would be to characterize the nigrostriatal projection in the disease state. To accomplish this aim, we turned to the MitoPark model of Parkinson disease (Ekstrand et al., 2007). The MitoPark mouse is a genetic model of PD, created by conditionally knocking out exons 6 and 7 of mitochondrial transcription factor A (Tfam) from dopamine neurons via a cross to DAT-IRES-Cre mice (Backman et al., 2006). Tfam is responsible for mitochondrial transcription and mitochondrial genome replication, and its loss results in mice with dopamine neurons that are respiratory-chain-deficient. This cellular stress ultimately leads to the preferential and progressive loss of nigrostriatal dopamine neurons, recapitulating many of the core symptoms and pathological alterations commonly observed in the Parkinsonian state (Ekstrand et al., 2007). Thus, we set out to characterize the molecular adaptations underlying this progressive degenerative effect.

To profile nigrostriatal dopamine neurons in the MitoPark mouse model, we utilized DAT-IRES-Cre; Tfam fl/fl mice (Ekstrand et al., 2007). We set out to profile these neurons prior to their death, and achieved this aim by performing cell-type-specific Retro-TRAP studies at a presymptomatic time point. We selected the earliest reasonable time point perform profiling studies, 10 weeks (first surgery at 6 weeks, second surgery at 8 weeks, and IPs at 10 weeks). Additionally, at 10 weeks, the

midbrain dopamine neurons appear relatively undisturbed (Ekstrand et al., 2007). To assure that these mice were indeed presymptomatic in our own hands at 10 weeks, we performed an open field test (OFT), which indeed confirmed that these mice exhibited similar, intact locomotor function to their wild-type littermates (Figure 5.21). Additionally, we later confirmed that these mice were indeed Parkinsonian, exhibiting characteristic hypokinesia after 14 weeks (Figure 5.21). These data reflect the timeline observed in previous studies on the MitoPark mouse (Ekstrand et al., 2007).

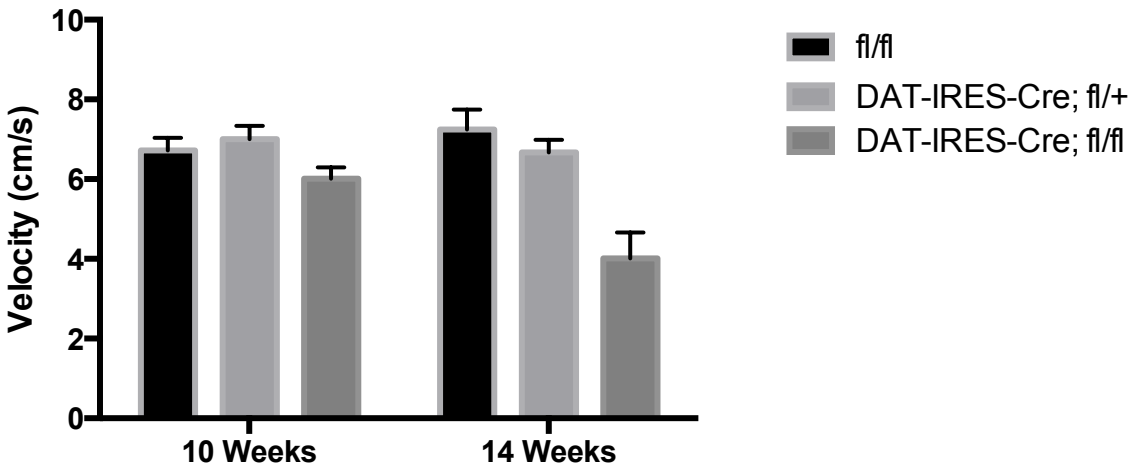

Figure 5.21. Locomotor Function of MitoPark Mice in the Open Field Test. MitoPark mice exhibit a time-dependent decrease in gross locomotor function (paired comparison within treatment over time: $p < 0.01$; between group comparison at 10 weeks: n.s., at 14 weeks: $p < 0.0001$) due to degeneration of the nigrostriatal projection (Ekstrand et al., 2007). Littermate controls have intact, unchanged locomotor function. All data are displayed as mean ± SEM.

To perform cell-type-specific Retro-TRAP within the nigrostriatal dopaminergic circuit of MitoPark mice, we followed the same protocol as before for the nigrostriatal projection; this time, however, we used DAT-IRES-Cre +/-; Tfam fl/fl mice (as compared with DAT-IRES-Cre +/-; Tfam +/+ in the original case). After performing IPs, we confirmed that we were able to significantly deplete for the deleted exons (exons 6-7 deleted, probe for exons 5-6) from dopamine neurons using qPCR, and this was comparatively depleted as compared to other Tfam exons (2-3, $p = 0.001$). We then sought to identify molecular alterations that may provide a potential mechanism for the phenotype observed in Parkinsonian patients, as well as the phenocopy MitoPark model. We first assessed the effect on dopaminergic character by investigating the expression changes in the dopamine transporter *Slc6a3* (DAT). In the nigrostriatal projection, we observed significant downregulation of DAT expression in the MitoPark disease state (Figure 5.22). Interestingly, when we looked at global dopaminergic DAT expression by looking at FLAG IPs (specific to all midbrain dopamine neurons) normalized to our Input sample, we found no alteration in DAT expression (Figure 5.22), suggesting that the molecular adaptations observed are specific to nigrostriatal circuit, and not the disease model itself.

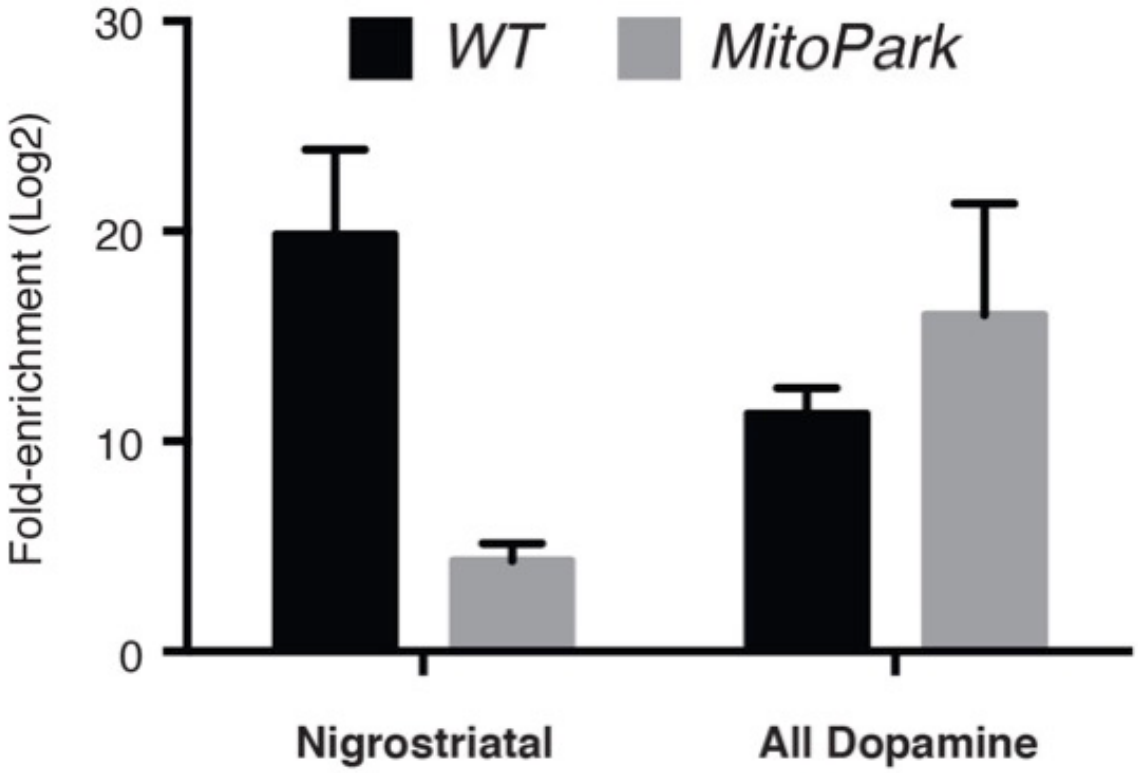

Figure 5.22. Reduced Expression of Dopamine Transporter DAT in Pre-Symptomatic MitoPark Mouse Model of PD. DAT expression is reduced in the nigrostriatal DA projection of MitoPark mice (Slc6a3, $p < 0.05$), whereas expression within other DA neurons remains fully intact. All data are displayed as mean ± SEM.

5.11 Identification of a novel function for gastrin-releasing peptide (GRP)

In our molecular profiling studies, one common transcript that was repeatedly enriched in projections targeting the nucleus accumbens was that of gastrin-releasing peptide (GRP). Notably, its receptor gastrin-releasing peptide receptor (GRPR) also appears to be expressed in the nucleus accumbens shell (Figure 5.23). The origin of this GRP enrichment was ultimately found within the ventral tegmental area (VTA), particularly the mesolimbic projection (Figure 5.12E). This was confirmed both through identification in the Allen Brain Atlas *in situ* hybridizations (data not shown), as well as conclusively with triple-labeling within the VTA using a combination of immunohistochemistry (to label midbrain dopamine neurons and the partially overlapping mesolimbic projection) and fluorescence *in situ* hybridization (FISH) marking *Grp* mRNA (Figure 5.12E). Very little is known about central nervous system function of GRP; however, given that it is highly enriched within the mesolimbic projection, we postulated that this peptide could play an important role in modulating reward-related behaviors.

Figure 5.23. Gastrin-releasing Peptide Receptor (GRPR) Expression in the Nucleus Accumbens, from GENSAT Database. Gastrin-releasing peptide receptor (GRPR)-EGFP mice from GENSAT show a pattern of expression apparent in the nucleus accumbens. This is consistent with expression of gastrin-releasing peptide (GRP) mRNA found in the ventral tegmental area.

To address the possibility that GRP modulates valence, we performed conditioned place preference (CPP) studies in tandem with GRP infusion bilaterally into the nucleus accumbens (NAc). In performing dose-response studies, we found that lower levels of GRP (0.25 μg) may be mildly appetitive, whereas higher levels of GRP (1.0 μg were highly aversive) (Figure 5.24). This bidirectional modulation of valence was rather surprising given the wealth of evidence suggesting the appetitive role of midbrain dopamine neuron activity (Schultz, 1998; Tsai et al., 2009). However, this effect is not totally unprecedented given previous evidence on bidirectional neurpeptidergic modulation of reward within the nucleus accumbens (Lemos et al., 2012). One hypothesis to explain our surprising results is that GRP exists within this circuit to act as a 'brake' on dopaminergic function in the NAc. Such could be the case during acquisition of cocaine-induced conditioned place preference (CPP).

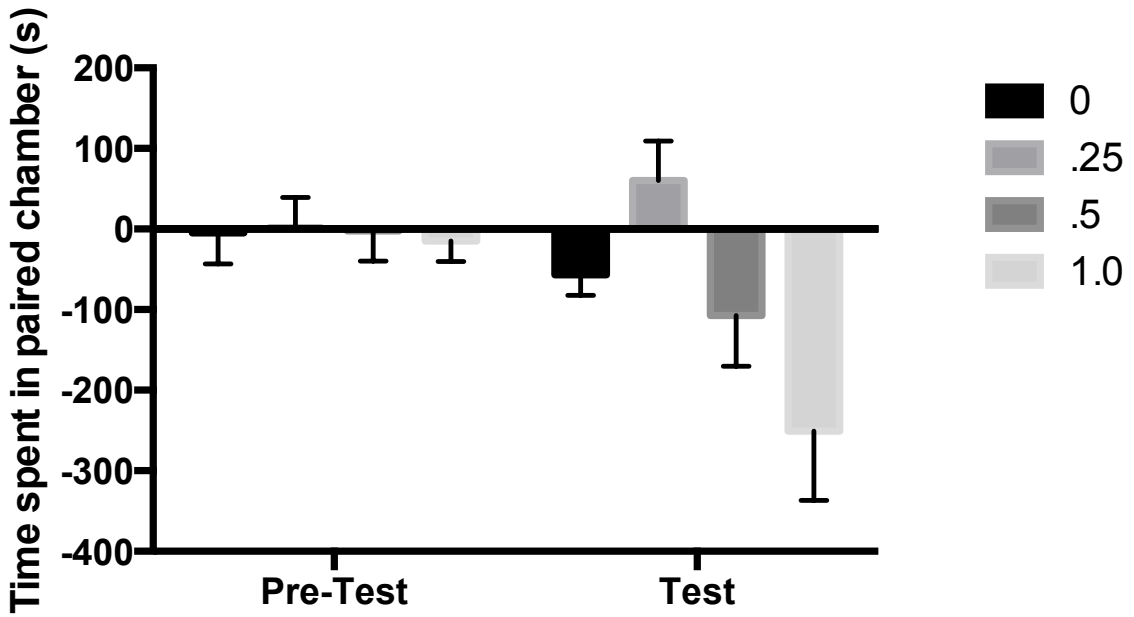

Figure 5.24. Dose-response of Gastrin-releasing Peptide Administration Bilaterally to the Nucleus Accumbens. Gastrin-releasing peptide in the nucleus accumbens is mildly appetitive at low doses and shifts to being aversive at a higher dose level ($p < 0.05$). All data are displayed as mean ± SEM.

We thus set out to see if we could alter cocaine-induced CPP through simultaneous infusion of GRP bilaterally into the NAc. We investigated the effects of low dose GRP infusion into the NAc under a variable cocaine regimen (0, 5, or 10 mg/kg). Cocaine CPP can be elicited by 5 and 10 mg/kg cocaine, with the most robust CPP at 10 mg/kg (Koo et al., 2012). At the low dose cocaine regimen, we surprisingly found that GRP administration caused an appetitive to aversive shift in cocaine CPP ($p < 0.01$, Figure 5.25). However, when administered to mice on the high dose cocaine regimen, GRP was found to enhance cocaine CPP ($p < 0.05$, Figure 5.25). Together, these data suggest that GRP has a bidirectional effect on valence, and complex interactions with cocaine in the mesolimbic dopaminergic circuitry that remains to be fully determined. Future work will focus on the role of GRP release specifically from mesolimbic dopamine neurons in the context of health and addiction-related behavioral states.

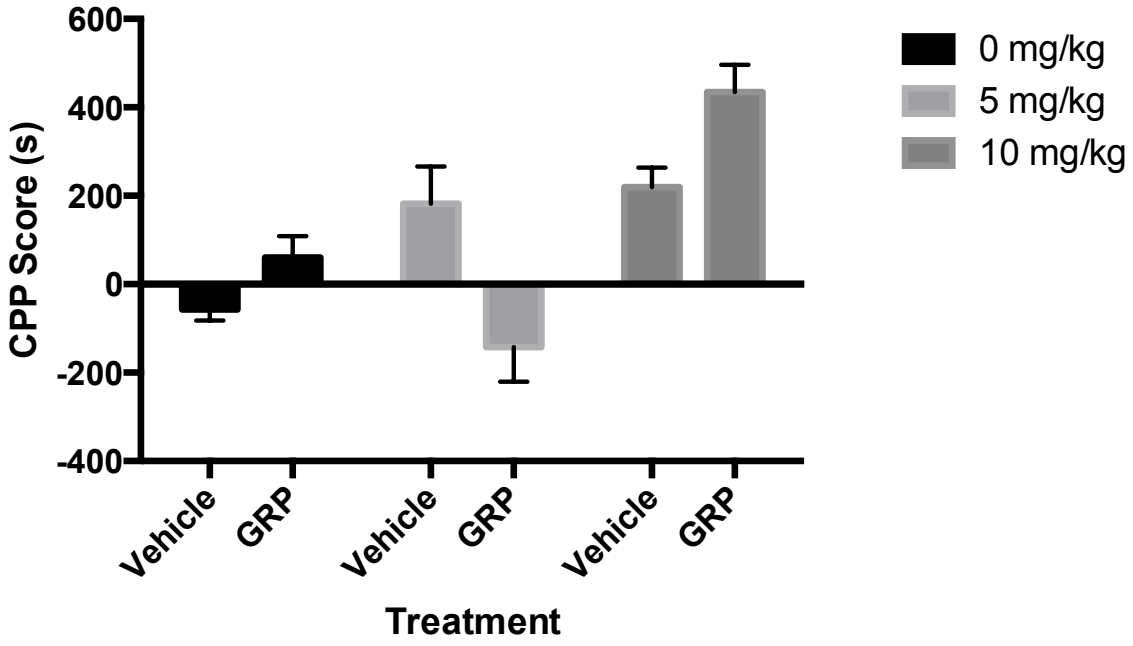

Figure 5.25. Effect of Infusion of Gastrin-Releasing Peptide Into the Nucleus Accumbens on Cocaine CPP. At a low dose of cocaine (5 mg/kg), GRP infusion caused an appetitive to aversive shift in cocaine CPP ($p < 0.01$). At a high dose of cocaine, GRP infusion caused a synergistic increase in cocaine CPP ($p < 0.05$). All data are displayed as mean ± SEM.

These studies demonstrate the particular utility of using an unbiased approach to molecular profiling of neural circuits, particularly Retro-TRAP, which ultimately enables the identification of novel proteins within the nervous system, with as yet unidentified functions. The discovery of GRP within the mesolimbic projection is just one of many examples of the power of such a technique, and certainly more functional proteins with currently understudied roles will be uncovered. One case of this will be the application of Retro-TRAP to the mesolimbic and nigrostriatal dopamine circuits, which will hopefully unveil a number of differentially expressed molecules, which ultimately give rise to the differential susceptibility of these two cell types in the disease state.

CHAPTER 6: DISCUSSION

There is currently a significant effort underway to systematically identify all of the brain's component cell types, and then to functionally establish the role of these cell types in the behaving organism. This approach has been particularly effective, though incomplete. A cell type, to current first-order approximations, is defined as an anatomically restricted population of neurons with a unique molecular identifier (e.g. dopamine, serotonin, parvalbumin, etc.). Additional, but not mutually exclusive criteria for cell type classification include (but are not limited to) electrophysiological properties, morphology, and connectivity. A critical question then becomes the resolution at which we can appreciate cell types. I wish to conclude this work by first summarizing some the major accomplishments of the described thesis work (particularly with regards to refining our definition of cell types within the brain by virtue of anatomy/connectivity and the molecular dissection of brainstem neural circuits), and then discussing critical future directions for refining our definition of cell types within the brain and how they contribute to adaptive behavior.

As neurotechnologies continue to improve, our ability to resolve the function of smaller and smaller subpopulations of neurons increases. Neural circuits can now be targeted for activation (gain-of-function) and inhibition (loss-of-function) by virtue of their expression of a principal marker genes (Tye and Deisseroth, 2012), connectivity (Tye and Deisseroth, 2012), and even contextual/temporally-restricted activity (Guenthner et al., 2013; Liu et al., 2012; Ramirez et al., 2013). In some cases,

some intersections of these criteria (e.g. cell-type- and projection-specific) are currently possible and will become more practical to implement in the years to come.

To understand the behavioral function(s) of the dorsal raphe nucleus, I utilized projection- and cell-type-specific approaches to dissect out the role of three different cell types in the behaving animal. These cell types, defined by expression of serotonin, the GABAergic transporter *Vgat*, and the non-canonical glutamate transporter *VGluT3*, each play different roles in modulating behavioral output. Studies prior to this had suggested key roles of the dorsal raphe in modulating locomotion (Warden et al., 2012; Waterhouse et al., 2004) and reward (McDevitt et al., 2014; Qi et al., 2014; Rompre and Miliaressis, 1985), but none had parsed out the specific cell types underlying these behaviors. Still, many questions remain. For instance, dorsal raphe 5-HT and VGluT3 neurons have substantial degrees of overlap, yet activation of one subpopulation elicits vigorous locomotor function and suppression of appetite, while the other does not appear to acutely effect baseline behavioral function at all. Future studies will require the development and application of novel transgenic mouse lines and molecular logic gates (Fenno et al., 2014) to access the intersection, union, and complements of these subpopulations. Knowledge of their differential input/output architecture may also provide clues critical to understanding the context within which these neural circuits are designed to function.

To address questions such as those that remain from the studies of the dorsal raphe, it is clear that technology development will play a critical role. One area that was particularly necessary was that of molecular profiling within neural circuits. The development of translating ribosome affinity purification (TRAP, Doyle et al., 2008; Heiman et al., 2008) conferred neuroscientists with the critical capability of molecularly profiling cell types based on the expression of a principal marker gene. With the development of Retro-TRAP, we extended this class of TRAP-related technologies to enable profiling of cell types not only based on expression of a principal marker gene, but connectivity, as well. This methodology, for the first time, enabled us to project molecular information onto the connectivity map of the mouse brain.

The following are some concluding thoughts on the importance of the previously described studies and possibilities for future work, building on these tools and basic discoveries.

6.1 Dorsal raphe control of innate behaviors

The behavioral function of the dorsal raphe is poorly understood. This is no surprise given its molecular heterogeneity and the remarkable complexity and collateralization of projections originating from the locus. In the current work, we sought to reduce complexity of the cellular heterogeneity component by targeting three different cell types that are significantly represented in the raphe: 5-HT, VGluT3, and GABA. In acute dissection of behavioral functions, we surprisingly

found a limited role for serotonergic function, whereas the GABAergic and glutamatergic neurons were able to robustly and rapidly modulate innate, survival-related behaviors. The work also provides neuroanatomic evidence for the output pathways through which these cell types may control their various behavioral functions.

To understand how the brain provides the dorsal raphe with contextual information, it will be critical to identify the cell-type-specific inputs onto each of the identified DRN cell types, and to investigate whether these inputs are sufficient to elicit the studied behaviors. One possibility to achieve this aim (discussed further below) will be a modification of Retro-TRAP, where we utilize a simultaneous monosynaptic rabies approach within a Cre-driver mouse crossed to the SYN-NBL10 mouse. This would enable a relatively rapid approach to defining the cell types that target the DRN.

6.2 Viral TRAP for rapid molecular profiling of defined cell types

Translating ribosome affinity purification (TRAP) has been highly successful in achieving molecular profiles of a diverse array of cell types in health (Doyle et al., 2008; Nakajima et al., 2014) and disease states (Mellen et al., 2012; Schmidt et al., 2012). This approach initially relied on BAC transgenesis to target the EGFPL10a transgene directly to cell types of interest (Heiman et al., 2008); however, more recently, a number of reporter lines have been developed that utilize crosses with Cre-driver lines to conditionally express epitope-tagged ribosomal proteins in

specific cell populations (Sanz et al., 2009; Stanley et al., 2013; Liu et al, 2014; Zhao et al., 2014). In the current work, we sought to extend the TRAP method to take advantage of viral-mediated gene transfer, enabling rapid and anatomically-restricted molecular profiling using pre-existing Cre-driver lines and eliminating the need to cross multiple mouse lines.

The broad availability of Cre-driver lines (Gerfen et al., 2013; Gong et al., 2003) allows the viral TRAP strategy to immediately be applied to myriad cell types without the need to generate novel transgenic strains or cross existing lines. AAV-mediated overexpression of the TRAP transgene also enables profiling data to be generated as early as three weeks post-infection, allowing for substantial temporal flexibility when designing experiments. Furthermore, viral delivery of the EGFPL10a transgene into adult mouse tissue eliminates the possibility of recombination and activation of the tagged ribosomal protein in unwanted cell types that may transiently express Cre during development (Lam et al., 2011; Lammel et al., 2015). Such developmentally ectopic expression imposes a significant limitation on the utility of Cre-dependent TRAP and RiboTag reporter strains when used in combination with Cre driver lines that have dynamic expression patterns in development (Sanz et al., 2009; Stanley et al., 2013). Lastly, the AAV-FLEX-EGFPL10a vector provides a simple strategy to extend the TRAP technique to other species such as rats, for which a number of Cre driver lines exist (Steinberg et al., 2013; Witten et al., 2011).

The current viral approach to translational profiling has a broad dynamic range, allowing for enrichments of control and cell type markers, with concomitant depletion of markers for glia and other non-targeted cell types. Therefore, vTRAP provides a method to obtain highly cell-type-specific gene expression data similar to transgenic strategies. Importantly, we found that the translational profiles obtained from vTRAP correlated very highly with those from bacTRAP (data not shown), demonstrating the ability to reproducibly target and profile the same cell population using either the viral or transgenic approaches.

It is also possible that translational profiling using vTRAP could be further improved by allowing more time for increased EGFPL10a expression. AAVs often require at least 2 weeks for maximal expression (Kaspar et al., 2002), and due to the low turnover rate of neuronal ribosomal proteins (Price et al., 2010), may need an extended period of time for higher levels of integration into the ribosome. Nonetheless, we find that we can robustly profile multiple different neural populations even within three weeks after stereotactic injections of viruses. Indeed, our polysome biochemistry also demonstrates that it is even possible to label ribosomes as early as 1-week post-injection. Together, these data demonstrate a rapid approach to anatomically-restricted, cell-type-specific molecular profiling.

Other factors surrounding enrichment may also need to be taken into consideration. Cre-dependent 'FLEX/DIO' constructs used in AAVs have been demonstrated to exhibit a minor degree of leakiness (Miyamichi et al., 2013), which may be due to a

number of possibilities such as antisense transcription from the 3' UTR (Kim et al., 2012) or promiscuous recombination of the lox sites during plasmid preparation (A.R.N., unpublished data). Thus, when using Cre-dependent AAVs, it will be important to carefully titer the virus and ensure that there has not been any recombination of the vector during its preparation, prior to drawing conclusions about expression of a given marker gene. Furthermore, it is highly recommended that identified candidate marker genes are confirmed using an independent method, such as IHC and/or FISH.

Additionally, AAVs are commonly used in neuroscience as vectors to deliver a number light-activated channels and pumps (channelrhodopsins, halorhodopsins, archaerhodopsins), designer receptors (DREADDs), genetically-encoded calcium indicators (GECIs), and siRNAs. The viruses we report here can potentially be used in tandem with these above approaches and could facilitate our understanding of the molecular adaptations underlying changes in neural activity, as well as correlated behavioral alterations observed after experimental perturbation.

Finally, genome editing technologies such as TALENs and CRISPR have advanced to the point where it is possible to acutely manipulate gene expression and epigenetic states using viral-mediated gene transfer (Konermann et al., 2013; Platt et al., 2014; Ran et al., 2015; Swiech et al., 2015). To assess the effects of these engineered molecular perturbations, profiling technologies could be multiplexed onto these manipulations with co-injection of AAV-FLEX-GFPL10. The use of vTRAP technology

in tandem with genome engineering could facilitate our understanding of the role of targeted genetic alterations on central nervous system function.

6.3 Retro-TRAP for molecular connectomics

Numerous studies have focused on the comprehensive, high-resolution mapping of the connectivity within the central nervous system (Helmstaedter et al., 2013; Maisak et al., 2013; Takemura et al., 2013). This work, along with studies dating back to the mid-1980s elucidating the connectome of the nematode *C. elegans* (White et al., 1986), have worked towards the important goal of relating neural structure to its function (Lichtman and Denk, 2011; Morgan and Lichtman, 2013). However, connectomic information is necessary but not sufficient to characterize the role of neural populations within a functioning circuit, in part because neural circuitry is labile to neuromodulation, which is essential to its function but invisible to neuroanatomical reconstruction (Bargmann, 2012). Thus, to understand how neural circuits give rise to behavior, the synthesis of connectomic and molecular information is essential.

The identification of markers for specific neurons enables an array of studies delineating their function through use of electrophysiology, molecular profiling, and neural activation/inhibition using optogenetics or chemical genetics (Armbruster et al., 2007; Boyden et al., 2005). Recently, translational profiling approaches have made it possible to profile neurons based on the expression of cell-type-specific marker genes (Heiman et al., 2008), as well as changes in their activity (Knight et al.,

2012); however, these approaches do not provide neuroanatomical information about the neurons being profiled. Thus, means for simultaneously generating connectomic and molecular information would help advance our understanding of how neural circuits give rise to behavior.

6.3.1 Projection-specific translational profiling

GFP is commonly encoded in retrograde tracing viruses to identify presynaptic inputs to a defined locus within the brain. However, while GFP expression can be used to confirm a neuroanatomical connection, it does not reveal the molecular composition of the cell-type. Additionally, many of the retrograde viruses used, such as rabies virus, are often acutely toxic to the cells they infect, potentially altering transcriptomic profiles (Osakada and Callaway, 2013; Wickersham et al., 2007). To enable molecular profiling of a presynaptic cell-type, we required an efficient retrograde virus expressing GFP that had minimal toxicity to the infected cells. Canine adenovirus (CAV) had previously been used for restoration of nigrostriatal dopamine release in a model of dopamine deficiency, demonstrating the long-term preservation of neural function (Hnasko et al., 2006).

We focused our efforts on inputs to the nucleus accumbens (NAc), as they are known to play an important role in such diverse behaviors as feeding (Georgescu et al., 2005), social interaction (Dolen et al., 2013), and reward processing (Lammel et al., 2012). Dysfunction of these neural populations is also implicated in a variety of

disease states, such as obesity (Ludwig et al., 2001), addiction (Luscher and Malenka, 2011), and depression (Chaudhury et al., 2013; Tye et al., 2013).

This work additionally enables the molecular definition of anatomically interspersed populations of neurons within the brain based on their projection pattern. The ventral tegmental area (VTA), for example, is a heterogeneous nucleus with distinct subsets of dopaminergic neurons that can be classified based on their projections to a number of postsynaptic targets such as the medial prefrontal cortex, nucleus accumbens, and hippocampus. However, these populations are not dissociable by manual dissection, making the profiling of these distinct neuronal populations impossible using established techniques such as bacTRAP and RiboTag. Thus, it is likely that molecular profiling of genetically-defined projective cell-types will be an important application of projection-specific translational profiling. Indeed, it is already becoming clear that different projections from a molecularly defined nucleus can have differential behavioral effects relevant to reward processing (Lammel et al., 2012), as well as depression (Chaudhury et al., 2013). Toward this end, we extended the current approach to profile VTA dopamine neurons projecting to the nucleus accumbens using CAV-GFP, and a Cre-driver line with an AAV that we generated.

The data reported here further indicate that NBL10 could be incorporated into other vector systems for a variety of studies. For example, a monosynaptic rabies virus expressing GFP could be used in tandem with the SYN-NBL10 mouse (crossed

to a Cre-driver line) to profile neurons synapsing onto a molecularly-defined postsynaptic target (see Wall et al., 2013). Similarly, this system could be adapted to identify markers for neurons post-synaptic to genetically-defined cells using Cre-dependent anterograde strains of herpes simplex virus (Lo and Anderson, 2011).

Molecularly profiling neurons based on their pattern of connectivity represents a methodology that is conceptually distinct from a number of recent efforts, which have been made to obtain molecular genetic information from connectomic-based experiments. Approaches such as single-synapse proteomic analysis (Micheva et al., 2010) and the Allen Brain Institute's cell-type-specific, virally-targeted expression of GFP (connectivity.brain-map.org) have made significant progress in this area; however, these methodologies require either highly-sensitive microscopy methods or numbers of transgenic mouse lines expressing Cre recombinase. Additionally, these approaches require an *a priori* defined cell-type to be targeted. Thus, an unbiased approach to studying molecular connectivity within the brain as reported here should be of general use.

Alternate strategies have also been employed to molecularly profile neurons based on their projection pattern, particularly within the VTA. However, these approaches such as laser capture microdissection (Lammel et al., 2008; Li et al., 2013) have low RNA yields, require specialized instrumentation and are difficult to implement, and are therefore not amenable to high-throughput analyses. Another possible approach to projection-specific molecular profiling would be through fluorescence-activated

cell sorting (FACS) of retrogradely-labeled, fluorophore-positive neurons (see Sugino et al., 2006); however, the current isolation protocols for neuronal FACS (Lobo et al., 2006) appear to induce cellular stress, and the resulting molecular profiles have reduced sensitivity in comparison to techniques like bacTRAP. Projection-specific translational profiling using TRAP-based methodologies, therefore, allows for access to translating mRNAs with high efficiency, enabling detailed molecular analyses using quantitative PCR and RNA-seq.

6.3.2 Intersectional genetic applications of NBL10-based TRAP

The NBL10-based approach could be engineered to further molecularly refine subpopulations of neural cell-types defined by the intersection of two markers. For example, to translationally profile a neural cell-type defined by two marker genes (e.g. genes A and B), one could drive expression of NBL10 on the gene A promoter, and cross this mouse to a gene B-GFP mouse. This particular approach would allow for increasing granularity in the systematic analysis of CNS cell-types that are currently characterized by a single marker gene. Furthermore, AAV-FLEX-NBL10 could be used for this purpose, as well. A GFP line could be crossed to a partially overlapping Cre-driver line, and the offspring could be injected with AAV-FLEX-NBL10 to profile the intersection of these two cell-types. The data reported here indicate that this approach is feasible and would potentially enable an intersectional strategy for molecular profiling of neurons allowing a further refinement of the analysis of a variety of neuronal subpopulations.

6.4 Summary

Through these investigations, we have begun to uncover a previously unappreciated role for local cell type diversity in modulating behavior. Future work will seek to uncover the role of the dorsal raphe at a much higher behavioral and cell-subtype-specific resolution. Additionally, novel tool development will inform future studies and elucidate underlying molecular mechanisms, which currently are beyond the sensitivity of available tools. Importantly, we are at a unique inflection point where the molecular profiling technologies are finally being matched with the substantial progress of *in vivo* genome editing. Thus, candidate marker genes within identified cell types can now be selectively targeted *in vivo* for knockdown with high specificity (Ran et al., 2015), and will likely be repurposed for titrating gene expression levels. Together, these technologies will enable a feedback loop between marker gene discovery and perturbation that will enable the elucidation of the complex mechanisms that define the molecular and neural basis of behavior.

REFERENCES

Amat, J., Baratta, M.V., Paul, E., Bland, S.T., Watkins, L.R., and Maier, S.F. (2005). Medial prefrontal cortex determines how stressor controllability affects behavior and dorsal raphe nucleus. Nat Neurosci *8*, 365-371.

Amilhon, B., Lepicard, E., Renoir, T., Mongeau, R., Popa, D., Poirel, O., Miot, S., Gras, C., Gardier, A.M., Gallego, J., et al. (2010). VGLUT3 (vesicular glutamate transporter type 3) contribution to the regulation of serotonergic transmission and anxiety. J Neurosci *30*, 2198-2210.

Aponte, Y., Atasoy, D., and Sternson, S.M. (2011). AGRP neurons are sufficient to orchestrate feeding behavior rapidly and without training. Nature neuroscience *14*, 351-355.

Arlotta, P., Molyneaux, B.J., Chen, J., Inoue, J., Kominami, R., and Macklis, J.D. (2005). Neuronal subtype-specific genes that control corticospinal motor neuron development in vivo. Neuron *45*, 207-221.

Armbruster, B.N., Li, X., Pausch, M.H., Herlitze, S., and Roth, B.L. (2007). Evolving the lock to fit they key to create a family of G protein-coupled receptors potently activated by an inert ligand. Proc. Natl. Acad. Sci. USA *104*, 5163-5168.

Atasoy, D., Aponte, Y., Su, H.H., and Sternson, S.M. (2008). A FLEX switch targets Channelrhodopsin-2 to multiple cell types for imaging and long-range circuit mapping. J. Neurosci. *28*, 7025-7030.

Backman, C.M., Malik, N., Zhang, Y., Shan, L., Grinberg, A., Hoffer, B.J., Westphal, H., and Tomac, A.C. (2006). Characterization of a mouse strain expressing Cre recombinase from the 3' untranslated region of the dopamine transporter locus. Genesis *44*, 383-390.

Bargmann, C.I. (2012). Beyond the connectome: how neuromodulators shape neural circuits. Bioessays *34*, 458-465.

Boyden, E.S., Zhang, F., Bamberg, E., Nagel, G., and Deisseroth, K. (2005). Millsecond-timescale, genetically targeted optical control of neural activity. Nat. Neurosci. *8*, 1263-1268.

Bru, T., Salinas, S., and Kremer, E.J. (2010). An update on canine adenovirus type 2 and its vectors. Viruses *2*, 2134-2153.

Challis, C., Boulden, J., Veerakumar, A., Espallergues, J., Vassoler, F.M., Pierce, R.C., Beck, S.G., and Berton, O. (2013). Raphe GABAergic neurons mediate the acquisition of avoidance after social defeat. J Neurosci *33*, 13978-13988.

Chaudhury, D., Walsh, J.J., Friedman, A.K., Juarez, B., Ku, S.M., Koo, J.W., Ferguson, D., Tsai, H.C., Pomeranz, L., Christoffel, D.J., et al. (2013). Rapid regulation of depression-related behaviours by control of midbrain dopamine neurons. Nature *493*, 532-536.

Chung, C.Y., Seo, H., Sonntag, K.C., Brooks, A., Lin, L., and Isacson, O. (2005). Cell type-specific gene expression of midbrain dopaminergic neurons reveals molecules involved in their vulnerability and protection. Hum. Mol. Genet. *14*, 1709-1725.

Croizier, S., Franchi-Bernard, G., Colard, C., Poncet, F., La Roche, A., and Risold, P.Y. (2010). A comparative analysis show morphofunctional differences between the rat and mouse melanin-concentrating hormone systems. PLoS One *5*, e15471.

Damier, P., Hirsch, E.C., Agid, Y., and Graybiel, A.M. (1999a). The substantia nigra of the human brain. I. Nigrosomes and the nigral matrix, a compartmental organization based on calbindin D(28K) immunohistochemistry. Brain *122*, 1421-1436.

Damier, P., Hirsch, E.C., Agid, Y., and Graybiel, A.M. (1999b). The substantia nigra of the human brain. II. Patterns of loss of dopamine-containing neurons in Parkinson's disease. Brain *122*, 1437-1448.

Dolen, G., Darvishzadeh, A., Huang, K.W., and Malenka, R.C. (2013). Social reward requires coordinated activity of nucleus accumbens oxytocin and serotonin. Nature *501*, 179-184.

Doyle, J.P., Dougherty, J.D., Heiman, M., Schmidt, E.F., Stevens, T.R., Ma, G., Bupp, S., Shrestha, P., Shah, R.D., Doughty, M.L., et al. (2008). Application of a translational profiling approach for the comparative analysis of CNS cell types. Cell *135*, 749-762.

Dugas, J.C., Mandemakers, W., Rogers, M., Ibrahim, A., Daneman, R., and Barres, B.A. (2008). A novel purification method for CNS projection neurons leads to the identification of brain vascular cells as a source of trophic support for corticospinal motor neurons. J Neurosci *28*, 8294-8305.

Ekstrand, M.I., Terzioglu, M., Galter, D., Zhu, S. Hofstetter, C., Lindqvist, E., Thams, S., Bergstrand, A., Hansson, F.S., Trifunovic, A., et al. (2007). Progressive parkinsonism in mice with respiratory-chain-deficient dopamine neurons. Proc Natl Acad Sci USA *104*, 1325-1330.

Ekstrand, M.I., Nectow, A.R., Knight, Z.A., Latcha, K.N., Pomeranz, L.E., and Friedman, J.M. (2014). Molecular profiling of neurons based on connectivity. Cell *157*, 1230-1242.

Fenno LE, Mattis, J., Ramakrishnan, C., Hyun, M., Lee, S.Y., He, M., Tucciarone, J., Selimbeyoglu, A., Berndt, A., Grosenick, L., et al. (2014). Targeting cells with single vectors using multiple-feature Boolean logic. Nat Methods *11*, 763-772.

Fremeau, R.T., Burman, J., Quereshi, T., Tran, C.H., Proctor, J., Johnson, J., Zhang, H., Sulzer, D., Copenhagen, D.R., Storm-Mathisen, J., et al. (2002). The identification of vesicular glutamate transporter 3 suggests novel modes of signaling by glutamate. Proc Natl Acad Sci USA *99*, 14488-14493.

Gagnon, D., and Parent, M. (2014). Distribution of VGLUT3 in highly collateralized axons from the rat dorsal raphe nucleus as revealed by single-neuron reconstructions. PloS one *9*, e87709.

Georgescu, D., Sears, R.M., Hommel, J.D., Barrot, M., Bolanos, C.A., Bednarek, M.A., Bibb, J.A., Maratos-Flier, E., Nestler, E.J., and DiLeone, R.J. (2005). The hypothalamic neuropeptide melanin-concentrating hormone acts in the nucleus accumbens to modulate feeding behavior and forced-swim performance. J. Neurosci. *25*, 2933-2940.

Gerfen, C.R., Paletzki, R., and Heintz, N. (2013). GENSAT BAC cre-recombinase driver lines to study the functional organization of cerebral cortical and basal ganglia circuits. Neuron *80*, 1368-1383.

Gong, S., Zheng, C., Doughty, M.L., Losos, K., Didkovsky, N., Schambra, U.B., Nowak, N.J., Joyner, A., Leblanc, G., Hatten, M.E.*, et al.* (2003). A gene expression atlas of the central nervous system based on bacterial artificial chromosomes. Nature *425*, 917-925.

Gorlich, A., Antolin-Fontes, B., Ables, J.L., Frahm, S., Slimak, M.A., Dougherty, J.D., and Ibanez-Tallon, I. (2013). Reexposure to nicotine during withdrawal increases the pacemaking activity of cholinergic habenular neurons. Proc Natl Acad Sci USA *110*, 17077-17082.

Grgic, I., Hofmeister, A.F., Genovese, G., Bernhardy, A.J., Sun, H., Maarouf, O.H., Bijol, V., Pollak, M.R., and Humphreys, B.D. (2014). Discovery of new glomerular disease-relevant genes by translational profiling of podocytes in vivo. Kidney international *86*, 1116-1129.

Guenthner, C.J., Miyamichi, K., Yang, H.H., Heller, H.C., and Luo, L. (2013). Permanent genetic access to transiently active neurons via TRAP: targeted recombination in active populations. Neuron *78*, 773-784.

Haber, S.N., Ryoo, H., Cox, C., and Lu, W. (1995). Subsets of midbrain dopaminergic neurons in monkeys are distinguished by different levels of mRNA for the dopamine transporter: comparison with the mRNA for the D2 receptor, tyrosine hydroxylase and calbindin immunoreactivity. J Comp Neurol *362*, 400-410.

Haemmerle, C.A., Campos, A.M., and Bittencourt, J.C. (2015). Melanin-concentrating hormone inputs to the nucleus accumbens originate from distinct hypothalamic sources and are apposed to GABAergic and cholinergic cells in the Long-Evans rat brain. Neuroscience *289*, 392-405.

Heiman, M., Schaefer, A., Gong, S., Peterson, J.D., Day, M., Ramsey, K.E., Suarez-Farinas, M., Schwarz, C., Stephan, D.A., Surmeier, D.J., et al. (2008). A translational profiling approach for the molecular characterization of CNS cell types. Cell *135*, 738-748.

Heisler, L.K., Jobst, E.E., Sutton, G.M., Zhou, L., Borok, E., Thornton-Jones, Z., Liu, H.Y., Zigman, J.M., Balthasar, N., Kishi, T., et al. (2006). Serotonin reciprocally regulates melanocortin neurons to modulate food intake. Neuron *51*, 239-249.

Helmstaedter, M., Briggman, K.L., Turaga, S.C., Jain, V., Seung, H.S., and Denk, W. (2013). Connectomic reconstruction of the inner plexiform layer in the mouse retina. Nature *500*, 168-174.

Hnasko, T.S., Perez, F.A., Scouras, A.D., Stoll, E.A., Gale, S.D., Luquet, S., Phillips, P.E., Kremer, E.J., and Palmiter, R.D. (2006). Cre recombinase-mediated restoration of nigrostriatal dopamine in dopamine-deficient mice reverses hypophagia and bradykinesia. Proc. Natl. Acad. Sci. USA *103*, 8858-8863.

Jacobs, B.L., and Fornal, C.A. (1993). 5-HT and motor control: a hypothesis. Trends Neurosci *16*, 346-352.

Jego, S., Glasgow, S.D., Herrera, C.G., Ekstrand, M., Reed, S.J., Boyce, R., Friedman, J., Burdakov, D., and Adamantidis, A.R. (2013). Optogenetic identification of a rapid eye movement sleep modulatory circuit in the hypothalamus. Nat. Neurosci. *16*, 1637-1643.

Jennings, J.H., Sparta, D.R., Stamatakis, A.M., Ung, R.L., Pleil, K.E., Kash, T.L., and Stuber, G.D. (2013). Distinct extended amygdala circuits for divergent motivational states. Nature *496*, 224-228.

Jensen, P., Farago, A.F., Awatramani, R.B., Scott, M.M., Deneris, E.S., and Dymecki, S.M. (2008). Redefining the serotonergic system by genetic lineage. Nat Neurosci *11*, 417-419.

Johnson, M.D. (1994). Synaptic glutamate release by postnatal rat serotonergic neurons in microculture. Neuron *12*, 433-442.

Kaspar, B.K., Vissel, B., Bengoechea, T., Crone, S., Randolph-Moore, L., Muller, R., Brandon, E.P., Schaffer, D., Verma, I.M., Lee, K.F., et al. (2002). Adeno-associated

virus effectively mediates conditional gene modification in the brain. Proc Natl Acad Sci USA *99*, 2320-2325.

Kempadoo, K.A., Tourino, C., Cho, S.L., Magnani, F., Leinninger, G.M., Stuber, G.D., Zhang, F., Myers, M.G., Deisseroth, K., de Lecea, L., et al. (2013). Hypothalamic neurotensin projections promote reward by enhancing glutamatergic transmission in the VTA. J. Neurosci. *33*, 7618-7626.

Kim, J., Zhao, T., Petralia, R.S., Yu, Y., Peng, H., Myers, E., and Magee, J.C. (2012). mGRASP enables mapping mammalian synaptic connectivity with light microscopy. Nat Methods *9*, 96-102.

Kim, S.Y., Adhikari, A., Lee, S.Y., Marshel, J.H., Kim, C.K., Mallory, C.S., Lo, M., Pak, S., Mattis, J., Lim, B.K., et al. (2013). Diverging neural pathways assemble a behavioural state from separable features in anxiety. Nature *496*, 219-223.

Knight, Z.A., Tan, K., Birsoy, K., Schmidt, S., Garrison, J.L., Wysocki, R.W., Emiliano, A., Ekstrand, M., and Friedman, J.M. (2012). Molecular profiling of activated neurons by phosphorylated ribosome capture. Cell *151*, 1126-1137.

Konermann, S., Brigham, M.D., Trevino, A.E., Hsu, P.D., Heidenreich, M., Cong, L., Platt, R.J., Scott, D.A., Church, G.M., and Zhang, F. (2013). Optical control of mammalian endogenous transcription and epigenetic states. Nature *500*, 472-476.

Koo, J.W., Mazei-Robison, M.S., Chaudhury, D., Juarez, B., LaPlant, Q., Ferguson, D., Feng, J., Sun, H., Scobie, K.N., Damez-Werno, D., et al. (2012). BDNF is a negative regulator of morphine action. Science *338*, 124-128.

Kozorovitskiy, Y., Saunders, A., Johnson, C.A., Lowell, B.B., and Sabatini, B.L. (2012). Recurrent network activity drives striatal synaptogenesis. Nature *485*, 646-650.

Krashes, M.J., Shah, B.P., Madara, J.C., Olson, D.P., Strochlic, D.E., Garfield, A.S., Vong, L., Pei, H, Watabe-Uchida, M., Uchida, N., et al. (2014). An excitatory paraventricular nucleus to AgRP neuron circuit that drives hunger. Nature *507*, 238-242.

Kravitz, A.V., Freeze, B.S., Parker, P.R., Kay, K., Thwin, M.T., Deisseroth, K., and Kreitzer, A.C. (2010). Regulation of parkinsonian motor behaviours by optogenetic control of basal ganglia circuitry. Nature *466*, 622-626.

Kremer, E.J., Boutin, S., Chillon, M., and Danos, O. (2000). Canine adenovirus vectors: an alternative for adenovirus-mediated gene transfer. Journal of virology *74*, 505-512.

Kriaucionis, S., and Heintz, N. (2009). The nuclear DNA base 5-hydroxymethylcytosine is present in Purkinje neurons and the brain. Science *324*, 929-930.

Lam, D.D., Leinninger, G.M., Louis, G.W., Garfield, A.S., Marston, O.J., Leshan, R.L., Scheller, E.L., Christensen, L., Donato, J., Jr., Xia, J., et al. (2011). Leptin does not directly affect CNS serotonin neurons to influence appetite. Cell Metabolism *13*, 584-591.

Lammel, S., Hetzel, A., Hackel, O., Jones, I., Liss, B., and Roeper, J. (2008). Unique properties of mesoprefrontal neurons within a dual mesocorticolimbic dopamine system. Neuron *57*, 760-773.

Lammel, S., Ion, D.I., Roeper, J., and Malenka, R.C. (2011). Projection-specific modulation of dopamine neuron synapses by aversive and rewarding stimuli. Neuron *70*, 855–862.

Lammel, S., Lim, B.K., Ran, C., Huang, K.W., Betley, M.J., Tye, K.M., Deisseroth, K., and Malenka, R.C. (2012). Input-specific control of reward and aversion in the ventral tegmental area. Nature *491*, 212-217.

Lammel, S., Steinberg, E.E., Foldy, C., Wall, N.R., Beier, K., Luo, L., and Malenka, R.C. (2015). Diversity of transgenic mouse models for selective targeting of midbrain dopamine neurons. Neuron *85*, 429-438.

Lein, E., Hawrylycz, M.J., Ao, N., Ayres, M., Bensinger, A., Bernard, A., Boe, A.F., Boguski, M.S., Brockway, K.S., Byrnes, E.J., et al. (2007). Genome-wide atlas of gene expression in the adult mouse brain. Nature *445*, 168-176.

Lemos, J.C., Wanat, M.J., Smith J.S., Reyes, B.A., Hollon N.G., Van Bockstaele, E.J., Chavkin C., and Phillips, P.E. (2012). Severe stress switches CRF action in the nucleus accumbens from appetitive to aversive. Nature *490*, 402-406.

Li, X., Qi, J., Yamaguchi, T., Wang, H.L., and Morales, M. (2013). Heterogeneous composition of dopamine neurons of the rat A10 region: molecular evidence for diverse signaling properties. Brain Struct. Funct. *218*, 1159-1176.

Lichtman, J.W., and Denk, W. (2011). The big and the small: challenges of imaging the brain's circuits. Science *334*, 618-623.

Lim, B.K., Huang, K.W., Grueter, B.A., Rothwell, P.E., and Malenka, R.C. (2012). Anhedonia requires MC4R-mediated synaptic adaptations in nucleus accumbens. Nature *487*, 183-189.

Liu, J., Krautzberger, A.M., Sui, S.H., Hofmann, O.M., Chen, Y., Baetscher, M., Grgic, I., Kumar, S., Humphreys, B.D., Hide, W.A., et al. (2014). Cell-specific translational profiling in acute kidney injury. J Clin Invest *124*, 1242-1254.

Liu, X., Ramirez, S., Pang, P.T., Puryear, C.B., Govindarajan, A., Deisseroth, K., and Tonegawa, S. (2012). Optogenetic stimulation of a hippocampal engram activates fear memory recall. Nature *484*, 381-385.

Liu, Z., Zhou, J., Li, Y., Hu, F., Lu, Y., Ma, M., Feng, Q., Zhang, J.E., Wang, D., Zeng, J., et al. (2014). Dorsal raphe neurons signal reward through 5-HT and glutamate. Neuron *81*, 1360-1374.

Lo, L., and Anderson, D.J. (2011). A Cre-dependent, anterograde transsynaptic viral tracer for mapping output pathways of genetically marked neurons. Neuron *72*, 938-950.

Lobo, M.K., Karsten, S.L., Gray, M., Geschwind, D.H., and Yang, X.W. (2006). FACS-array profiling of striatal projection neuron subtypes in juvenile and adult mouse brains. Nat. Neurosci. *9*, 443-452.

Lobo, M.K., Covington, H.E., Chaudhury, D., Friedman, A.K., Sun, H., Damez-Werno, D., Dietz, D.M, Zaman, S., Koo, J.W., Kennedy, P.J., et al. (2010). Cell-type-specific loss of BDNF signaling mimics optogenetic control of cocaine reward. Science *330*, 385-390.

Lou, S., Duan, B., Vong, L., Lowell, B.B., and Ma, Q. (2013). Runx1 controls terminal morphology and mechanosensitivity of VGLUT3-expressing C-mechanoreceptors. J. Neurosci. *33*, 870-882.

Lowry, C.A., Evans, A.K., Gasser, P.J., Hale, M.W., Staub, D.R., and Shekhar, A. (2008). Topographic organization and chemoarchitecture of the dorsal raphe nucleus and the median raphe nucleus. Serotonin and Sleep, 25-67.

Ludwig, D.S., Tritos, N.A., Mastaitis, J.W., Kulkarni, R., Kokkotou, E., Elmquist, J., Lowell, B., Flier, J.S., and Maratos-Flier, E. (2001). Melanin-concentrating hormone overexpression in transgenic mice leads to obesity and insulin resistance. J. Clin. Invest. *107*, 379-386.

Luscher, C., and Malenka, R.C. (2011). Drug-evoked synaptic plasticity in addiction: from molecular changes to circuit remodeling. Neuron *69*, 650-663.

Maisak, M.S., Haag, J., Ammer, G., Serbe, E., Meier, M., Leonhardt, A., Schilling, T., Bahl, A., Rubin, G.M., Nern, A., et al. (2013). A directional tuning map of Drosophila elementary motion detectors. Nature *500*, 212-216.

McDevitt, R.A., Tiran-Cappello, A., Shen, H., Balderas, I., Britt, J.P., Marino, R.A., Chung, S.L., Richie, C.T., Harvey, B.K., and Bonci, A. (2014). Serotonergic versus nonserotonergic dorsal raphe projection neurons: differential participation in reward circuitry. Cell Rep *8*, 1857-1869.

Mellen, M., Ayata, P., Dewell, S., Kriaucionis, S., and Heintz, N. (2012). MeCP2 binds to 5hmC enriched within active genes and accessible chromatin in the nervous system. Cell *151*, 1417-1430.

Micheva, K.D., Busse, B., Weiler, N.C., O'Rourke, N., and Smith, S.J. (2010). Single-synapse analysis of a diverse synapse population: proteomic imaging methods and markers. Neuron *68*, 639-653.

Miyamichi, K., Shlomai-Fuchs, Y., Shu, M., Weissbourd, B.C., Luo, L., and Mizrahi, A. (2013). Dissecting local circuits: parvalbumin interneurons underlie broad feedback control of olfactory bulb output. Neuron *80*, 1232-1245.

Morgan, J.L., and Lichtman, J.W. (2013). Why not connectomics? Nat. Methods *10*, 494-500.

Mosharov, E.V., Larsen, K.E., Kanter, E., Phillips, K.A., Wilson, K., Schmitz, Y., Krantz, D.E., Kobayashi, K., Edwards, R.H., and Sulzer, D. (2009). Interplay between cytosolic dopamine, calcium, and α-synuclein causes selective death of substantia nigra neurons. Neuron *62*, 218-229.

Molyneaux, BJ., Goff, L.A., Brettler, A.C., Chen, H.H., Brown, J.R., Hrvatin, S., Rinn, J.L., and Arlotta, P. (2015). DeCoN: genome-wide analysis of in vivo transcriptional dynamics during pyramidal neuron fate selection in neocortex. Neuron *85*, 275-288.

Muyldermans, S. (2013). Nanobodies: natural single-domain antibodies. Annu. Rev. Biochem. *82*, 775-797.

Nakajima, M., Gorlich, A., and Heintz, N. (2014). Oxytocin modulates female sociosexual behavior through a specific class of prefrontal cortical interneurons. Cell *159*, 295-305.

Nelson, A.B., Bussert, T.G., Kreitzer, A.C., and Seal, R.P. (2014). Striatal cholinergic neurotransmission requires VGLUT3. J Neurosci *34*, 8772-8777.

Oh, Y.S., Gao, P., Lee, K.W., Ceglia, I., Seo, J.S., Zhang, X., Ahn, J.H., Chait, B.T., Patel, D.J., Kim, Y., et al. (2013). SMARCA3, a chromatin-remodeling factor, is required for p11-dependent antidepressant action. Cell *152*, 831-843.

Oka, Y., Ye, M., and Zuker, C.S. (2015). Thirst driving and suppressing signals encoded by distinct neural populations in the brain. Nature. In Press.

Osakada, F., and Callaway, E.M. (2013). Design and generation of recombinant rabies virus vectors. Nat. Protoc. *8*, 1583-1601.

Platt, R.J., Chen, S., Zhou, Y., Yim, M.J., Swiech, L., Kempton, H.R., Dahlman, J.E., Parnas, O., Eisenhaure, T.M., Jovanovic, M., et al. (2014). CRISPR-Cas9 knockin mice for genome editing and cancer modeling. Cell *159*, 440-455.

Price, J.C., Guan, S., Burlingame, A., Prusiner, S.B., and Ghaemmaghami, S. (2010). Analysis of proteome dynamics in the mouse brain. Proc Natl Acad Sci USA *107*, 14508-14513.

Qi, J., Zhang, S., Wang, H.L., Wang, H., de Jesus Aceves Buendia, J., Hoffman, A.F., Lupica, C.R., Seal, R.P., and Morales, M. (2014). A glutamatergic reward input from the dorsal raphe to ventral tegmental area dopamine neurons. Nature Communications *5*, 5390.

Ramirez, S., Liu, X., Lin, P.A., Suh, J., Pignatelli, M., Redondo, R.L., Ryan, T.J., and Tonegawa, S. (2013). Creating a false memory in the hippocampus. Science *341*, 387-391.

Ran, F.A., Cong, L., Yan, W.X., Scott, D.A., Gootenberg, J.S., Kriz, A.J., Zetsche, B., Shalem, O., Wu, X., Makarova, K.S., et al. (2015). In vivo genome editing using Staphylococcus aureus Cas9. Nature. In Press.

Ries, J., Kaplan, C., Platonova, E., Eghlidi, H., and Ewers, H. (2012). A simple, versatile method for GFP-based super-resolution microscopy via nanobodies. Nat. Methods *9*, 582-584.

Rompre, P.P., and Miliaressis, E. (1985). Pontine and mesencephalic substrates of self-stimulation. Brain research *359*, 246-259.

Rothbauer, U., Zolghadr, K., Tillib, S., Nowak, D., Schermelleh, L., Gahl, A., Backmann, N., Conrath, K., Muyldermans, S., Cardoso, M.C., et al. (2006). Targeting and tracing antigens in live cells with fluorescent nanobodies. Nat. Methods *3*, 887-889.

Russo, S.J., and Nestler, E.J. (2013). The brain reward circuitry in mood disorders. Nat Rev Neurosci *14*, 609-625.

Sanz, E., Yang, L., Su, T., Morris, D.R., McKnight, G.S., and Amieux, P.S. (2009). Cell-type-specific isolation of ribosome-associated mRNA from complex tissues. Proc. Natl. Acad. Sci. USA *106*, 13939-13944.

Schmidt, E.F., Warner-Schmidt, J.L., Otopalik, B.G., Pickett, S.B., Greengard, P., and Heintz, N. (2012). Identification of the cortical neurons that mediate antidepressant responses. Cell *149*, 1152-1163.

Schultz, W. (1998). Predictive reward signal of dopamine neurons. J Neurophysiol *80*, 1-27.

Scott, M.M., Wylie, C.J., Lerch, J.K., Murphy, R., Lobur, K., Herlitze, S., Jiang, W., Conlon, R.A., Strowbridge, B.W., and Deneris, E.S. (2005). A genetic approach to access serotonin neurons for in vivo and in vitro studies. Proc Natl Acad Sci USA *102*, 16472-16477.

Seal, R.P., and Edwards, R.H. (2006). The diverse roles of vesicular glutamate transporter 3. Handb Exp Pharmacol, 137-150.

Sesack, S.R., and Grace, A.A. (2010). Cortico-basal ganglia reward network: microcircuitry. Neuropsychopharmacology *35*, 27-47.

Shimada, M., Tritos, N.A., Lowell, B.B., Flier, J.S., and Maratos-Flier, E. (1998). Mice lacking melanin-concentrating hormone are hypophagic and lean. Nature *396*, 670-674.

Silva, J.P., von Meyenn, F., Howell, J., Thorens, B., Wolfrum, C., and Stoffel, M. (2009). Regulation of adaptive behaviour during fasting by hypothalamic Foxa2. Nature *462*, 646-650.

Sugino, K., Hempel, C.M., Miller, M.N., Hattox, A.M., Shapiro, P., Wu, C., Huang, Z.J., and Nelson, S.B. (2006). Molecular taxonomy of major neuronal classes in the mouse forebrain. Nat. Neurosci. *9*, 99-107.

Stachniak, T.J., Ghosh, A., and Sternson, S.M. (2014). Chemogenetic synaptic silencing of neural circuits localizes a hypothalamus-->midbrain pathway for feeding behavior. Neuron *82*, 797-808.

Stanley, S.A., Domingos, A.I., Kelly, L., Garfield, A., Damanpour, S., Heisler, L., and Friedman, J. (2013). Profiling of glucose-sensing neurons reveals that GHRH neurons are activated by hypoglycemia. Cell Metab. *18*, 596-607.

Steinberg, E.E., Keiflin, R., Boivin, J.R., Witten, I.B., Deisseroth, K., and Janak, P.H. (2013). A causal link between prediction errors, dopamine neurons and learning. Nature Neurosci *16*, 966-973.

Sulzer, D. (2007). Multiple hit hypotheses for dopamine neuron loss in Parkinson's disease. Trends Neurosci *30*, 244-250.

Svenningsson, P., Chergui, K., Rachleff, I., Flajolet, M., Zhang, X., El Yacoubi, M., Vaugeois, J.M., Nomikos, G.G., and Greengard, P. (2006). Alterations in 5-HT1B receptor function by p11 in depression-like states. Science *311*, 77-80.

Swiech, L., Heidenreich, M., Banerjee, A., Habib, N., Li, Y., Trombetta, J., Sur, M., and Zhang, F. (2015). In vivo interrogation of gene function in the mammalian brain using CRISPR-Cas9. Nature biotechnology *33*, 102-106.

Takemura, S.Y., Bharioke, A., Lu, Z., Nern, A., Vitaladevuni, S., Rivlin, P.K., Katz, W.T., Olbris, D.J., Plaza, S.M., Winston, P., et al. (2013). A visual motion detection circuit suggested by Drosophila connectomics. Nature *500*, 175-181.

Tang, J.C., Szikra, T., Kozorovitskiy, Y., Teixiera, M., Sabatini, B.L., Roska, B., and Cepko, C.L. (2013). A nanobody-based system using fluorescent proteins as scaffolds for cell-specific gene manipulation. Cell *154*, 928-939.

Thomas, A., Lee, P.J., Dalton, J.E., Nomie, K.J., Stoica, L., Costa-Mattioli, M., Chang, P., Nuzhdin, S., Arbeitman, M.N., and Dierick, H.A. (2012). A versatile method for cell-specific profiling of translated mRNAs in Drosophila. PloS one *7*, e40276.

Tsai, H.C., Zhang, F., Adamantidis, A., Stuber, G.D., Bonci, A., de Lecea, L., and Deisseroth, K. (2009). Phasic firing in dopaminergic neurons is sufficient for behavioral conditioning. Science *324*, 1080-1084.

Tsien, R.Y. (1998). The green fluorescent protein. Annu. Rev. Biochem. *67*, 509-544.

Tye, K.M., and Deisseroth, K. (2012). Optogenetic investigation of neural circuits underlying brain disease in animal models. Nature reviews Neuroscience *13*, 251-266.

Tye, K.M., Mirzabekov, J.J., Warden, M.R., Ferenczi, E.A., Tsai, H.C., Finkelstein, J., Kim, S.Y., Adhikari, A., Thompson, K.R., Andalman, A.S., et al. (2013). Dopamine neurons modulate neural encoding and expression of depression-related behaviour. Nature *493*, 537-541.

Wall, N.R., Wickersham, I.R., Cetin, A., De La Parra, M., and Callaway, E.M. (2010). Monosynaptic circuit tracing in vivo through Cre-dependent targeting and complementation of modified rabies virus. Proc. Natl. Acad. Sci. USA *107*, 21848-21853.

Wall, N.R., De La Parra, M., Callaway, E.M., and Kreitzer, A.C. (2013). Differential innervation of direct- and indirect-pathway striatal projection neurons. Neuron *79*, 347-360.

Wang, Y., and Jiao, Y. (2014). Translating ribosome affinity purification (TRAP) for cell-specific translation profiling in developing flowers. Methods in molecular biology *1110*, 323-328.

Warden, M.R., Selimbeyoglu, A., Mirzabekov, J.J., Lo, M., Thompson, K.R., Kim, S.Y., Adhikari, A., Tye, K.M., Frank, L.M., and Deisseroth, K. (2012). A prefrontal cortex-brainstem neuronal projection that control response to behavioural challenge. Nature *492*, 428-432.

Waterhouse, B.D., Devilbiss, D., Seiple, S., and Markowitz, R. (2004). Sensorimotor-related discharge of simultaneously recorded, single neurons in the dorsal raphe nucleus of the awake, unrestrained rat. Brain research *1000*, 183-191.

Watson, F.L., Mills, E.A., Wang, X., Guo, C., Chen, D.F., and Marsh-Armstrong, N. (2012). Cell type-specific translational profiling in the Xenopus laevis retina. Developmental dynamics : an official publication of the American Association of Anatomists *241*, 1960-1972.

Weissbourd, B., Ren, J., DeLoach, K.E., Guenthner, C.J., Miyamichi, K., and Luo, L. (2014). Presynaptic partners of dorsal raphe serotonergic and GABAergic neurons. Neuron *83*, 645-662.

White, J.G., Southgate, E., Thomson, J.N., and Brenner, S. (1986). The structure of the nervous system of the nematode caenorhabditis elegans. Phil. Trans. R. Soc. Lond. (B) *314*, 1-340.

Wickersham, I.R., Finke, S., Conzelmann, K.K., and Callaway, E.M. (2007). Retrograde neuronal tracing with a deletion-mutant rabies virus. Nat. Methods *4*, 47-49.

Wise, R.A. (2009). Roles for nigrostriatal—not just mesocorticolimbic—dopamine in reward and addiction. Trends Neurosci *32*, 517-524.

Witten, I.B., Steinberg, E.E., Lee, S.Y., Davidson, T.J., Zalocusky, K.A., Brodsky, M., Yizhar, O., Cho, S.L., Gong, S., Ramakrishnan, C., et al. (2011). Recombinase-driver rat lines: tools, techniques, and optogenetic application to dopamine-mediated reinforcement. Neuron *72*, 721-733.

Wu, Q., Clark, M.S., and Palmiter, R.D. (2012). Deciphering a neuronal circuit that mediates appetite. Nature, *483*, 594-597.

Zhou, P., Zhang, Y., Ma, Q., Gu, F., Day, D.S., He, A., Zhou, B., Li, J., Stevens, S.M., Romo, D., et al. (2013). Interrogating translational efficiency and lineage-specific transcriptomes using ribosome affinity purification. Proc Natl Acad Sci USA *110*, 15395-15400.